PRINCIPLE AND PERFORMANCE OF CONCANAVALIN A-SUGAR AFFINITY BASED CLOSED-LOOP INSULIN DELIVERY SYSTEM

A Thesis Submitted to the

College of Graduate and Postdoctoral Studies

In Partial Fulfilment of the Requirements

For the Degree of Doctor of Philosophy

In the Division of Biomedical Engineering

University of Saskatchewan

Saskatoon

By

Ruixue Yin

PERMISSION TO USE

In presenting this thesis/dissertation in partial fulfillment of the requirements for a Postgraduate degree from the University of Saskatchewan, I agree that the Libraries of this University may make it freely available for inspection. I further agree that permission for copying of this thesis/dissertation in any manner, in whole or in part, for scholarly purposes may be granted by the professor or professors who supervised my thesis/dissertation work or, in their absence, by the Head of the Department or the Dean of the College in which my thesis work was done. It is understood that any copying or publication or use of this thesis/dissertation or parts thereof for financial gain shall not be allowed without my written permission. It is also understood that due recognition shall be given to me and to the University of Saskatchewan in any scholarly use which may be made of any material in my thesis/dissertation.

DISCLAIMER

Reference in this thesis/dissertation to any specific commercial products, process, or service by trade name, trademark, manufacturer, or otherwise, does not constitute or imply its endorsement, recommendation, or favoring by the University of Saskatchewan. The views and opinions of the author expressed herein do not state or reflect those of the University of Saskatchewan, and shall not be used for advertising or product endorsement purposes.

Requests for permission to copy or to make other uses of materials in this thesis/dissertation in whole or part should be addressed to:

Head of the Division of Biomedical Engineering, College of Engineering
University of Saskatchewan
Engineering Building, 57 Campus Drive
Saskatoon, Saskatchewan S7N 5A9 Canada

OR

Dean
College of Graduate and Postdoctoral Studies
University of Saskatchewan
116 Thorvaldson Building, 110 Science Place
Saskatoon, Saskatchewan S7N 5C9 Canada

ABSTRACT

A closed-loop control system that delivers insulin in response to a change of the glucose level is a highly desirable therapy for diabetes patients. An example of such a system is the Concanavalin A (Con A)-sugar affinity based chemically controlled closed-loop insulin delivery system (Con A-based system in short) that integrates a glucose sensing element and a glucose-triggered insulin release system into a single system using glucose-responsive materials. This thesis concerns this system, primarily focusing on the principle or mechanism of the Con A-based system owing to the controversy regarding the principle that the affinity of glucose with Con A is much lower than that of polysaccharides with Con A and therefore glucose cannot trigger the dissociation of Con A-polysaccharides binding in the current literature. The other focus of this thesis is on the feasibility of tailored design to individual patients.

Four specific research objectives were defined for this thesis. **Objective 1:** Investigate the glucose-responsive principle of Con A-sugar affinity-based hydrogel networks with the characterization methods such as isothermal titration calorimetry and attempt to resolve the aforementioned controversy. **Objective 2**: Examine the feasibility of modulating the insulin release behavior by varying the composition of the Con A-based system. **Objective 3**: Develop a methodology for design of the Con A-based system to tailor to individual patients in order to prolong the insulin supply period. **Objective 4**: Develop a mathematical model for improving the design in Objective 3.

The study involves both experiments and mathematical modeling, including analysis with the isothermal titration calorimetry method, and use of the ligand binding equilibrium theory. As well, the study attempts to develop a robotic system perspective to the insulin delivery system. The following conclusions can be drawn from the study: (1) the robotic system perspective to drug delivery systems can provide a general framework for systematic study of drug delivery systems; (2) the principle of glucose triggering the dissociation of Con A-sugar networks is valid because (a) the glucose molecules and the terminal groups (on DexG) have a similar

binding affinity with Con A sites and (b) the glucose can bind with the remaining Con A sites based on the ligand binding equilibrium theory; (3) the amount of remaining Con A sites and DexG molecules after the formation of the Con A-DexG network can be determined, so a modulated insulin release is possible; (4) an integrated design of chemically controlled closed-loop insulin delivery system, specifically by integration of Con A-based glucose-responsive microspheres into a biodegradable chitosan scaffold, can prolong the insulin supply period; (5) a mathematical model for the Con A-based system controlled by swelling and variable diffusion theory has been established and validated, so the glucose-responsive behavior of Con A-DexG hydrogel can be predicted with the model.

There are a couple of contributions with this thesis. First, a systems perspective to drug delivery is available, which can help to design a hybrid (chemical, mechanical) intelligent drug delivery system. Second, the principle of Con A-sugar affinity-based hydrogel networks has been confirmed along with the resolution of the existing controversy on how and why the Con A-based system works. Third, a modulated insulin release with a prolonged supply duration is demonstrated, which opens room for personalized insulin delivery. Finally, a mathematical model with two variables (swelling ratio and diffusion coefficient) is available in the field of insulin delivery, which is an indispensable tool for the design of individualized delivery systems.

In further studies, several aspects may be considered as follows: (1) improvement of the mathematical model for the Con A-based system; (2) combination of glucose level and the characteristics of patients that are responsible for individual requirements for personalized design; (3) optimization of the design to improve the stability, reliability, robustness and/or resilience of the system; (4) incorporation of different insulin sources in the chemically controlled closed-loop system to improve the sustainability of insulin delivery.

ACKNOWLEDGEMENTS

First of all, I would like to show my earnest appreciation and gratitude to my supervisor Professor Wenjun (Chris) Zhang for his incomparable help throughout my PhD study. He has taught me a lot by using his powerful generalization and FCBPSS theory in learning the nature of everything. His immense knowledge, genius in doing research, powerful logic and remarkable enthusiasm greatly inspire me to overcome the challenges in my study. Besides the study, he helped me a lot to my family and my life. In particular, he taught me how to educate and guide my little child, and he and Ms Annie Meng supported me both mentally and financially when my mom suffered from a serious health problem. It was a great honor to meet Chris and Annie in my life.

I would also like to thank my colleagues and friends for their mental or physical help and support during my study life. They are Bing Zhang, Chenwang Yuan, Xue Yong, Ang Chen, Dong He, Xu Wang and his wife Amy, and Hongbo Zhang. Special thanks go to Dr. Jason Maley from SSSC (Sask Structural Science Centre) for his willingness to help me with the characterizations presented in this thesis.

Last but not the least, I want to express my deepest gratitude to my family. My mom is a very strong person who has suffered from diabetes for more than 30 years. Her braveness and willingness to learn how to treat diabetes patients are the original motivation for me to do insulin delivery research. My father and my husband have been so supportive and understanding for every decision I have made over years. My little boy has brought a lot of joy for my life and drives me to grow up to be a more responsible human being.

This thesis is dedicated to

my parents, my husband, and my little boy Aden.

TABLE OF CONTENTS

LIST OF TABLES

LIST OF FIGURES

LIST OF ABBREVIATIONS AND ACRONYMS

Symbols/Abbreviations	Description
Con A	Concanavalin A
DexG	Glycidyl methacrylate modified dextran
ITC	Isothermal titration calorimetry
$C_{\text{Con A total}}$	Initial concentration of Con A
$C_{\text{DexG total}}$	Initial concentration of DexG
$C_{\text{Glu total}}$	Initial concentration of glucose
k_1	Equilibrium constant of DexG-Con A binding reaction
k_2	Equilibrium constant of glucose-Con A binding reaction
C_{DexGConA}	The concentration of resultant DexG-Con A complex
C_{GluConA}	The concentration of resultant Glu-Con A complex
c_{p}	The concentration of polymer DexG in the hydrogel
c_{covalent}	The concentration of covalent crosss-links
DS	Degree of substitution
$\overline{M_n}$	Number average molecular mass of the polymer chain
$\overline{M_c}$	Number average molecular mass of the polymer chain between cross-links
$\bar{v}$	Partial specific volume of the polymer
V_1	Molar volume of water
χ_1	Flory-Huggins polymer-solvent interaction parameter
$v_{2,r}$	Polymer fraction of the hydrogel after gel formation
$v_{2,s}$	Polymer fraction of the hydrogel at equilibrium swelling
Q	Swelling ratio
C_{n}	Flory characteristic ratio
M_{r}	Molecular mass of repeat unit
l	The unit length along the polymer backbone

ξ	Mesh size of the hydrogel network
a	Hydrodynamic radius of the solute (insulin)
D_0	Liquid phase diffusivity of the solute (insulin)
D	Hydrogel phase diffusivity of the solute (insulin)

CHAPTER 1 INTRODUCTION

1.1 Background

1.1.1 Diabetes and insulin

Diabetes mellitus is a group of metabolic disorders in which there are high blood sugar levels over a prolonged period. Diabetes is due to either the inability of the pancreas to produce insulin (i.e., Type 1) or the improper response of cells to the insulin produced (i.e., Type 2) [1, 2]. Insulin is a protein hormone secreted by β-cells of the pancreas to lower blood glucose levels by facilitating the cellular uptake of circulating glucose into tissues in the body and converting excess glucose, i.e., one beyond the maximum glycogen storage, into fat. The function of insulin also includes regulating carbohydrate, lipid and protein metabolism, and promoting cell proliferation and growth [3].

Globally, by estimation, 463 million adults were living with diabetes in 2019, compared to 108 million adults in 1980 [4]. The chronic effects of diabetes can cause serious complications, including eye disease, neuropathy, cardiovascular disease, gastrointestinal disorders, kidney disease, impaired sexual function, bone and rheumatic disorders, endocrine diseases, central nervous system problems, and psychological and psychiatric conditions [5].

Diabetes is generally divided into two major types: insulin dependent diabetes mellitus (IDDM), known as Type 1 diabetes, and non-insulin dependent diabetes mellitus (NIDDM), known as Type 2 diabetes. The characteristic of Type 1 diabetes is the inability of producing insulin resulting from the autoimmune destruction of pancreatic β-cells, while Type 2 diabetes is caused by a combination of insulin resistance (i.e., the attenuated biological response to insulin) and the insufficient insulin secretion to overcome the resistance [6, 7]. For Type 1 and advanced Type 2 diabetic patients, the current treatment usually requires regular monitoring of blood

glucose (BG) levels (e.g., by finger-prick blood tests) and subsequently multi-injection of different types of exogenous insulin (ultra-short acting, short acting, lente, semilente, and ultralente insulin with different onsets and duration of action) throughout the day [8].

Unfortunately, the aforementioned traditional insulin injection therapy is imprecise in terms of the control of BG levels, and it may result in hypoglycemia if the insulin dosage is too high [9, 10]. Also, hypoglycemia is an acute complication of diabetes and may lead to impairment of the counter-regulatory system, loss of consciousness, seizures and even death [11]. Besides, the multi-dose injection of insulin per day is painful and depends largely on the compliance of the procedure of insulin injection by patients [12]. For the convenience of later discussions, the traditional approach to insulin delivery that focuses on patient's self-administration at different times of the day is called off-line closed-loop insulin delivery. An alternative approach to insulin delivery is to build an artificial insulin-secreting-cell on-line closed-loop insulin delivery system, which mimics the function of the pancreas. This alternative approach has been attracting a great deal of attention in the field of diabetes treatment.

1.1.2 Closed-loop insulin delivery

Broadly speaking, the on-line closed-loop insulin delivery, also known as artificial pancreas, can be defined as a system that is able to control insulin release continuously and automatically as a direct response to blood glucose levels [1]. In general, the on-line closed-loop insulin delivery system can be divided into three categories: electromechanically controlled system, bio-controlled system, and chemically controlled system.

The electromechanically controlled closed-loop insulin delivery system, also known as traditional artificial pancreas in a narrow sense, is a system that combines a continuous glucose sensor, a computerized control algorithm, and an insulin infusion pump to achieve closed-loop insulin delivery (see Fig. 1.1) [13]. The main problem with this system is delays in insulin delivery (see Fig. 1.1), including insulin absorption delay, insulin action delay as well as glucose

sensing delay. The insulin absorption delay is due to the subcutaneous administration of insulin. The insulin action delay is a function of insulin in the plasma reaching cells to take action. Measuring glucose levels in the interstitial fluid causes the glucose sensing delay due to the interstitium-plasma delay of glucose concentration. In addition, there's also the delay of electronical signal processing for the electromechanically controlled insulin delivery system [9, 12].

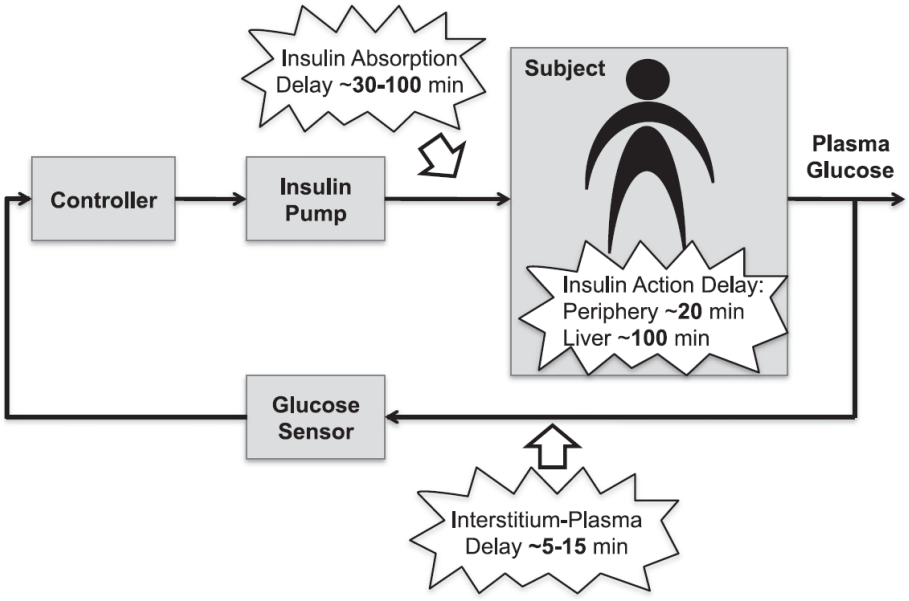

Fig. 1.1. Diagram of the electrochemically controlled closed-loop insulin delivery system. Reprinted with kind permission from [13].

The bio-controlled closed-loop insulin delivery system, also known as a bio-artificial pancreas or islet transplantation, involves the encapsulation of isolated islet cells in biocompatible materials to avoid potential damage from mechanical stress and the host immune system, while allowing the diffusion of nutrients, oxygen and waste and enabling glucose-responsive release of insulin [14, 15]. The main problem with this system is effectiveness and safety, and this problem hinders this system from clinical applications.

The chemically controlled closed-loop insulin delivery system is to integrate a glucose sensing element and a glucose-triggered insulin release system into a single system using glucose-responsive materials (see Fig. 1.2), and the sensor and insulin delivery portal are highly coupled

[1]. The glucose-responsive materials, usually hydrogels, modify their physical and/or chemical properties to release insulin in response to a variation of glucose concentration. In this system, the three distinct systems in Fig. 1.1 above, namely the controller, insulin pump, and glucose sensor, become integrated and signal communication among them is accomplished physically or mechanically rather than electronically or biologically. In fact, the chemically controlled closed-loop insulin delivery system also has the benefit of the bio-controlled closed loop insulin delivery system, i.e., protection of the system from a host system by encapsulating islet cells [16]. This thesis concerns the chemically controlled closed-loop insulin delivery system.

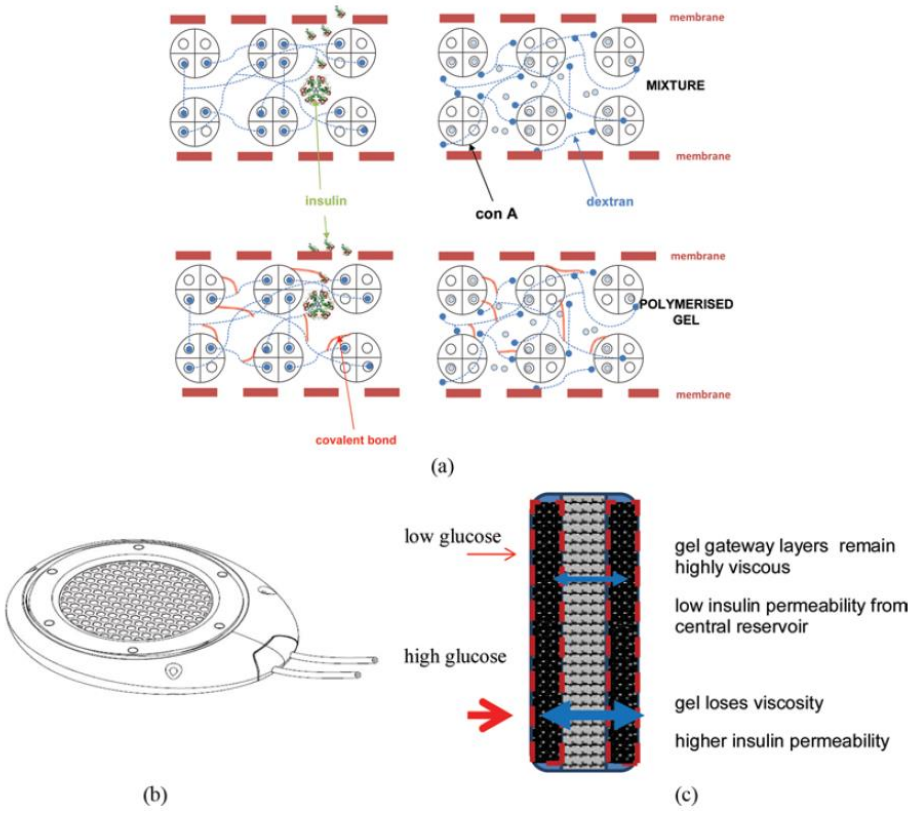

Fig. 1.2. A chemically controlled closed-loop insulin delivery system developed by Taylor's group: (a) mechanism scheme of glucose-responsive materials: the glucose molecules can displace dextran terminals to induce gel phase change; (b) implantable insulin delivery device; (c) overview of the glucose-responsive action: the gel keeps highly viscous at low glucose level, while the gel changes quickly into liquid when glucose has permeated it. Reprinted with kind permission from [25].

There are three categories of the chemically controlled closed-loop insulin delivery system,

namely (i) glucose oxidase [17], (ii) concanavalin A (Con A)-sugar affinity [18] and (iii) phenylboronic acid [19]. Among them, the Con A-sugar affinity based system (Con A-based system for short) has the strongest specificity to glucose [20, 21] as well as good biocompatibility [22, 23]. It is worth noting that free native Con A shows non-cytotoxicity at a concentration of up to 20 μg/mL[22, 23] and in the case of insulin delivery, the required concentration of Con A is usually less than 10 μg/mL [23]. This means that Con A-based system is safe. The first *in vivo* testing in a live diabetic domestic pig has been undertaken by Taylor's group using an implantable artificial pancreas which is made from crosslinkable dextran-Con A complex [24]. This thesis was focused on the Con A-based system.

1.1.3 Con A-sugar based glucose-responsiveness

In the past decade, the glucose-responsive behavior of Con A-sugar based hydrogels, microgels, films and nanoparticles has been investigated in the context of drug delivery and biosensors [26-29]. The current understanding of the principle or mechanism of the Con A-based system can be outlined, illustrated in Fig. 1.3. (1) A Con A system is composed of Con A and its receptor—polysaccharide or glyco-polymer molecules. (2) A Con-A can bind four glucose residues with the polysaccharide/glyco-polymer, but this binding can be dissociated (see Fig. 1.3). (3) This dissociation is governed by the competitive movements of free glucose and glucose-residues against the polysaccharide and/or glyco-polymer molecule, i.e., the free glucose moving to the Con A receptor to dissociate the glucose-residue from the Con A-receptor binding while the dissociated glucose residue moving in an opposite direction of the free glucose [30].

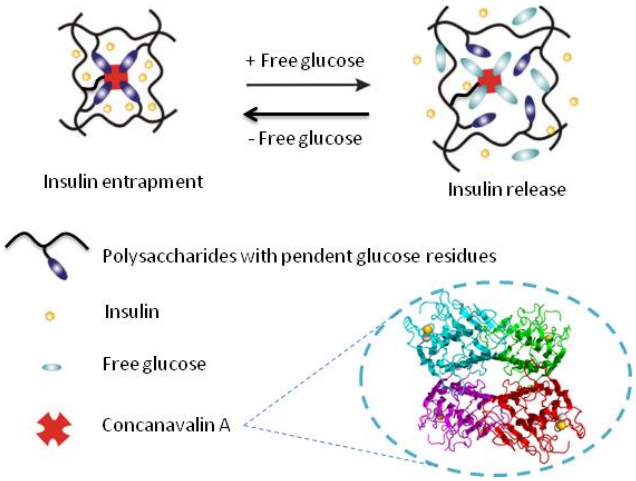

Fig. 1.3. The cross-linked hydrogel network based on Con A-sugar specific affinity and the mechanism of reversible structural changes for glucose-responsiveness.

It is worth mentioning that the polymer in the Con A-based system can be glycogen, dextran and its derivatives, and other glucose-containing synthetic polymers [25, 31, 32]. The controversy in the literature regarding the mechanism of the Con A-based system lies in the (3) in the aformentioned script. There is a report [33] that the binding affinity of Con A/glucose in free solution is much lower than that of Con A/glucose-residue on polysaccharide, measured by isothermal titration calorimetry (ITC), which suggests that free glucose may not likely seize the sugar-binding sites from Con A-polysaccharide complex or polymer. Further, Li and co-workers [26] demonstrated that the low affinity of glucose with Con A was not able to trigger the dissociation of Con A-glycogen binding at physiological pH value (pH 7.4).

1.1.4 Clinical-level issues for the Con A-based system

Besides the controversy in understanding how the Con A-based system works, there are some clinical-level issues this thesis was interested in, and they are: **Issue (1) - Personalized treatment**. In the clinic, it has been found that individuals are significantly different in the areas such as manifestations of disease, symptoms, co-morbidities, genetic predisposition, and variance in molecular sensitivity to drugs, in particular insulin resistance for diabetes patients. This calls for a modulated or tailored insulin delivery approach [34, 35]. For instance, a

sufficient insulin supply determined based on the degree of insulin resistance of individual patients may overcome the reduced efficiency of insulin and maintain normal glucose tolerance [36]. **Issue (2) - Sustainable insulin supply**. The administration route of CCCID systems may be subcutaneous or intraperitoneal injection or minimally invasive implantation. Therefore, they are expected to continue the glucose sensing and insulin release for a long term, which can dramatically release the burden of patients in physical pain and compliance.

1.2 Objectives and Scope

Based on the discussion above, four specific research objectives were defined for this thesis and they are presented in the following:

- ***Objective 1****: Investigate the glucose-responsive principle of Con A-sugar affinity-based hydrogel networks and attempt to resolve the aforementioned controversy.*
- ***Objective 2****: Examine the feasibility of modulating the insulin release behavior by varying the composition of the Con A-based system.*
- ***Objective 3****: Develop a methodology for design of the Con A-based system to tailor to individual patients in order to prolong the insulin supply period.*
- ***Objective 4****: Develop a mathematical model for improving the design of Con A-based system.*

In the research for Objective 1, only the characterization method of Isothermal Titration Calorimetry (ITC) was used, because the molecules tested in ITC are untethered, which is similar as the formation of Con A-sugar network. In the research for Objective 4, the purpose is to examine the feasibility of the model, and therefore, validity of the model was mainly concerned.

1.3 Organization of the thesis

This thesis is organized in a manuscript-based style. At the beginning of each chapter, a brief introduction is included to describe the relation between the manuscript and the context of the

thesis. The status of each manuscript is also given at the beginning of each chapter. To produce a coherent and defendable thesis, all published or prepared manuscripts have been formatted on the consistently.

The remaining part of the thesis is organized as follows: Chapter 2 is a comprehensive review of the literature related to the proposed objectives in Chapter 1. Chapter 3 proposes a supply-demand feedback control system for systematic generalizing a drug delivery system along with its process. Chapter 4 investigates the glucose-responsive principle of Con A-sugar affinity-based hydrogel networks with the isothermal titration calorimetry method and ligand competition theory. This chapter will also study the feasibility of modulating the insulin release behavior by design of the composition of the Con A-based system. Chapter 5 proposes an integrated system to prolong insulin supply duration for the Con A-based system. Chapter 6 constructs a mathematical model for the glucose-responsive process of the Con A-based system with the help of the swelling and variable diffusion coefficient theory. Conclusions and several future studies are given in Chapter 7. Appendix A shows details of the characterization method and results of GPC-LLS, GPC and NMR tests. Appendix B exhibits the insulin calibration curve and SEM images of insulin-loaded microspheres obtained with different shearing time at high speed. The list of published manuscripts is given in Appendix C at the end of the thesis, and the copyright permissions of all published figures and manuscripts used in this thesis are in Appendix D.

1.4 Contributions of the primary investigator

It is noted that all published or prepared manuscripts are co-authored. However, it is mutual understanding of all authors that Ruixue Yin, as the first author, is the primary investigator. The contributions of other authors are limited to the advisory and editorial capacity.

REFERENCES

[1] Di J, Yu J, Ye Y, Ranson D, Jindal A, Gu Z. Engineering synthetic insulin-secreting cells using hyaluronic acid microgels integrated with glucose-responsive nanoparticles. Cellular and Molecular Bioengineering. 2015;8:445-54.

[2] Gordijo CR, Koulajian K, Shuhendler AJ, Bonifacio LD, Huang HY, Chiang S, et al. Nanotechnology‐enabled closed loop insulin delivery device: In vitro and in vivo evaluation of glucose‐regulated insulin release for diabetes control. Advanced Functional Materials. 2011;21:73-82.

[3] Wilcox G. Insulin and insulin resistance. Clinical biochemist reviews. 2005;26:19-39.

[4] Global diabetes data report 2010-2045, IDF Diabetes Atlas 9th edition, 2019.

[5] G. PJCaW. Textbook of Diabetes (3 ed.). Malden, MA: Blackwell Science Ltd. 1997;1.

[6] U. SD. in Human Physiology: An Integrated Approach ,
4th edition. Pearson Education , San Francisco, USA. 2007;Ch. 6.

[7] Pickup JC, Zhi ZL, Khan F, Saxl T, Birch DJ. Nanomedicine and its potential in diabetes research and practice. Diabetes/metabolism Research and Reviews. 2008;24:604-10.

[8] Owens DR, Zinman B, Bolli GB. Insulins today and beyond. The lancet. 2001;358:739-46.

[9] Ravaine V, Ancla C, Catargi B. Chemically controlled closed-loop insulin delivery. Journal of Controlled Release. 2008;132:2-11.

[10] Bratlie KM, York RL, Invernale MA, Langer R, Anderson DG. Materials for diabetes therapeutics. Advanced Healthcare Materials. 2012;1:267-84.

[11] Shafiee G, Mohajeri-Tehrani M, Pajouhi M, Larijani B. The importance of hypoglycemia in diabetic patients. Journal of Diabetes & Metabolic Disorders. 2012;11:17.

[12] Veiseh O, Tang BC, Whitehead KA, Anderson DG, Langer R. Managing diabetes with nanomedicine: challenges and opportunities. Nature Reviews Drug Discovery. 2015;14:45-57.

[13] Cobelli C, Renard E, Kovatchev B. Artificial pancreas: past, present, future. Diabetes. 2011;60:2672-82.

[14] Baker K. Comparison of bioartificial and artificial pancreatic transplantation as promising therapies for Type I Diabetes Mellitus. Bioscience Horizons: The International Journal of

Student Research. 2016;9:hzw002.

[15] Sakata N, Sumi S, Yoshimatsu G, Goto M, Egawa S, Unno M. Encapsulated islets transplantation: past, present and future. World Journal of Gastrointestinal Pathophysiology. 2012;3:19-26.

[16] Uchiyama T, Watanabe J, Ishihara K. Implantable polymeric artificial pancreas. Journal of Biomaterials Science, Polymer Edition. 2004;15:1237-62.

[17] Qi W, Yan X, Duan L, Cui Y, Yang Y, Li J. Glucose-sensitive microcapsules from glutaraldehyde cross-linked hemoglobin and glucose oxidase. Biomacromolecules. 2009;10:1212-6.

[18] Kim JJ, Park K. Modulated insulin delivery from glucose-sensitive hydrogel dosage forms. Journal of Controlled Release. 2001;77:39-47.

[19] Jin X, Zhang X, Wu Z, Teng D, Zhang X, Wang Y, et al. Amphiphilic random glycopolymer based on phenylboronic acid: synthesis, characterization, and potential as glucose-sensitive matrix. Biomacromolecules. 2009;10:1337-45.

[20] Edelman GM, Cunningham BA, Reeke GN, Becker JW, Waxdal MJ, Wang JL. The covalent and three-dimensional structure of concanavalin A. Proceedings of the National Academy of Sciences. 1972;69:2580-4.

[21] Yin R, Wang K, Du S, Chen L, Nie J, Zhang W. Design of genipin-crosslinked microgels from concanavalin A and glucosyloxyethyl acrylated chitosan for glucose-responsive insulin delivery. Carbohydrate Polymers. 2014;103:369-76.

[22] Vetri V, Carrotta R, Picone P, Di Carlo M, Militello V. Concanavalin A aggregation and toxicity on cell cultures. Biochimica et Biophysica Acta (BBA)-Proteins and Proteomics. 2010;1804:173-83.

[23] Ye T, Yan S, Hu Y, Ding L, Wu W. Synthesis and volume phase transition of concanavalin A-based glucose-responsive nanogels. Polymer Chemistry. 2014;5:186-94.

[24] Taylor M, Gregory R, Tomlins P, Jacob D, Hubble J, Sahota T. Closed-loop glycaemic control using an implantable artificial pancreas in diabetic domestic pig (Sus scrofa domesticus). International Journal of Pharmaceutics. 2016;500:371-8.

[25] Sahota T, Tomlins P, Taylor MJ. Long-Term Stability of Glucose Responsive Dextran Methacrylate-Concanavalin A Methacrylamide Gels as Part of an Implantable Artificial

Pancreas. International Journal of Polymeric Materials and Polymeric Biomaterials. 2015;64:946-54.

[26] Li J, Qu X, Payne GF, Zhang C, Zhang Y, Li J, et al. Biospecific Self‐Assembly of a Nanoparticle Coating for Targeted and Stimuli‐Responsive Drug Delivery. Advanced Functional Materials. 2015;25:1404-17.

[27] Tanna S, Sahota TS, Sawicka K, Taylor MJ. The effect of degree of acrylic derivatisation on dextran and concanavalin A glucose-responsive materials for closed-loop insulin delivery. Biomaterials. 2006;27:4498-507.

[28] Yin R, Wang K, Han J, Nie J. Photo-crosslinked glucose-sensitive hydrogels based on methacrylate modified dextran–concanavalin A and PEG dimethacrylate. Carbohydrate Polymers. 2010;82:412-8.

[29] Sato K, Imoto Y, Sugama J, Seki S, Inoue H, Odagiri T, et al. Sugar-induced disintegration of layer-by-layer assemblies composed of concanavalin A and glycogen. Langmuir. 2005;21:797-9.

[30] Tanna S, Taylor MJ, Sahota TS, Sawicka K. Glucose-responsive UV polymerised dextran–concanavalin A acrylic derivatised mixtures for closed-loop insulin delivery. Biomaterials. 2006;27:1586-97.

[31] Lu C, Chen X, Xie Z, Lu T, Wang X, Ma J, et al. Biodegradable amphiphilic triblock copolymer bearing pendant glucose residues: preparation and specific interaction with concanavalin A molecules. Biomacromolecules. 2006;7:1806-10.

[32] Zhu Y, Tong W, Gao C. Molecular-engineered polymeric microcapsules assembled from Concanavalin A and glycogen with specific responses to carbohydrates. Soft Matter. 2011;7:5805-15.

[33] Benzeval I, Bowyer A, Hubble J. The influence of degree-of-branching and molecular mass on the interaction between dextran and Concanavalin A in hydrogel preparations intended for insulin release. European Journal of Pharmaceutics and Biopharmaceutics. 2012;80:143-8.

[34] Cnop M, Landchild MJ, Vidal J, Havel PJ, Knowles NG, Carr DR, et al. The concurrent accumulation of intra-abdominal and subcutaneous fat explains the association between insulin resistance and plasma leptin concentrations. Diabetes. 2002;51:1005-15.

[35] DeFronzo R, Simonson D, Ferrannini E. Hepatic and peripheral insulin resistance: a common feature of type 2 (non-insulin-dependent) and type 1 (insulin-dependent) diabetes mellitus. Diabetologia. 1982;23:313-9.
[36] Kahn SE, Hull RL, Utzschneider KM. Mechanisms linking obesity to insulin resistance and type 2 diabetes. Nature. 2006;444:840-6.

CHAPTER 2 LITERATURE REVIEW

2.1 Introduction

This chapter presents a review of the literature in relation to the proposed objectives in Chapter 1. Section 2.2 provides the basic knowledge of the hydrogel network and the structure-function relationship for hydrogel design. Section 2.3 discusses three characterization methods for the binding behaviour among molecules in the Con A-based system. Section 2.4 presents the literature on mathematical modeling of hydrogel-based drug delivery systems including the Con A-based system.

2.2 Hydrogel network and structure-function relationship of the network

Hydrogels are water-swollen polymeric networks, consisting of crosslinked molecules (hydrophilic polymers) that can swell but do not dissolve in water [1, 2]. The ability to swell under biological conditions makes them an ideal class of materials for biomedical applications, such as drug delivery and tissue engineering [3]. The structure-function relationship has been discussed considerably in hydrogel design and manufacturing literature [4] but not in a systematic way. In the following, a general knowledge architecture of systems called FCBPSS (F: function, C: context, B: behavior, P: principle, SS: state and structure) [5] is employed to discuss hydrogel systems for a more comprehensive understanding.

2.2.1 Hydrogel structure

Hydrogels possess a 3D network structure, crosslinked physically or chemically or both [1, 2]. Stimuli-responsive hydrogels, also known as "smart" or "intelligent" hydrogels, present the unique property of undergoing structural changes in response to environmental stimulus. These stimuli-responsive hydrogels exhibit both sensor and effector functions. They can sense a

stimulus as a signal and transduce it through structural changes, while the structural change itself can play the role of effector [6]. The stimulus responsible for the structural change of hydrogels can be physical (temperature, light, electric and magnetic field), chemical (pH, ionic strength, chemical and biological agents), or both [7]. The glucose-responsive hydrogels/microgels developed in our previous studies [8-10] are a kind of stimuli-responsive hydrogels. In general, the structure of the hydrogel network-based stimuli-responsive system is shown in Fig. 2.1. The macromolecules (polymers) form a crosslinked molecular network. The linkage can be both covalent bonding and physical bonding. The network absorbs water to an equilibrium swelling state, enabling the transport of macromolecular drugs, nutrients, and cellular wastes. When a hydrogel network receives a stimulus, the physical bonding linkages or even some covalent bonding linkages may be (reversibly) disrupted, resulting in the change of swelling state.

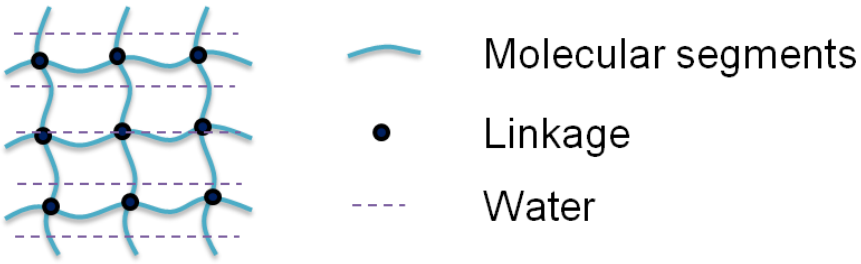

Fig. 2.1. Schematic structure of a crosslinked hydrogel network.

2.2.2 Structure-function relationship in hydrogel design

The structure-function relationship of hydrogels has been investigated both experimentally and theoretically. In general, the network has two statuses: neutral status and electronically charged status. For neutral hydrogel networks, the equilibrium volume is a balance between the osmotic pressure and the elasticity of the polymer network. When a hydrogel network contacts the aqueous environment, it tends to absorb the aqueous solvent and swell driven by the osmotic pressure, thus expanding the distance between the polymer bone and the aqueous solvent. Meanwhile, the polymer chains between any two cross-linkages generate the elastic restoring

force resulting from the expansion. The elastic restoring force is controlled by the number of cross-linkages: the higher the cross-linker density, the lower the swelling ratio. With the increase of swelling, the osmotic pressure and elastic restoring force reach a balance, leading to the equilibrium swelling state of the hydrogel. For electronically charged hydrogel networks, the swelling equilibrium volume is mainly governed by the electrostatic repulsion between the charged monomer units and the osmotic pressure exerted by the mobile counter-ion concentration inside the hydrogel [11, 12]. The swelling ratio depends on the charge density of the hydrogel as well as the ionic strength of the surrounding environment.

Different structures of a hydrogel network are responsible for different functions of the network, including the degradation of the network, diffusion of bioactive molecules and migration of cells through the network [13]. However, for years, a "trial-and-error" approach has been applied to validate hydrogel structures, with *ex post* modifications being made on an existing design based on the *in vitro* or *in vivo* experimental results. This empirical approach is too time-consuming and costly [14].

Recently, *in silico* experiments have been applied to assist the design process for hydrogel networks. With *in silico* experiments, mathematical models may be developed to help identify the key parameters and mechanisms that govern the transport of substances inside hydrogel networks [15]. The characterization of water-sorption capabilities (i.e., swelling) is the first step towards understanding the structure of a hydrogel network and how the network plays the function of substance transport. Four important parameters have been defined to characterize swelling, which are (1) the swelling ratio Q (including the mass swelling ratio Q_m and the volume swelling ratio Q_v); (2) the polymer volume fraction in the swollen state $\upsilon_{2,s}$; (3) the number average molecular weights between cross-links M_c; and (4) the network mesh size ξ. Relationships among these parameters have also been studied, e.g., $\upsilon_{2,s} = Q_v^{-1}$ [1, 15]. Along with the swelling equilibrium principle, the other governing laws involved for the substance transport in hydrogel networks are Fick's second law for diffusion, mass transfer and mass conservation [16, 17].

To be comprehensive, the FCBPSS view of the structure-function relationship, swelling parameters and equations, and the governing laws for the substance transport of hydrogels are presented as follows:

- "Structure": the crosslinked network shown in Figure 1 and its components.
- "State": the variables (parameters) related to swelling and substance transport of hydrogels.
- "Behavior": the relationship between state variables (swelling parameters).
- "Principle": Governing laws for swelling and substance transport, including swelling equilibrium, diffusion, mass transfer and mass conservation.
- "Function": Transport of substances for different biomedical applications, such as drug delivery, tissue engineering.
- "Context": Human body.

2.3 Con A-sugar binding interaction characterization methods

There are several methods for testing the affinity of Con A with sugar. From a point of view of association and dissociation, isothermal titration calorimetry (ITC) is for the association process, and atomic force microscopy (AFM) is for the dissociation process, while surface plasmon resonance (SPR) can measure both association and dissociation kinetics. Further, each method is suitable in a particular context. For instance, ITC can only be used for free solution measurement [18], i.e., both Con A and its sugar ligand can freely move in the solution; whereas, SPR requires the ligand to be immobilized on the sensor surface [19], i.e., only Con A can move freely during the test. Moreover, for AFM test [20], Con A may need to attach to the AFM tips, while the sugar ligand can be immobilized on a hard surface or in a hydrogel phase that is most similar to real application in insulin delivery. In the literature, Li [21] and Benzeval [22] have not paid attention to the context of using ITC as a method to measure Con A-sugar affinity. Con A-sugar affinity measured in a free solution by ITC may not represent the affinity in the case of glucose-triggered dissociation process in their applications of insulin delivery systems and biosensors. In this thesis, different measurement methods were taken in their particular contexts and combined to explore the glucose-responsive mechanism of Con A-sugar affinity-based

hydrogel networks.

2.3.1 Isothermal titration calorimetry method

Isothermal Titration Calorimetry (ITC) is the application of calorimetric technique in the measurement of the energetics of biomedical reactions or molecular interactions, including ligand-binding phenomena, enzyme-substrate interactions, and interactions among components of multi-molecular complexes. The heat of the biomedical reactions is directly observed in the form of enthalpy [18]. The results are calculated based on a group of molecules (per mol of molecules, 6.02×10^{23}).

The ITC technique can provide data on the strength of the affinity interaction, while it cannot provide information on the kinetics. It requires neither the sugar ligand nor the lectin (Concanavalin A in this case) to be immobilized, i.e., the sugar ligand and lectin can be in free-moving phase in the testing solution [23, 24]. Therefore, the resulting data can better represent how the two components behave in the hydrogel formation process. But the information generated by ITC does not provide information regarding the affinity in the hydrogel dissociation process triggered by glucose, where the two components are immobilized rather than in a free solution.

Mandal's group investigated the thermodynamics of binding of Con A with a series of linear and branched chain oligosaccharides to determine the primary binding epitope of different carbohydrate chains for Con A [25]. Benzeval and co-workers investigated the influence of the degree-of-branching and molecular mass on the interaction between dextran and Con A for the purpose of the hydrogel preparation intended for insulin delivery, and proposed that the knowledge of the differing strengths of the affinity bond between the lectin and the various different dextran sizes available would enable the composition of the hydrogel to be tailored to the desired response rate [22]. Li and co-workers [21] detected a lower affinity of glucose with Con A compared with glycogen-Con A interaction, and demonstrated that the low affinity of glucose with Con A was not able to trigger the dissociation of Con A-glycogen binding in

physiological pH value (pH 7.4). However, they may neglect that the context of the dissociation process is different from the ITC test, i.e., the Con A molecules are partially immobilized during the dissociation process. *Overall, the use of the ITC technique in understanding the mechanism of Con A-sugar affinity-based glucose-responsive systems must be combined with other methods by awareness of the importance of context.*

2.3.2 Surface plasmon resonance (SPR) method

The basic physical principle of SPR is using an optical method to measure the refractive index near (within 300 nm) a sensor surface. To perform the test, one molecule (usually the ligand, e.g., the sugar ligand for Con A) is immobilized onto the sensor surface. Meanwhile, the analyte (i.e., the binding partner, e.g., Con A) is injected in aqueous solution (e.g., buffer) under continuous flow. An increase in the refraction can be observed as the analyte binds to the ligand which leads to the accumulation of protein on the sensor surface [19]. Similar to the ITC method, the results are also calculated based on a group of molecules (per mol of molecules, $6.02*10^{23}$).

The change in refractive index is measured in real time; therefore, the SPR technique is able to provide information on kinetics [26]. It can detect both association (the period during which the analyte is being injected) and dissociation (the period after the end of the injection) process. It is noted that it is the equilibrium association or dissociation constant obtained by SPR, as both association and dissociation take place in association or dissociation process [27].

The SPR technique has been applied to understand the interaction of Con A with a series of sugar ligands in recent years. Yu et al. quantitatively analyzed the binding kinetics and equilibrium constant of Con A with a bio-mimicking glycocalyx layer on the surface, indicating that the mode of binding changed from multivalent to monovalent by varying the spatial distribution of carbohydrate ligands within the surface-grafted polymer layer [27]. The SPR data in this literature reveals that *for the binding of Con A with a low concentration of immobilized polysaccharide, the association constant may be equal to the binding of Con A*

with the monosaccharide in free solution. However, for the binding of Con A with a high concentration of immobilized polysaccharide, the association constant is much higher than the binding of Con A with monosaccharide in free solution. This is a strong evidence that drives us to pay attention to the importance of context for the affinity test. Benzeval's work [28] provided the very different data from ITC and SPR on the affinity test of carboxymethyl-dextran with Con A. He ascribed the differences to the multivalent nature of the components and stated SPR was not effective in measuring the dextran-Con A binding. However, we believe that the difference in the affinity data from ITC and SPR should be considered as the significant effect of the context, and we shall make use of such difference in the investigation of Con A principle as well as in the design of Con A-sugar based hydrogel networks.

Other studies using SPR to test the affinity of Con A with different carbohydrates are described as follows. Munoz and co-workers provided a detailed evaluation of multivalent carbohydrate-Con A interactions by introducing monodispersed glycodendrimers as multivalent analytes and immobilized Con A on the sensor surface of SPR equipment. They believed that the obtained information on the glycoconjugate binding efficiency and real time structural data will contribute to the optimization of glycoconjugate architectures for particular purposes [29]. Furthermore, Sandoval-Altamirano et al. performed SPR in the design and synthesis of mannose derivatives with different chain lengths and chain numbers for the purpose of modifying the affinity of mannosyl glycol-vesicle with target lectins [30]. These studies were relevant to the study in this thesis.

2.3.3 Atomic force microscopy method

The basic principle for AFM is the force measurement between the probe tip and the sample surface. Specifically, the probe tip is attached to a cantilever-type spring, and the cantilever (also called lever) will deflect in response to the force between the tip and sample. Images of the sample surface are taken by scanning the sample relative to the probe tip and digitizing the deflection of the lever or the z-movement of the piezo as a function of the lateral position x, y

[20]. The AFM technique is applicable to insulating, semi-conductive or conductive samples [31]. AFM technique has a high force sensitivity (10^{-11} to 10^{-6} N), a high dynamic range (0.001 – 5000 nN), a high positional accuracy (0.01 nm) and is available under physiological conditions. Therefore, AFM has been successfully employed to study the structure of single bio-molecules or bio-membranes, and molecular forces at single-molecule level, such as intra-molecular unfolding forces of individual proteins, intermolecular forces between ligands and receptors or lectins [32].

For the measurement of intermolecular protein-ligand interactions (including Con A-sugar ligand affinity), no matter the ligand or the protein, one molecule should be attached to the probe tip and the other attached to the substrate surface [33]. During the experiment, the tip needs to be brought into contact with the sample surface so as to form a protein-ligand complex. Then, the force required for dissociation, also defined as unbinding force or rupture force, can be recorded by pulling on the complex until the protein-ligand interaction bond breaks [32]. Ratto et al. [33] reported a study to measure the rupture force for a single Con A-mannose bond using AFM. The double-tethered method not only improves the reliability of the measurement but also enables to distinguish the nonspecific binding between the tip and sample from the specific binding of Con A and mannose. Yu et al. measured the unbinding force of Con A with the immobilized mannose surface layer by AFM, indicating that the binding mode between Con A and mannose layer changes from multiple to single with variation of mannose residue concentration. This result was consistent with their results obtained from SPR [27]. Beside the unbinding force, the dissociation rate (constant), binding width of the binding pocket, the energy landscape and the dynamics of the binding can also be obtained [34]. Gour and Verma applied AFM to explore the interaction dynamics of newly synthesized mannose derivates with Con A and proposed molecular models for the interaction between Con A and mannose derivates using AFM [35].

Overall, by using AFM to measure the interaction between Con A and sugar ligand, the Con A and ligand are both immobilized, and the result is measure at a single-molecule level. To understand the glucose-responsive mechanism of Con A-sugar affinity-based hydrogel

networks, it may provide more accurate information on the dissociation process of Con A-sugar ligand as both Con A and the polysaccharide can be viewed as immobilized in the hydrogel network.

2.3.4 Conclusions

For the understanding of the glucose-responsive principle of Con A-sugar affinity-based hydrogel networks, we may divide the whole process into three stages and use a proper method to detect the association/dissociation constant by considering the particular context.

1) Hydrogel network formation from free solution: Using ITC to test the association constant of the binding of polysaccharide and glucose with Con A.
2) Glucose-triggered dissociation of the hydrogel network - both the association of Con A/glucose bonds and the dissociation of Con A/polysaccharide bonds occur in this stage: Using AFM to detect the dissociation of immobilized Con A/immobilized polysaccharide bonds and using SPR to detect the association of immobilized Con A/free glucose bonds may help to understand this stage.
3) Hydrogel network reformation - the dissociation of Con A/glucose bonds and association of Con A/polysaccharide bonds: Using SPR to measure the dissociation of immobilized Con A/free glucose bonds and the association of free Con A/immobilized polysaccharide bonds.

2.4 Modeling of hydrogel-based drug delivery systems

2.4.1. Equilibrium properties

The equilibrium swelling/de-swelling properties of the randomly crosslinked hydrogel network is described by the Flory-Erman model based on the elasticity of polymer networks, i.e. [16, 36]

$$\ln(1-\upsilon_{2m})+\upsilon_{2m}+\chi\upsilon_{2m}^{2}=-\frac{\xi}{V_0}V_1\upsilon_{2m}^{1/3}\left(1+\frac{\mu}{\xi}K\upsilon_{2m}^{-2/3}\right) \quad (2\text{-}1)$$

where χ is the solvent-polymer interaction parameter, V_1 is the molar volume of the solvent, V_0 is the reference volume (the volume of polymerizing mixture), υ_{2m} is the volume fraction of polymer at swelling equilibrium, μ is the junction density, and ζ is the cycle rank (i.e., the number of independent circuits in the hydrogel network). Among the above parameters, μ and ζ are related to the density of polymer and the average molecular weight of the crosslink. All the above parameters plus K can be calculated by empirical equations or experiments [16, 37].

2.4.2 Kinetics of swelling for spherical hydrogels

The equation of motion of a hydrogel network was proposed by Tanaka, Hocker and Benedek (THB) [38]. For a hydrogel composed of a crosslinked network and immersed in a solvent, a displacement vector **u** (**r**, *t*) represents the displacement of a point in the network from its final equilibrium location after the hydrogel is completely swollen (For $t = \infty$, $u = 0$). The kinetics of the swelling for a hydrogel can be described by the change of the displacement vector as a function of space and time as shown in equation (2-2):

$$\partial\,\mathbf{u}/\partial\,t = \text{div}\ \tilde{\sigma}/f \quad (2\text{-}2)$$

where f is the friction coefficient between the network and fluid medium, and $\tilde{\sigma}$ is the stress tensor.

For the swelling of a spherical hydrogel, the displacement vector is spherically symmetric and given by

$$\mathbf{u}\,(\mathbf{r}, \mathrm{t}) = u\,(r, t)\,\mathbf{r}/r \quad (2\text{-}3)$$

and the stress in the radial direction is described as

$$\sigma_{rr} = \frac{\left(K'+\frac{4G}{3}\right)du}{dr} + \frac{2\left(K'-\frac{2G}{3}\right)u}{r} \quad . \quad (2\text{-}4)$$

where K' and G are the bulk and shear modulus of the polymer network, respectively.

The magnitude of the displacement follows the equation of motion below [39]:

$$\frac{\partial u}{\partial t} = D\frac{\partial}{\partial r}\left\{\frac{1}{r^2}\left[\frac{\partial}{\partial r}\left(r^2 u\right)\right]\right\} \quad (2\text{-}5)$$

where $D = (K' + \frac{4G}{3})/f$ is called the diffusion coefficient of the hydrogel in a specific solvent.

2.4.3 Transport of substances

Mathematical models for the transport of drug substances from a hydrogel system as a function of time have been developed and categorized into three types: diffusion-controlled (also known as Case I), swelling-controlled (also known as Case II) and chemically controlled. This thesis focused on the modeling of Case I and Case II, as the chemically controlled delivery, in which the molecule release is determined by the reaction occurring between the polymer network and the releasable drug, is not related to the work in this thesis. When the drug diffusion rate is lower than the hydrogel swelling, i.e., drug diffusion is the rate-limiting step, diffusion-controlled drug transport occurs in the hydrogel system. In contrast, the hydrogel system undergoes a swelling-controlled delivery mode when the swelling of hydrogel is lower than the drug diffusion rate.

The diffusion-controlled (Case I) is the most widely used mechanism for describing drug transport in a hydrogel system. For a hydrogel system with uniform drug distribution (known as matrix system, different from a reservoir system where the drug solution is surrounded by a hydrogel membrane), drug diffusion from a highly swollen state can be described using Fick's second law, i.e. [15]:

$$\frac{\mathrm{d}C_\mathrm{A}}{\mathrm{d}t} = D\frac{\mathrm{d}^2C_\mathrm{A}}{\mathrm{d}x^2} \tag{2-6}$$

where C_A is drug concentration and D is the drug diffusion coefficient. In equation (2-6), the drug diffusion coefficient is assumed as a constant. For concentration-dependent drug diffusivity, the following equation is used:

$$\frac{\partial C_\mathrm{A}}{\partial t} = \frac{\partial}{\partial x}\left(D(C_\mathrm{A})\frac{\partial C_\mathrm{A}}{\partial x}\right) \tag{2-7}$$

For a spherical matrix system, the following equation is given [40]:

$$\frac{\partial C}{\partial t} = \frac{D}{r^2}\frac{\partial}{\partial r}\left(r^2\frac{\partial c}{\partial r}\right) \tag{2-8}$$

After the determination of D, equations (2-6)-(2-8) can be solved together with proper initial and boundary conditions, resulting in a so-called drug release kinetics profile. It is noted that drug diffusion coefficients may be a function of drug concentration and drug diffusivity for

hydrogel systems may also depend on the degree of swelling and the crosslinking density of the hydrogel network. In other words, the diffusion coefficient may be sensitive to environmental changes and/or the structural changes of the hydrogel network and may vary during the release period. The drug diffusion coefficient D can be determined empirically or using free volume, hydrodynamic or obstruction theories [41].

An empirical equation developed by Peppas et al., also known as the power law, is a simple method to describe drug transport [42]:

$$\frac{M_t}{M_\infty} = k \cdot t^n \tag{2-9}$$

where M_t is the mass of water gained or lost at time t, M_∞ is the initial mass of water contained in the polymer, k is a structural/geometric constant for the system and n is the release exponent which represents the release mechanism. For $n = 0.5$, the system follows Fickian or diffusion-controlled (Case I) mechanism, while for $n = 1$, the system undergoes swelling-controlled (Case II) mechanism. When $0.5 < n < 1$， the intermediate case (known as anomalous diffusion) occurs [43]. Moreover, the release exponent n values are relative to the geometry of the hydrogel system. For Case I mode, $n = 0.5$ for slab matrix, while $n = 0.45$ for cylinder matrix and 0.43 for spheres [15].

Modeling of the swelling-controlled (Case II) mechanism usually involves moving boundary conditions, where drug molecules are released at the interface of rubbery and glassy phases of swollen hydrogels. The empirical power law, i.e., equation (2-9), for Case I mechanism can also be used in swelling-controlled delivery systems with the modification taking into account both the drug diffusion and polymer relaxation [44]:

$$\frac{M_t}{M_\infty} = k_1 t^m + k_2 t^{2m} \tag{2-10}$$

where k_1, k_2 and m are constants, and the two terms on the right side represent the diffusion and polymer relaxation, respectively.

The actual drug transport in hydrogels may follow a mixed mechanism of Case I and Case II.

Harmon et al. developed a model that is suitable for Case I, Case II, and anomalous drug transport processes [45]. The total flux J is assumed to include two parts: one owing to the diffusion with a concentration gradient and the other due to the stress relaxation of polymer chains with a propagation speed v. For one-dimensional volume variation of hydrogels, the equation is given as follows:

$$J = -D\frac{\partial C}{\partial x} + v(C - C_0) \quad \text{for } 0 \le |x| \le l \tag{2-11}$$

where C and C_0 are concentrations at x and $x = 0$, respectively.

Furthermore, mass conservation can be applied to get drug transport kinetics [16]:

$$\frac{\partial C}{\partial t} + v.\nabla C = \nabla.(D\,\nabla C) \tag{2-12}$$

2.4.4 Conclusions

Overall, combining the above principles related to swelling and drug delivery, including swelling equilibrium equations, swelling kinetics, diffusion laws, power law and mass conservation, we may be able to construct a mathematical model of the Con A-sugar affinity based closed-loop insulin delivery system to predict the drug release kinetics under different glucose concentrations and the relationship between drug release and hydrogel composition. The glucose-responsive process can be viewed as changing the parameter values (such as the volume fraction of polymer at swelling equilibrium $v_{2m,}$ the drug delivery coefficient D) under the environment with different glucose concentrations, thus resulting in different outputs of the model.

REFERENCES

[1] Zhu J, Marchant RE. Design properties of hydrogel tissue-engineering scaffolds. Expert Review of Medical Devices. 2011;8:607-26.

[2] Lutolf MP. Spotlight on hydrogels. Nature Materials. 2009;8:451-3.

[3] Ulijn RV, Bibi N, Jayawarna V, Thornton PD, Todd SJ, Mart RJ, et al. Bioresponsive hydrogels. Materials Today. 2007;10:40-8.

[4] Slaughter BV, Khurshid SS, Fisher OZ, Khademhosseini A, Peppas NA. Hydrogels in regenerative medicine. Advanced Materials. 2009;21:3307-29.

[5] Zhang W, Wang J. Design theory and methodology for enterprise systems. Enterprise Information Systems; 2016.

[6] Ravaine V, Ancla C, Catargi B. Chemically controlled closed-loop insulin delivery. Journal of Controlled Release. 2008;132:2-11.

[7] Yin R, Zhang N, Wang K, Long H, Xing T, Nie J, et al. Material design and photo-regulated hydrolytic degradation behavior of tissue engineering scaffolds fabricated via 3D fiber deposition. Journal of Materials Chemistry B. 2017;5:329-40.

[8] Yin R, Tong Z, Yang D, Nie J. Glucose-responsive insulin delivery microhydrogels from methacrylated dextran/concanavalin A: preparation and in vitro release study. Carbohydrate Polymers. 2012;89:117-23.

[9] Yin R, Bai M, Zhang B, Wang K, Zhang H, Yang S, et al. Understanding drug delivery from a system perspective: Concept and demonstration. Nano/Micro Engineered and Molecular Systems (NEMS), 2017 IEEE 12th International Conference on: IEEE; 2017. p. 698-701.

[10] Yin R, Wang K, Han J, Nie J. Photo-crosslinked glucose-sensitive hydrogels based on methacrylate modified dextran–concanavalin A and PEG dimethacrylate. Carbohydrate Polymers. 2010;82:412-8.

[11] Tanaka T. Phase transitions in gels and a single polymer. Polymer. 1979;20:1404-12.

[12] Tanaka T, Fillmore D, Sun S-T, Nishio I, Swislow G, Shah A. Phase Transitions in Ionic Gels. Physical Review Letters. 1980;45:1636-9.

[13] Hoffman AS. Hydrogels for biomedical applications. Advanced Drug Delivery Reviews. 2012;64:18-23.

[14] Giannitelli SM, Accoto D, Trombetta M, Rainer A. Current trends in the design of scaffolds for computer-aided tissue engineering. Acta Biomaterialia. 2014;10:580-94.

[15] Lin C-C, Metters AT. Hydrogels in controlled release formulations: network design and mathematical modeling. Advanced Drug Delivery Reviews. 2006;58:1379-408.

[16] Ninawe PR, Hatziavramidis D, Parulekar SJ. Delivery of drug macromolecules from thermally responsive gel implants to the posterior eye. Chemical Engineering Science. 2010;65:5170-7.

[17] Abdekhodaie M, Wu X. Modeling of a glucose sensitive composite membrane for closed-loop insulin delivery. Journal of Membrane Science. 2009;335:21-31.

[18] Freire E, Mayorga OL, Straume M. Isothermal titration calorimetry. Analytical Chemistry. 1990;62:950A-9A.

[19] Van Der Merwe PA. Surface plasmon resonance. Protein-ligand Interactions: Hydrodynamics and Calorimetry. 2001;1:137-70.

[20] Meyer E. Atomic force microscopy. Progress in Surface Science. 1992;41:3-49.

[21] Li J, Qu X, Payne GF, Zhang C, Zhang Y, Li J, et al. Biospecific Self‐Assembly of a Nanoparticle Coating for Targeted and Stimuli‐Responsive Drug Delivery. Advanced Functional Materials. 2015;25:1404-17.

[22] Benzeval I, Bowyer A, Hubble J. The influence of degree-of-branching and molecular mass on the interaction between dextran and Concanavalin A in hydrogel preparations intended for insulin release. European Journal of Pharmaceutics and Biopharmaceutics. 2012;80:143-8.

[23] Leavitt S, Freire E. Direct measurement of protein binding energetics by isothermal titration calorimetry. Current Opinion in Structural Biology. 2001;11:560-6.

[24] Pierce MM, Raman C, Nall BT. Isothermal titration calorimetry of protein–protein interactions. Methods. 1999;19:213-21.

[25] Mandal DK, Kishore N, Brewer CF. Thermodynamics of lectin-carbohydrate interactions. Titration microcalorimetry measurements of the binding of N-linked carbohydrates and ovalbumin to concanavalin A. Biochemistry. 1994;33:1149-56.

[26] Myszka DG. Kinetic analysis of macromolecular interactions using surface plasmon resonance biosensors. Current Opinion in Biotechnology. 1997;8:50-7.

[27] Yu K, Creagh AL, Haynes CA, Kizhakkedathu JN. Lectin interactions on surface-grafted glycostructures: Influence of the spatial distribution of carbohydrates on the binding kinetics and rupture forces. Analytical Chemistry. 2013;85:7786-93.

[28] Benzeval I. Development of responsive polymers for drug delivery applications: University of Bath; 2009.

[29] Munoz EM, Correa J, Riguera R, Fernandez-Megia E. Real-time evaluation of binding mechanisms in multivalent interactions: a surface plasmon resonance kinetic approach. Journal

of the American Chemical Society. 2013;135:5966-9.

[30] Sandoval-Altamirano C, Sanchez SA, Ferreyra NF, Gunther G. Understanding the interaction of concanavalin a with mannosyl glycoliposomes: A surface plasmon resonance and fluorescence study. Colloids and Surfaces B: Biointerfaces. 2017;158:539-46.

[31] Binnig G, Quate CF, Gerber C. Atomic force microscope. Physical Review Letters. 1986;56:930.

[32] Lee C-K, Wang Y-M, Huang L-S, Lin S. Atomic force microscopy: determination of unbinding force, off rate and energy barrier for protein–ligand interaction. Micron. 2007;38:446-61.

[33] Ratto TV, Langry KC, Rudd RE, Balhorn RL, Allen MJ, McElfresh MW. Force spectroscopy of the double-tethered concanavalin-A mannose bond. Biophysical Journal. 2004;86:2430-7.

[34] Cai X-E, Yang J. The binding potential between the cholera toxin B-oligomer and its receptor. Biochemistry. 2003;42:4028-34.

[35] Gour N, Verma S. Synthesis and AFM studies of lectin–carbohydrate self-assemblies. Tetrahedron. 2008;64:7331-7.

[36] Flory PJ, Erman B. Theory of elasticity of polymer networks. Macromolecules. 1982;15:800-6.

[37] Queslel J, Mark J. Theoretical equilibrium moduli and swelling extents for randomly cross-linked networks. European Polymer Journal. 1986;22:273-6.

[38] Tanaka T, Hocker LO, Benedek GB. Spectrum of light scattered from a viscoelastic gel. The Journal of Chemical Physics. 1973;59:5151-9.

[39] Tanaka T, Fillmore DJ. Kinetics of swelling of gels. The Journal of Chemical Physics. 1979;70:1214-8.

[40] Zhou Y, Wu X. Modeling and analysis of dispersed-drug release into a finite medium from sphere ensembles with a boundary layer. Journal of Controlled Release. 2003;90:23-36.

[41] Amsden B. Solute diffusion within hydrogels. Mechanisms and models. Macromolecules. 1998;31:8382-95.

[42] Peppas N, Bures P, Leobandung W, Ichikawa H. Hydrogels in pharmaceutical formulations. European Journal of Pharmaceutics and Biopharmaceutics. 2000;50:27-46.

[43] Wu S, Li H, Chen JP. Modeling investigation of volume variation kinetics of fast response hydrogels. Journal of Macromolecular Science, Part C: Polymer Reviews. 2004;44:113-30.
[44] Peppas NA, Sahlin JJ. A simple equation for the description of solute release. III. Coupling of diffusion and relaxation. International Journal of Pharmaceutics. 1989;57:169-72.
[45] Harmon JP, Lee S, Li J. Methanol transport in PMMA: The effect of mechanical deformation. Journal of Polymer Science Part A: Polymer Chemistry. 1987;25:3215-29.

CHAPTER 3 SYSTEM PERSPECTIVE TO DRUG DELIVERY

This chapter is derived from an article published in ***Proceedings of the 12th IEEE International Conference on Nano/Micro Engineered and Molecular Systems****, 698-701, April 9-12, 2017, Los Angeles, USA.*

3.1 Introduction

Drug delivery, the process of administering an active pharmaceutical ingredient to achieve therapeutic effect, has seen dramatic advances in the past few decades [1]. The modern drug delivery technology has been fueled with the advances in material science and engineering for the sustained drug delivery [2], pulsatile drug delivery [3], and targeted (on-site) drug delivery [4]. One of the most important common features with modern drug delivery methods is the varying degree of automatic feedback control of the drug release process. Generally, modern drug delivery methods are expected (1) to improve bioavailability by preventing the premature degradation and enhancing uptake, (2) to maintain the drug concentration within the therapeutic window for a prescribed time by controlling the drug release process, and (3) to reduce adverse side effects by targeting to a specific disease site and target cell. Micro-/nano-scale formulations are a promising direction of drug delivery technology, owing to the benefits including allowance for subcutaneous or intramuscular injection, increased resolution, fast responsiveness, biodegradability and biocompatibility [5, 6].

The ultimate goal of drug delivery is to supply a precise amount of drug to a target diseased cell or tissue with minimal adverse side effects [1]. Therefore, drug delivery is not just about the drug along with its transport but also about the diseased cell or tissue, and the nature of drug delivery is to establish and maintain the balance of the supply (drug) and demand (diseased cell or tissue). In this chapter, for the first time, drug delivery is viewed as drug supply chain system, and is described using the ontology of system design and control [7, 8]. A glucose-responsive insulin delivery microgel system is taken as an example for the system view of drug delivery.

3.2 Drug supply system

3.2.1 From drug delivery to drug supply chain

In the context of this thesis, there are two important steps in drug delivery, namely drug dosage form preparation and drug transport. It is worth mentioning that drug preparation is also called drug formulation, the result of which is the drug dosage form. Drug transport is also called drug release. The principle of drug delivery is the supply-demand balance. Demand of a drug (e.g., insulin) comes from disease (e.g., elevated level of glucose). A disease (high level sugar due to over glucose in body) makes sense because a needed balance in body is lost, e.g., insufficient amount of insulin created in body. The idea of the so-called response-based drug delivery is to deliver drugs in response to demands (Fig. 3.1).

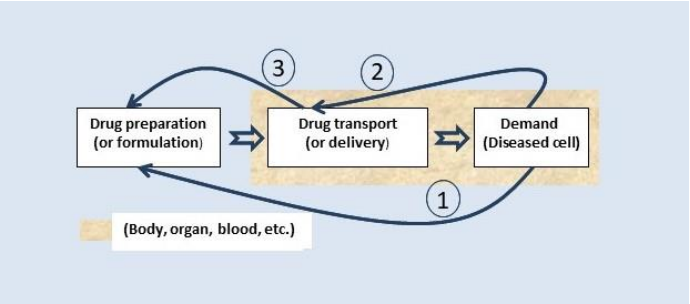

Fig. 3.1. Drug delivery viewed as drug supply chain. Line (1) denotes that the demand (derived from the state of diseased cells) calls for the adjustment at the stage of drug preparation; Line (2) denotes that the demand calls for the adjustment at the stage of drug transport; Line (3) denotes that the range of the adjustment at the stage of drug transport is not enough, which calls for the adjustment at the stage of drug preparation (in essence, a joint adjustment at the two stages (drug preparation and drug transport) is needed in order to track the demand.

3.2.2 The system perspective of drug supply chain

It is well known that any drug has side effects. Side effects imply that there is some unknown cause-effect relationship presented in the supply chain, and the worst situation of side effects is the positive feedback loop in that control input (modification of drug release) does not reduce the gap between the demand and supply but rather increases the gap [9]. To effectively manage side effects and possible positive feedback loops, a drug supply chain should be viewed as a system. Particularly, a drug supply chain system that consists of drugs, drug carriers, diseased cells or tissues, and the body (Fig. 3.1). Both drug and drug-carrier are physically integrated into one entity called drug system in this paper. The drug formulation in the drug literature corresponds to the production or preparation of the drug system; the drug transport or delivery follows the drug formulation. In the following, the drug supply chain system is called the drug supply system for brevity.

Drug supply systems are a dynamic system (i.e., states of the system change). The independent variable which gives a reference of the change of the state may be time and/or event [10]. Drug supply systems with the conventional drug dosage form, such as drug capsules, medicinal granules, tablets, and injection, are built as a time-based dynamic system, because the drug is released at one time only or several fixed times in these systems. However, for many modern drug supply systems, their dynamics are designed to be event-based (because the demand change is event-based). Further, the motives or driving forces for the change in a drug supply system may come from the external and/or internal exciters. The external driving force is for example magnetic field force, while the internal driving force is for example osmotic pressure (i.e., swelling force).

Modern drug supply systems can be viewed as a machine system with a varying degree of intelligence. Fig. 3.2 shows the general architecture of an intelligent drug supply system. It can be seen from Fig. 3.2 that an intelligent drug supply system has (1) the sensor which monitors both the supply and demand, (2) the actuator which drives the process of drug release and transport to diseased cells to the point that therapeutic effects take shape, (3) the plant which

includes drug and its carrier, (4) the reference which is derived from the demand of drugs and further derived from diseased cells and their states, and (5) the controller which first determines the discrepancy between the supply and demand, then determines the adjustment of the drug supply, and finally sends the signal to the actuator and supply system. Further, in Fig. 3.2, a drug source system provides drugs to the plant and an energy source system provides energy that is necessary to drive the (drug) actuation and to drive the drug supply to the plant. It is noted that the controller may also give instruction to the drug source and energy source system and may also give instruction to the organ, tissue or cell to control any other element than the drug conducive to controlling diseases.

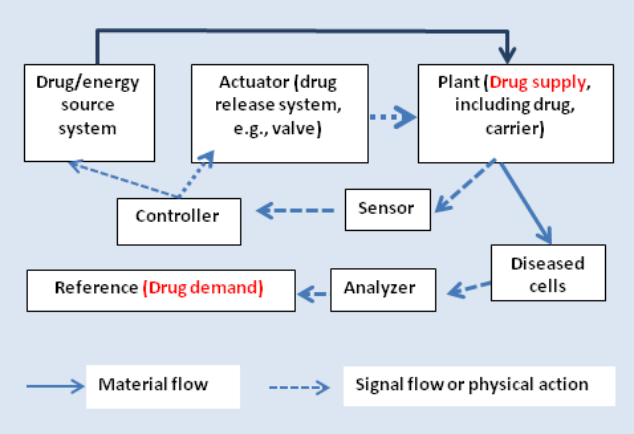

Fig. 3.2. The general architecture of an intelligent drug supply system.

It should be noted that the foregoing architecture serves as the reference architecture only, while real drug supply systems may deviate from this reference architecture both at the logical and physical levels to a certain degree. By logical level it is meant for the function of drug supply systems, for example the absence of a drug source or reservoir system. By physical level it is meant that several functions of a drug supply system may be integrated into one physical system. The benefit with such a reference system is that it allows us to examine the existing drug delivery technology more systematically.

3.2.3 Property, behavior, and performance of a drug supply system

Drug supply systems have the properties such as mechanical property (e.g., stiffness), chemical property (e.g., pH value), electrical property (e.g., conductivity), and so on. These properties are obtained from the structure and operation of a drug system (drug and its carrier), and the properties further determine the behavior and performance of a system. The performance of a drug supply system is generally the balance between the demand and supply, that is, the supply of a right amount of drug at the right time and the right place.

The behavior of a drug supply system refers to the stability, reliability, robustness and resilience of the system [11]. Stability refers to the behavior of a system for a sustainable performance (i.e., keeping the performance satisfactory with respect to the time and/or event progressing). In the case of a drug supply system, whether the drug can keep with or within its carrier during the transport of the drug system is the issue of stability. **Reliability** refers to the behavior of a system to maintain its performance during the entire life expectancy of the system. In the case of a drug supply system, whether the drug dosage form may structurally collapse before it reaches the target is the issue of reliability. **Robustness** refers to the behavior of a system to keep its performance when the system is under disturbance. In the case of a drug supply system, whether the drug keeps with or within the carrier under uncertain disturbances from its environment (e.g., change of pH value of the environment) is the issue of robustness. **Resilience** refers to the behavior of a system for recovery from an unexpected or unanticipated mishap. A resilient drug supply system has the ability of re-balancing the demand and supply after an unexpected loss of the balance through the change of the structure of a drug supply system and/or its operation which further leads to the change of drug substance flow. By noticing the behavior of a drug supply system, more efforts could be devoted to improving the stability, reliability, robustness and/or resilience of the system, thus enhancing both the performance and the safety of drug delivery.

3.3 Glucose-responsive insulin supply system

Glucose-responsive insulin delivery microgels are taken as an example to demonstrate the

benefit of the system perspective of drug delivery. The function of the glucose-responsive insulin supply (G-I for short) system is to automatically release a right amount of insulin into the body in response to the increase of the blood glucose level in the body [12]. The G-I system is viewed as a drug supply system with the insulin being a drug supplied to the body and the glucose being the marker of a demand. The G-I system is also viewed as a feedback system with the insulin being an input to the body and the glucose being a reference substance. It is noted that the reference in a feedback system may not be a signal but a material as well [11]. The G-I system is composed of polysaccharide chains, Con A, and glucose residues (Fig. 1.3 in Chapter 1). A covalent bonding exists among polysaccharides chains, and a physical bonding exists between Con A and glucose residues. The G-I system is a specialized network system. The G-I system operates based on the Concanavalin A (Con A)-sugar specific affinity principle (see Fig 1.3 in Chapter 1) [13] and in a water rich environment. That principle says that the Con-A can bind with more than one glucose residue from polysaccharide molecules and the bindings can be reversely dissociated and formed.

In the G-I network, the insulin is trapped in the network, so the network serves as a drug carrier or infrastructure [11]. When the free glucose is present in the body and diffused into the G-I system, the existing balance between the Con A and the glucose residues is broken, which thus causes the network swelling and consequently the insulin, which is originally trapped in the network, to be released to body. Due to the therapeutic effect of insulin, the free glucose in body reduces. It is noted that the whole network is in a water rich environment (providing a force constraint to the network), and thus the swelling of the network creates a shearing force between the insulin and its carrier, resulting in the separation of insulin from its carrier (i.e., insulin release).

In the above insulin release process, the compound of the Con A and glucose plays a role of the sensor to detect the “extra” glucose. The reference substance is built in the network, particularly the number of such compounds and their structures. The controller in the G-I system is: *given a specific amount of the free glucose, to release a specific amount of the insulin*. It is noted that the controller in this case is hardwired, realized by the design of the G-I network. The actuator

in the G-I system is the shearing force generation process, which is realized by the G-I network with its water environment. As can be seen from the above discussion, the controller, the actuator, and the sensor are highly coupled in a particular environment (i.e., the aqueous environment) with respect to their functions.

For the G-I system to work, power systems are needed for all the chemical and physical actions. They are a power system (based on the chemical affinity principle) for the Con A to bind the free glucose, a power system for the free glucose to diffuse into the G-I network, and a power system for the G-I network to swell and to drive the insulin out of the trapper.

The prescribed amount of insulin is stored inside the hydrogel network, which can last for several days to several months. The whole G-I system is injected or implanted into body. A prolonged insulin source can be achieved by injection or implantation of the insulin from an external source.

The sphere-like core-shell microgels fabricated from Con A-sugar based glucose-responsive materials are shown in Fig. 3.3a. The mean diameter calculated from SEM images is 5.23 μm (Fig. 3.3b). The *in vitro* insulin release behavior is evaluated to show the effectiveness of the G-I system (Fig. 3.3c). The pulsatile insulin release pattern for 5 cycles is displayed as the glucose concentration changed between 0 and 4 mg/mL. Under photo-irradiation of the shell layer, the amount of the accumulated insulin release is reduced (Fig. 3.3d), thus increasing the drug capacity of system (i.e., more insulin could be loaded into the core-shell microspheres without a need to release an excessive amount of insulin). In this way, the robustness of the system is improved in that the gap between the drug capacity and the threshold of the effective drug concentration is increased. The shell layer could act as both the protection and robust controller, both of which are very important, as body is highly uncertain.

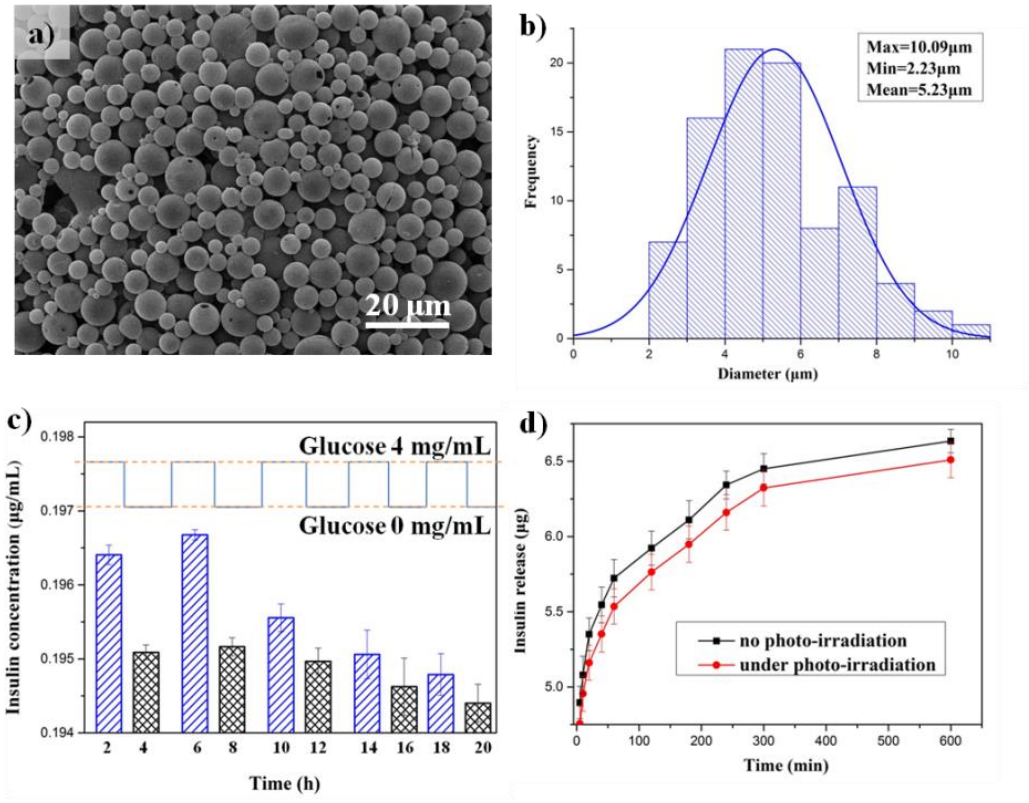

Fig. 3.3. Morphology and properties of glucose-responsive microgels: (a) SEM image, (b) diameter distribution, (c) in-vitro pulsatile release, and (d) photo-adjusted release behavior for robust control. Data is presented as mean ± SD (n = 3).

3.4 Concluding remark

The main contribution of this paper is a systems perspective to drug delivery, i.e., a supply-demand feedback control system, for generalizing a drug delivery system along with its process. Further, this system perspective establishes a fully soft robotic model to the drug delivery system [14]. Insulin delivery was taken as an example to illustrate the foregoing generalization and systems perspective.

There are a couple of benefits with this generalization. First, the biochemical view of protein-based or molecule-based drug delivery, a traditional view in drug delivery science and technology, can now be decomposed into engineering-meaningful sub-systems or components (i.e., sensor, actuator, controller, reference, plant). The significance of the decomposition is to

allow for a more rational design of a protein-based drug delivery system, particularly the separate design of the actuator, sensor, controller, and plant, and a possibility to model and simulate a drug delivery process. The separate design will reduce the complexity of design and will be conducive to innovation, as sub-systems are open to alternatives and a chance to combine the competent alternatives of the sub-systems into a more competent overall system is available. Second, this generalization can serve as a framework for incorporating engineered components into a natural molecular drug system. For instance, a soft-wired controller[1] may work together with a hard-wired controller to improve the drug delivery performance.

REFERENCES

[1] Kim S, Kim J-H, Jeon O, Kwon IC, Park K. Engineered polymers for advanced drug delivery. European Journal of Pharmaceutics and Biopharmaceutics. 2009;71:420-30.

[2] Putney SD, Burke PA. Improving protein therapeutics with sustained-release formulations. Nature Biotechnology. 1998;16:153-7.

[3] Kikuchi A, Okano T. Pulsatile drug release control using hydrogels. Advanced Drug Delivery Reviews. 2002;54:53-77.

[4] Veiseh O, Gunn JW, Zhang M. Design and fabrication of magnetic nanoparticles for targeted drug delivery and imaging. Advanced Drug Delivery Reviews. 2010;62:284-304.

[5] Byrne JD, Betancourt T, Brannon-Peppas L. Active targeting schemes for nanoparticle systems in cancer therapeutics. Advanced Drug Delivery Reviews. 2008;60:1615-26.

[6] Sinha V, Trehan A. Biodegradable microspheres for protein delivery. Journal of Controlled Release. 2003;90:261-80.

[7] Ang KH, Chong G, Li Y. PID control system analysis, design, and technology. IEEE Transactions on Control Systems Technology. 2005;13:559-76.

[8] Gero JS, Kannengiesser U. The situated function–behaviour–structure framework. Design Studies. 2004;25:373-91.

[9] Reynolds M, Holwell S. Systems approaches to managing change: a practical guide:

[1] A soft-wired controller refers to the controller which is based on electronics.

Springer; 2010.

[10] Zhang T, Zhang D, Gupta MM, Zhang W. Design of a general resilient robotic system based on axiomatic design theory. 2015 IEEE International Conference on Advanced Intelligent Mechatronics (AIM): IEEE; 2015. p. 71-8.

[11] Zhang W, Van Luttervelt C. Toward a resilient manufacturing system. CIRP Annals. 2011;60:469-72.

[12] Kim JJ, Park K. Modulated insulin delivery from glucose-sensitive hydrogel dosage forms. Journal of Controlled Release. 2001;77:39-47.

[13] Yin R, Wang K, Du S, Chen L, Nie J, Zhang W. Design of genipin-crosslinked microgels from concanavalin A and glucosyloxyethyl acrylated chitosan for glucose-responsive insulin delivery. Carbohydrate Polymers. 2014;103:369-76.

[14] Chen A, Yin R, Cao L, Yuan C, Ding HK and Zhang WJ. Soft robotics: Definition and research issues. 2017 24th International Conference on Mechatronics and Machine Vision in Practice (M2VIP), 2017, p. 366-70.

CHAPTER 4 PRINCIPLE OF CONCANAVALIN A-SUGAR AFFINITY BASED SYSTEM

This chapter is derived from an article published in ***International Journal of Biological Macromolecules****, 2019, 124, 724–732. Available online: https://doi.org/10.1016/j.ijbiomac.2018.11.261.*

4.1 Introduction

Diabetes mellitus is a group of metabolic disorders in which there are high blood sugar levels over a prolonged period. Diabetes is due to either the inability of the pancreas to produce insulin (i.e., Type 1) or the improper response of cells to the insulin produced (i.e., Type 2) [1]. Conventionally, multi-dose subcutaneous insulin injections throughout the day are required for the treatment of Type 1 and advanced Type 2 diabetes patients. Unfortunately, the multiple insulin injection therapy often leads to inadequate glycemic control accompanied by pain [2]. With the development of oral insulin delivery carriers, the oral administration of insulin could be an effective route to avoid trauma and distress caused by insulin injection [3]. However, this delivery method cannot achieve an automatic response to changes in blood glucose level. A closed-loop therapy is a highly desirable alternative to insulin injections and oral insulin delivery [1], which represents the glucose-responsive insulin delivery in response to the real-time glucose levels [4]. Till now, there are three basic approaches to achieve the closed-loop insulin delivery: (i) insulin infusion pumps directed by a control algorithm, which is further based on continuous glucose monitoring [5] (i.e., electromechanical-controlled), (ii) isolated islet cells encapsulated with biocompatible materials (i.e., bio-controlled), and (iii) chemical-controlled system by glucose-responsive hydrogels [6, 7].

Hydrogels are water-swollen polymeric networks consisting of crosslinked molecules that can swell but not dissolve in water [8, 9]. To a hydrogel-network based glucose-responsive system, the response rate to glucose stimulus is determined by the network structure change and the

resulting swelling property. Similar to the electromechanical closed-loop insulin delivery device, which is composed of the sensor, controller, actuator and body, the chemical-controlled system can be viewed as an intelligent machine system with the fact that its controller is hardwired (particularly realized by a smart design of the hydrogel-network) and further, the controller, actuator along with power generator, sensor and body are highly integrated in a particular aqueous environment with respect to their functions [10]. Typically, three kinds of glucose-responsive hydrogels were proposed in literature, which are glucose oxidase [11], concanavalin A (Con A) [12] and phenylboronic acid [13]. Among them, the Con A-sugar affinity-based system is very promising for clinical use due to its strongest specificity to glucose. The first *in vivo* test of such a system on a live diabetic domestic pig was performed in Taylor's group by using an implantable artificial pancreas made from crosslinkable-dextran/Con A complex [14]. Compared with other implantable devices, micro-/nanogels are more attractive for drug delivery, owing to its benefits including the allowance of subcutaneous or intramuscular injection, increased resolution, fast response, biodegradability and biocompatibility [15, 16]. It is worth mentioning that our group focused on the development of the glucose-responsive microgels by using polysaccharide-Con A interaction [6, 17].

In the past decade, the glucose-responsive behavior of Con A-sugar based hydrogels, microgels, films and nanoparticles were studied for drug delivery and biosensor [6, 18, 19]; however, the principle or mechanism of such a system, the Con A principle or mechanism in short, has not been well understood in the literature. Moreover, some counter-productive results relevant to the Con A principle have been reported in literature, which shows in particular that the binding affinity of Con A with glucose in the free solution is much lower than that of Con A with glucose-based polysaccharide, measured by isothermal titration calorimetry (ITC) [18]. Li and co-workers [18] also demonstrated that the low affinity of glucose with Con A was unable to trigger the dissociation of the Con A-glycogen binding in the physiological pH value (pH 7.4). Therefore, understanding the principle of the glucose-responsiveness of the Con A-sugar affinity-based chemical-controlled system warrants further study. In this chapter, a study on the principle of the Con A-sugar based glucose-responsive system through the binding affinity test by ITC and ligand binding theory is presented.

Additionally, we also performed the experiment to study whether different hydrogel-network compositions of the insulin-loaded microgels (based on Con A-sugar affinity) may respond to different glucose concentrations to examine the feasibility of a modulated insulin release control best tailored to individual patients. This experiment is a first step towards the realization of personalized diabetes care, which has received more and more attention nowadays [20, 21] due to its promise of achieving a more precise glucose control, improving the insulin sensitivity and reducing the risk of complications [22].

4.2 Materials and methods

4.2.1 Materials

Concanavalin A (extracted from Jack Bean, pre-activated, $\bar{M}_w$= 102 kDa, containing Ca^{2+} and Mn^{2+}) was purchased from Medicago Inc. (Canada). Polyethylene glycol (600) diamethacrylate (PEGDMA) was obtained from TCI Inc. (USA). Dextran ($\bar{M}_w$ = 40 and 70 kDa), glycidyl methacrylate (GMA), 4-(N, N-dimethylamino) pyridine (DMAP, 99%), brilliant blue G 250 (spectrographic grade), insulin (bovine pancreas), tris (99.9 %), dialysis membranes (MD34(8000-14000) D, Solarbio, USA), D-glucose, cyclohexane, ammonium persulfate, sodium bisulfite, dimethyl sulfoxide, span 80 and isopropyl alcohol were obtained from Sigma-Aldrich (USA). All the reagents were used as received.

4.2.2 Synthesis and characterization of glycidyl-methacrylated dextran (DexG)

The synthesis process and structural characterization of DexG can be found in [23, 24]. Briefly, dextran and glycidyl methacrylate (GMA) were dissolved in DMSO and the reaction was catalyzed by N, N-dimethylamino pyridine and took place at 33 ˚C under nitrogen purge for 48 h. Gel permeation chromatography (GPC) combined with laser light scattering (GPC-LLS) was performed to measure the molecular weight of unmodified and modified dextran. ^{1}H NMR

spectra were used to confirm the presence of double bonds from GMA and calculate the degree of substitution (DS) of DexG. The details of GPC, GPC-LLS and NMR measurements can be found in the APPENDIX 4.1. DexG with different molecular weight and DS were synthesized in this study for further experiments (see Table 4.1 in the section of results and discussion).

4.2.3 ITC measurement

ITC experiments were performed using a CSC 4200 (Calorimetry Science Corp.). Tris-HCl buffer (pH 7.4) was used for preparing Con A and its receptor (glucose, dextran and DexG) solutions. Con A was supplied as pre-activated with Ca^{2+} and Mn^{2+}. In each titration, 10 μL of ligand solution was injected into the Con A solution with a time interval of 200 s at 25 ℃. The heat during the binding process was measured. The dilution heat of the ligand titrated into the buffer without Con A was also measured. The data were fitted to an independent binding model and the binding affinity was represented by the constant *K*. The independent binding model is based on the concept that each ligand and each binding site have the same chance of combining, irrespective of the amount of binding that has already occurred. Also, the *n* value and thermodynamic parameters of the binding, including enthalpy change ΔH, entropy change ΔS and the Gibbs free energy change ΔG were also obtained from the experiments, where the ΔG was calculated by –RT ln K, and the ΔS was calculated by $(\Delta H-\Delta G)/T$ [25]. Other parameters were directly exported from the software of the instrument.

4.2.4 Microgels fabrication

Glucose-responsive microgels with different DexG/Con A compositions were fabricated by high-speed shear emulsification method according to our previous study [23]. Briefly, 39.9 g of organic phase containing 39 g of cyclohexane and 0.9 g of Span 80 as stabilizer was emulsified with aqueous phase (2 mL) containing a specific amount of DexG, Con A (in HCl-Tris buffer solution with pH 7.4), PEGDMA and insulin (dissolved in 0.01 M HCl) by stirring at 5,000 rpm for 2 min, followed by the addition of initiator solution (a mixture of 3 mM ammonium

persulfate and 3 mM sodium bisulfite). After continuous high-speed dispersion for 20 minutes, the emulsion was mechanically stirred for 24 h to achieve the purpose of further hardening and standing for the microgels. Then, 150 mL of isopropanol was added and the microgels were separated by centrifugation at 10, 000 rpm. After that, these obtained microgels were washed with isopropanol and deionized water 3 times, respectively [26]. Finally, the microgels were dried by freeze-drying.

4.2.5 SEM

The morphology and size distribution of the microgels were determined by a Hitachi S-4700 field-emission scanning electron microscope (SEM) at an accelerating voltage of 15 kV. Prior to the observation, the specimen was fixed on stubs and sputter coated with gold. Two hundred microgels from several SEM images were evaluated with the software Image J and an average diameter as well as a standard deviation was calculated.

4.2.6 Insulin loading measurement and in vitro insulin release test

The insulin entrapment capacity (EC) and loading capacity (LC) of the microgels was calculated by equations (4-1) and (4-2) [23], respectively. To test the amount of loaded insulin, a grind method plus a high-concentration glucose stimulus was implemented in the insulin release process with the aim to destroy and dissociate the hydrogel network inside the microgels. 10 mg of microgels were first grinded and then dispersed in a sealed dialysis bag with 3 mL of PBS (pH 7.4) solution. Then, the dialysis bag was put into the release medium (PBS, pH 7.4) with a glucose concentration of 20 mg/mL at 37 °C with a shock rate of 100 rpm. After 96 hours, the amount of released insulin was determined by the brilliant blue (G-250) label method, i.e., measuring the absorbance of brilliant blue G-250 labelled insulin (labelled by Van der Waals' force) at 595 nm by a UV spectrophotometer (Hitach U-3010) to get the insulin concentration according to the calibration curve. All measurements were replicated three times.

$$EC\% = \frac{Loaded\ Insulin}{Total\ insulin} \times 100\% \qquad (4\text{-}1)$$

$$LC\% = \frac{Loaded\ Insulin}{Microgels\ weight} \times 100\% \quad (4\text{-}2)$$

The *in vitro* release behavior of insulin from microgels with different compositions was investigated by measuring the amount of insulin released in the presence of different concentrations of glucose. Ten milligrams of microgels were first dispersed in a sealed dialysis bag with 3 mL of PBS (pH 7.4) solution with glucose concentration of 4 mg/mL. Then, the dialysis bag was put into the release medium (PBS, pH 7.4) with changed glucose concentration (4→10→1 mg/mL cycle with a specific time interval) at 37 °C with a shock rate of 100 rpm. At predetermined times, the released insulin in the medium was labeled by G-250 and the concentration was measured at 595 nm by using a UV spectrophotometer. The release study was continued after replacement with an equal volume of fresh solution to maintain a constant volume. All measurements were replicated three times.

4.2.7 CD and FL tests of released insulin

The activity of released insulin was determined by analysis of the structural stability by using both circular dichroism (CD) and fluorescence (FL) spectrophotometer. For the CD study, the released insulin and standard insulin were measured at 25 ˚C with a cell path length of 0.1 cm, a bandwidth of 1 nm, and a response time of 1 s. The standard insulin solution was prepared in PBS (pH 7.4) to a final concentration of 20 μg/mL. The samples were scanned from 190 to 250 nm at a resolution of 1.0 nm, and the data were compared at the characteristic peaks of about 208 nm and 223 nm. For the FL measurements, samples were tested at an excitation wavelength of 276 nm and emission wavelength of 305 nm, and the standard insulin solution was set to 0.01 mg/mL. For both CD and FL tests, each sample was repeated three times, and the final data was an average of three measurements.

4.2.8 In vitro cytotoxicity measurement of microgels

The cell viability of different microgels was assessed by using Cell Counting Kit-8 (CCK-8, Dojindo Molecular Technologies, Kumamoto, Japan) assay (Yue et al., 2017; Zheng et al., 2017) with human dermal fibroblasts cell line (HDF, Biovector Science lab, Inc.) as model cells. Briefly, HDF cells were cultured on 96-well culture plates at 2×10^4 cells/mL in 100 μL of growth medium DMEM containing 10 % (v/v) fetal bovine serum (FBS, Gibco, USA). Sterilized microgels were dispersed in the DEME medium with the concentration of 10 and 100 μg/mL. Cells were seeded to the medium without microgels for reference (negative control). The cell viability was evaluated after incubation for 1, 4 and 7 days by measuring the absorbance of the CCK-8 solution using a microplate reader (Bio-Rad, USA) at a wavelength of 450 nm. Cell viability (%) was calculated from $[A]_{test}/[A]_{n\text{-}control}\times100\%$, where $[A]_{test}$ and $[A]_{n\text{-}control}$ were the absorbance values of samples minus the medium and negative control minus the medium, respectively. For each sample, the final absorbance was the average value measured from six wells in parallel. It is noted that no positive control was applied in cytotoxicity experiments in this thesis, as the goal of *in vitro* cytotoxicity assay was trying to prove the samples were non-toxic. The expected results of experimental group should be similar to that of negative control while far from that of positive control. No significant difference compared with negative control would help to indicate the non-toxic of samples.

4.3 Results and discussion

4.3.1 Absolute molecular weight analysis of macromolecular ligands

The absolute molecular weight of macromolecular ligand samples (methacrylate modified and unmodified dextran in this study), in particular number-average molecular weight (*Mn*), is required for ITC test, as it determines the molar concentration of ligand which should be inputted for the data fitting process after titration [27]. To get the absolute *Mn* of methacrylate modified dextran (DexG in the following discussion) and unmodified dextran samples, we performed GPC-LLS measurements. The molecular weight and molecular weight dispersity of DexG and unmodified dextran samples are shown in Table A.1 and Table A.2 (APPENDIX A),

respectively. Comparing the measured molecular weight of DexG and unmodified dextran, it is noted that the introduction of methacrylate segments can significantly decrease the measured molecular weight by GPC-LLS, which may be attributed to the reduced molecular-chain entanglement caused by the hydrophobic methacrylate moieties. Similar results are obtained from GPC measurement (see Fig. A.1 in APPENDIX A), with the decrease of molecular weight after modification rather than an increase.

The molecular weight of unmodified dextran obtained from GPC-LLS measurement is chosen as the absolute molecular weight for the ITC test, due to the measured *Mw* of unmodified dextran being close to its theoretical *Mw*, and the measured *Mn* of unmodified dextran is similar to that in literature [28]. For the absolute molecular weight of DexG samples, an indirect measurement method is proposed in this study. The *Mn* of DexG is calculated as the molecular weight of unmodified dextran plus the molecular weight of the sum of all attached methacrylate moieties, which is shown in equation (4-3):

$$Mn = Mn^{\,d} + (Mn^{\,d} / 162) \times \mathrm{DS} \times 142.15 \qquad (4\text{-}3)$$

where $Mn^{\,d}$ is the number-average molecular weight of corresponding unmodified dextran obtained by GPC-LLS, 162 is the molecular weight of repeated unit in dextran molecule, 142.15 is the molecular weight of per methacrylate segment in DexG, and DS is the degree of substitution of methacrylate moieties in DexG molecules.

Further, to get the DS of DexG for the calculation of absolute molecular weight, proton nuclear magnetic resonance (^{1}H NMR) was performed. The results and detailed analysis are shown in the supplementary data (Fig. A.2, A.3 in APPENDIX A). The absolute molecular weight of unmodified dextran as well as the branching degree, DS and calculated molecular weight of DexG samples are shown in Table 4.1.

Table 4.1. The absolute molecular weight of unmodified dextran as well as the branching degree, DS and calculated molecular weight of DexG samples.

Sample	Dextran T40	DexG T40-20%	Dextran T70	DexG T70-20%	DexG T70-50%	DexG T70-70%
Mn of unmodified dextran by GPC-LLS (kDa)	33.69	33.69	62.58	62.58	62.58	62.58
Branching degree calculated by ^{1}H NMR	4.8%	4.8%	4.8%	4.8%	4.8%	4.8%
Mass ratio of GMA to Dextran in synthesis	--	20%	--	20%	50%	70%
Calculated DS by ^{1}H NMR	--	19.28%	--	20.60%	26.49%	58.10%
Calculated *Mn* of DexG (kDa)	--	39.38	--	73.88	77.11	94.45

4.3.2 Binding affinity analysis

The affinity of Con A with glucose, dextran and DexG was measured by ITC in free solution. The concentration of ligands and Con A in the titration process, and the results of Con A-glucose and Con A-dextran/DexG affinity are shown in Table 4.2. Figure 4.1 exhibits the titration curves of the ITC measurements using the molecular concentration of glucose, dextran and DexG for data fitting. The *K, ΔH, ΔG, ΔS* and *n* value of the binding are inserted in Fig. 4.1. All of the binding reactions show a negative *ΔG* value, indicating these reactions can happen spontaneously [25]. With higher *K* values, the affinity of ligand-Con A is higher. From Fig. 4.1 and Table 4.2, the *K* value of Glucose-Con A interaction is 323 ± 114 M^{-1}, which is similar to the value 296 ± 51.8 M^{-1} in Li's work, and the obtained *ΔH* and *ΔS* value of glucose-Con A binding (-4.77 kJ/mol and 0.032 kJ/(mol*K)) are also similar to the value in Li's work (-4.78 kJ/mol and 0.031 kJ/(mol*K)) [18]. Figure 4.1 also exhibits that the *K* values of Con A with

unmodified dextran (dextran T40 and T70) and methacrylate modified dextran (DexG) are in the order of magnitude 10^4-10^5 M^{-1}, which is much higher than the *K* value for Glucose-Con A interaction, indicating the affinity for Con A-polysaccharide binding is much higher than that for Con A-glucose binding. These ITC data are consistent with Li's work showing that the affinity for Con A-transferrin ($5.71 \pm 0.73 \times 10^6$ M^{-1}) was much higher than that for Con A-glucose (296 ± 51.8 M^{-1}) [18]. In addition, the ΔH values of Con A binding with dextran and DexG are much greater than that of Con A-glucose binding, and the ΔS values of Con A binding with dextran and DexG are negative. These results are also in agreement with the reported results in literature [25, 27].

Table 4.2. The concentration of ligands and Con A in the titration process and the results of Con A-glucose and Con A-dextran/DexG affinity.

Sample	Glucose	Dextran T40	DexG T40-20%	Dextran T70	DexG T70-20%	DexG T70-50%	DexG T70-70%
Molecular concentration (mM)	54.54	2.08	2.54	1.44	1.37	1.82	1.80
Terminal group concentration (mM)[a]	--	24.96	30.48	29.52	28.09	37.31	36.90
Con A concentration for titration (mM)	0.071	0.071	0.071	0.094	0.094	0.071	0.071
$K_{[MC]}$ [b] (M^{-1})	323±114	5349±657	7244±2186	11764±2209	5354±1394	13711±3532	6932±2510
$K_{[TC]}$ [b] (M^{-1})	--	424±43	524±142	584±111	260±69	704±200	231±49

[a] The terminal group concentration is calculated as the macromolecular concentration multiplied by the terminals/macromolecule ratio. And the terminals/macromolecule ratio is determined by ($Mn_{\text{unmodified dextran}}$/162) × branching degree + 2.

[b] For dextran and DexG, $K_{[MC]}$ represents the affinity obtained using the macromolecular concentration of dextran and DexG for ITC data fitting process, while $K_{[TC]}$ represents the affinity obtained using the terminal group concentration of dextran and DexG for ITC data fitting.

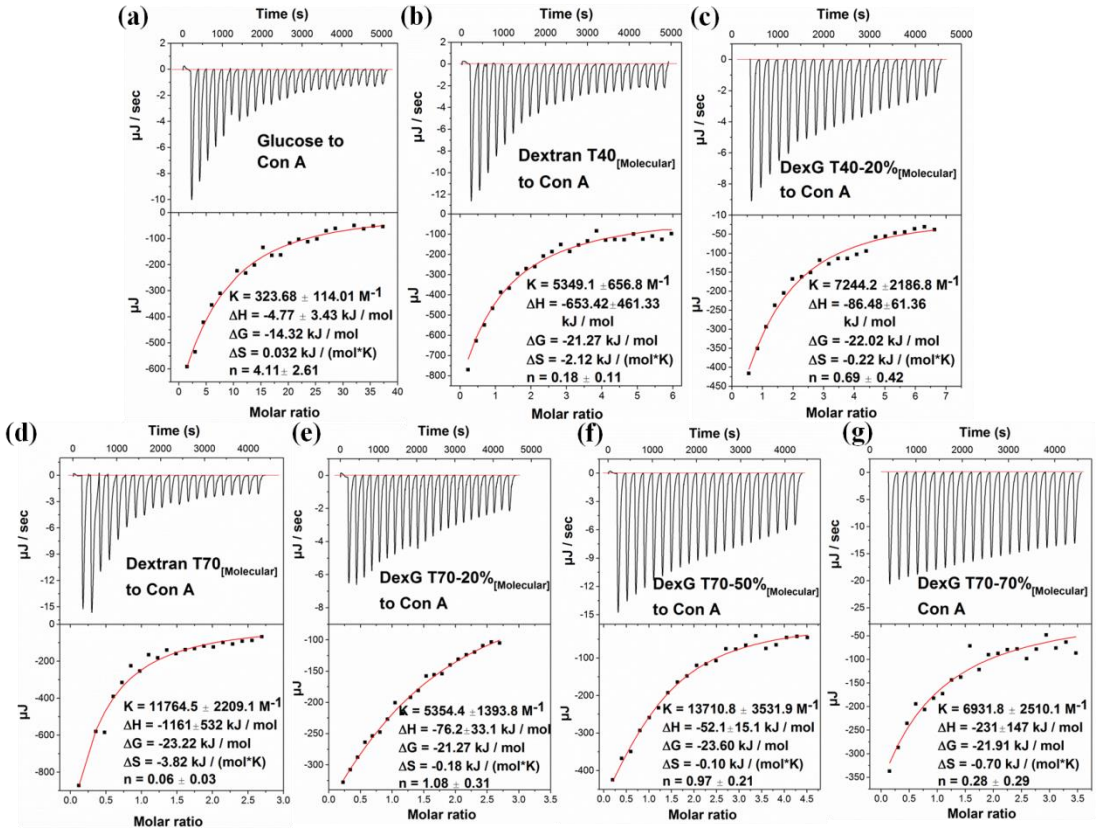

Fig. 4.1. ITC measurement on the interaction affinity of Con A with glucose (a) and a series of unmodified and methacrylate modified dextran (b-g), using the molecular concentration of ligand molecules for data fitting.

Furthermore, the influence of DS on the affnity of DexG with Con A can be seen from Fig. 4.1 b-g. For dextran T40, with 19.28% of substitued methacrylate groups (DexG T40-20%), the *K* value increases slightly compared with the *K* value of unmodified dextran. For dextran T70, with 20.60% of substitution (DexG T70-20%), the *K* value dramatically decreases compared with the *K* value of dextran T70, while the *K* value significantly increases to higher than the *K* value of dextran T70 with increased substitution of 26.49% (DexG T70-50%). However, the *K* value of DexG T70-70% with 58.10% of substitution decreases to lower than the *K* value of dextran T70 again. Interestingly, these results indicate that with a proper DS (19.28% for dextran T40 and 26.49% for dextran T70), the affinity of dextran with Con A could be enhanced. The possible reason may be that the introduction of methacrylate hydrophobic moieties onto dextran molecules enhances the interaction of dextran with Con A through the hydrophobic interaction. The reason for the decreased affinity of DexG T70-20% may be that some terminal

glucose residues are substituted by methacrylate groups, leading to less active terminal glucose residues which can react with Con A sites, and with 20.60% of substitution the DexG molecules can not form efficient hyodrophobic interaction with Con A to improve the affinity. Moreover, the decreased affinity of DexG T70-70% is caused by the excessive amount of substitution which will restrict the reaction of terminal glucose residues with Con A even with the assistance of hydrophobic interaction.

The characterization of Con A-sugar interaction in this study results in the same conclusion as in [18] that the binding affinity for Con A-glucose is much lower than that for Con A-polysaccharide. It seems that it cannot resolve the controversy in respect to the Con A principle. However, considering that it is the terminal groups on dextran molecules to bind on Con A sites and only the remaining terminal groups can move in the immobilized network after Con A-dextran hydrogel formation [25], the terminal group concentration of dextran or DexG were then used for ITC data fitting. The results are shown in Table 4.2. It can be seen that all of the $K_{[TC]}$ values for the interaction of Con A with the terminal groups on dextran or DexG are of the same magnitude as Con A-glucose interaction (10^3 M^{-1}), and even the $K_{[TC]}$ for Con A-DexG T70-20% and Con A-DexG T70-70% is lower than Con A-glucose affinity. It is noticed that in enzyme kinetics, competitive inhibition occurs when the inhibitor and the substrate have similar enzyme binding affinities (i.e., K_m and K_i are of the same order of magnitude) [29], and Bent's competitive ligand binding theory [30] also demonstrated that the competitive displacement of ligand A from PB complex can't be observed if K_A is much smaller than K_B when two ligands A and B can both bind to the same site of a third molecule P and the formation of ternary species PAB is not possible. Similarly, in this study, the $K_{[TC]}$ values and the K for Con A-glucose binding of the same order of magnitude indicated the competitive binding of glucose and the terminal groups on dextran/DexG molecules with the same binding site on Con A can happen theoretically. This is a strong evidence for the principle of glucose-responsiveness in Con A-sugar affinity-based system.

As for the phenomenon in Li's work that glucose was not able to trigger the disbanding of Con A-glycogen network, it was not reasonable to attribute this phenomenon to the much lower

affinity of Con A-glucose (10^3 M^{-1} magnitude) than Con A-glycogen (10^6 M^{-1} magnitude) [18]. Because one glycogen molecule has more than 3,000 branches, the *K* value for Con A-glycogen interaction might be at the same magnitude as Con A-glucose affinity if the terminal group concentration of glycogen was used for ITC measurement.

4.3.3 Mechanism/principle of Con A-sugar based glucose-responsiveness

In this chapter, we propose the principle of glucose-responsiveness in Con A-sugar based systems in light of affinity analysis and ligand competition theory [30], taking DexG T70-20%-Con A system as illustration (Scheme 4.1). The competitive binding between DexG (DeG) and glucose (Glu) with Con A can be expressed as the given equations according to the ligand competition theory.

$$\text{Con A} + \text{DeG} \rightleftharpoons \text{ConA- DeG} \qquad (4\text{-}4)$$

$$\text{Con A} + \text{Glu} \rightleftharpoons \text{ConA- Glu} \qquad (4\text{-}5)$$

The binding process of both equations (4-4) and (4-5) are in a dynamic equilibrium, and the equilibrium constants are given by:

$$K_{DeG} = [\text{Con A-DeG}] / [\text{Con A}]\,[\text{DeG}], \qquad (4\text{-}6)$$

$$K_{Glu} = [\text{Con A-Glu}] / [\text{Con A}]\,[\text{Glu}]. \qquad (4\text{-}7)$$

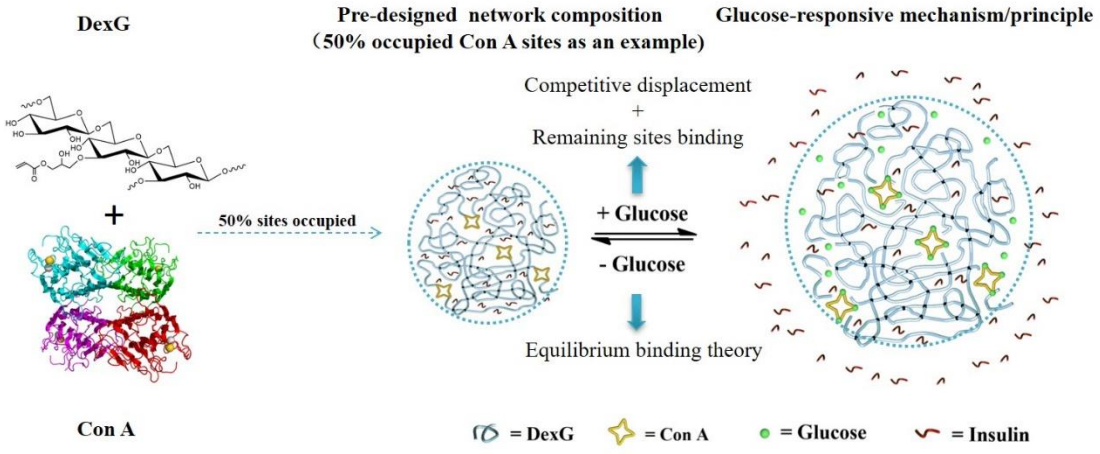

Scheme 4.1. Schematic illustration of Con A-DexG based system and its glucose-responsive mechanism/principle.

The Con A principle or mechanism can be explained with the combination of ITC analysis and dynamic equilibrium theory of ligand binding process. During the formation of Con A-DexG network, although the Con A tetramer has four sugar-interaction sites, it is conceivable that not all of these sites will be occupied after network formation owing to the steric hindrance within the network. Therefore, when free glucose diffuses into the network with a high concentration (such as 4 mg/mL), on one hand, the competitive displacement of glucose from Con A-DexG complex is possible to happen theoretically owing to the affinity of Con A-glucose is similar to the affinity of terminal groups on DexG T70-20% with Con A. On the other hand, the glucose molecules may have the chance to bind with the remaining Con A sites, further leading to the right shift of the equilibrium in equation (4-5). In this case, the concentration of available Con A will decrease and the equilibrium in equation (4-4) will correspondingly shift to the left, resulting in the dissociation of Con A-DexG complex. In contrast, when free glucose concentration decreases to a lower level (such as 1 mg/mL, known as normal glucose level), the equilibrium in equation (4-5) may spontaneously shift to the left according to the equilibrium theory, resulting in the increase of available Con A sites. More terminal moieties in DexG molecules will then bind to the available Con A sites, leading to the right shift of equation (4-4). In this way, the Con A-DexG network may reform. The equilibrium shift under different ligand concentrations is also similar to the concentration effect on competitive inhibition in enzyme kinetics [31], i.e., the competitive inhibition is proportional to inhibitor concentration, and the effect of the inhibition can be overcome if the substrate concentration is high enough. Therefore, it can be concluded that the concentration of glucose, the remaining Con A sites and the remaining terminal groups on DexG play important roles in the principle/mechanism of glucose-responsiveness in Con A-sugar affinity-based systems.

Regarding the conflict shown in Li's work [18], i.e., the inability of glucose to trigger the dissociation of Con A-glycogen deposited nanoparticles in physiological pH value (pH 7.4), on the basis of our explanation of Con A principle, it might be related to the low amount of remaining Con A sites after network formation and the low concentration of glucose for the trigger of equilibrium shift. In addition, Li and co-workers observed that glucose was able to

accelerate the disassembly of Con A-glycogen complex under acidic conditions at pH 5.5 or 5.0, which may be attributed to the looser network caused by the dimer aggregation of Con A instead of tetramer at pH 7.4 [27].

4.3.4 Design of network composition and preparation of microgels

On account of the Con A-DexG binding equilibrium equation (equation 4-4), it is possible to design the amount of remaining Con A sites and DexG molecules after the formation of Con A-DexG network by the calculation of Con A-DexG composition (Scheme 4.1). Table 4.3 gives three examples of designed compositions, where the sample 40/50/70-75% represents the amount of occupied Con A sites is 40/50/70 percent, respectively, and the percentage of reacted DexG molecules is 75%.

Table 4.3. Composition and insulin loading capability of microgels fabricated for modulated response.

Sample	Con A (mg)	DexG [a] (mg)	PEGDMA (mg)	Initiator	Loading Capacity (%)	Encapsulation Capacity (%)
40-75%	18.63	20.55	10 wt.%	3 wt. %	9.94	58.67
50-75%	23.29	30.82	10 wt.%	3 wt. %	11.03	77.18
70-75%	46.58	82.20	10 wt.%	3 wt. %	12.60	94.47

[a] DexG T70-20% was used here considering the molecular weight distribution, affinity and crosslinking property.

Taking 50-75% as an example, the calculation is given as follows. Suppose the initial concentration of Con A sites and DexG molecules are c_1 and c_2, respectively. It is noted here c_1 represents the concentration of Con A monomer because one Con A monomer has one binding site theoretically. It is assumed that there is only one Con A molecule binding with one DexG molecule. Although this is not strictly rigorous, the calculation is greatly simplified. After the formation of Con A-DexG network, if the concentration of generated Con A-DexG complex is

set to a, then the remaining concentration of Con A is c_1-a, and the concentration of DexG after reaction is c_2-a. Substitution of these relations into equation (4-6) gives

$$K_{DeG} = a / ((c_1\text{-}a) \times (c_2\text{-}a)). \quad (4\text{-}8)$$

In the case of 50-75% sample, we have

$$c_1 - a = c_1 \times (1\text{-}50\%), \quad (4\text{-}9)$$

$$c_2 - a = c_2 \times (1\text{-}75\%). \quad (4\text{-}10)$$

As K_{DeG} is determined as 5380 M^{-1} by the ITC test, the solutions for c_1 and c_2 can be obtained by the combination of equations (4-8)-(4-10).

The insulin-loaded microgels with designed Con A-DexG compositions were prepared through a high-speed shear emulsification method inherited from our previous study [17, 32]. The complex of Con A and DexG was formed prior to emulsification by virtue of the affinity links between lectin sites and sugar units. The covalent crosslinking of DexG molecules and PEGDMA crosslinker proceeded during emulsification, initiating by ammonium persulfate and sodium bisulfite at room temperature. The shape, morphology and size distribution of the microgels obtained from 50-75% composition (Table 4.3) as a typical example were observed by SEM and are shown in Fig. 4.2. The microgels exhibit a regular sphere-shape, a smooth surface free of cracks, and a normal size distribution with a mean diameter of 5.126±1.546 μm. The SEM image also displayed some aggregations of microgels. The main reason may lie in the Con A-sugar affinity and the surface hydrophilicity of the obtained microgels. Fig. A.4 exhibited the SEM images of DexG microgels without Con A (a) and Con A-DexG/Dex-CCH core-shell microgels (obtained from our previous study [32]) with hydrophobic surface (b). The elimination of Con A can reduce the aggregation of the microgels (Fig. A.4a); however, a lower degree of aggregation still exists, which might be due to the surface hydrophilicity. In the microgels shown in Fig. A.4b, the surface layer (Dex-CCH) is hydrophobic, and Con A is not contained in the surface layer. Therefore, there is no specific interaction among the microgels surface, leading to the non-aggregated status.

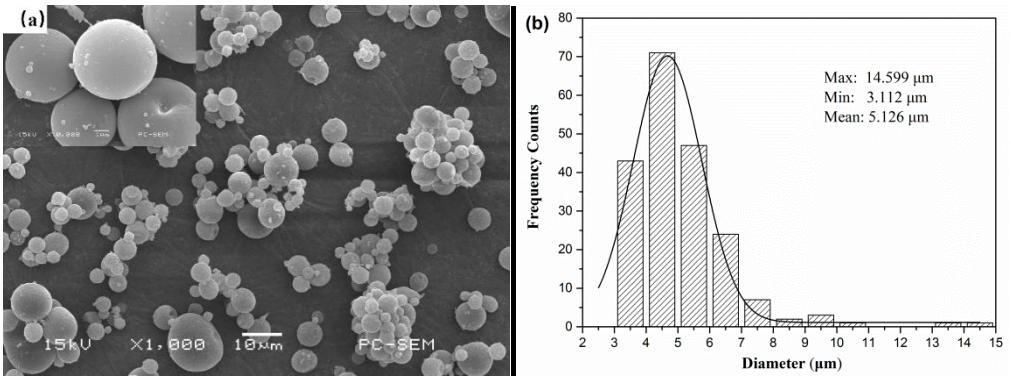

Fig. 4.2. SEM image of 50-75% microgels (a) and size distribution calculated based on several SEM images (b).

4.3.5 In vitro insulin release analysis

The insulin loading capacity and insulin encapsulation capacity of microgels 40/50/70-75% are shown in Table 4.3, indicating the increased insulin loading capacity and encapsulation capacity with more occupied Con A sites after the formation of Con A-DexG network. This is attributed to the denser network created with more Con A sites occupied by DexG molecules.

In general, insulin dosing is divided into two regimens: basal and bolus insulin. The basal insulin is required for fasting conditions; while bolus insulin is calculated to correct for meals or hyperglycemia condition [5]. In the development of closed-loop insulin pumps, a 24 h-cycle release mode with three boluses for simulating three meals a day has been applied to test the efficiency of insulin delivery [5]. Therefore, in this study, insulin delivery repeated in a 24 h-cycle with three boluses was implemented to test the glucose-responsive insulin release behavior of microgels.

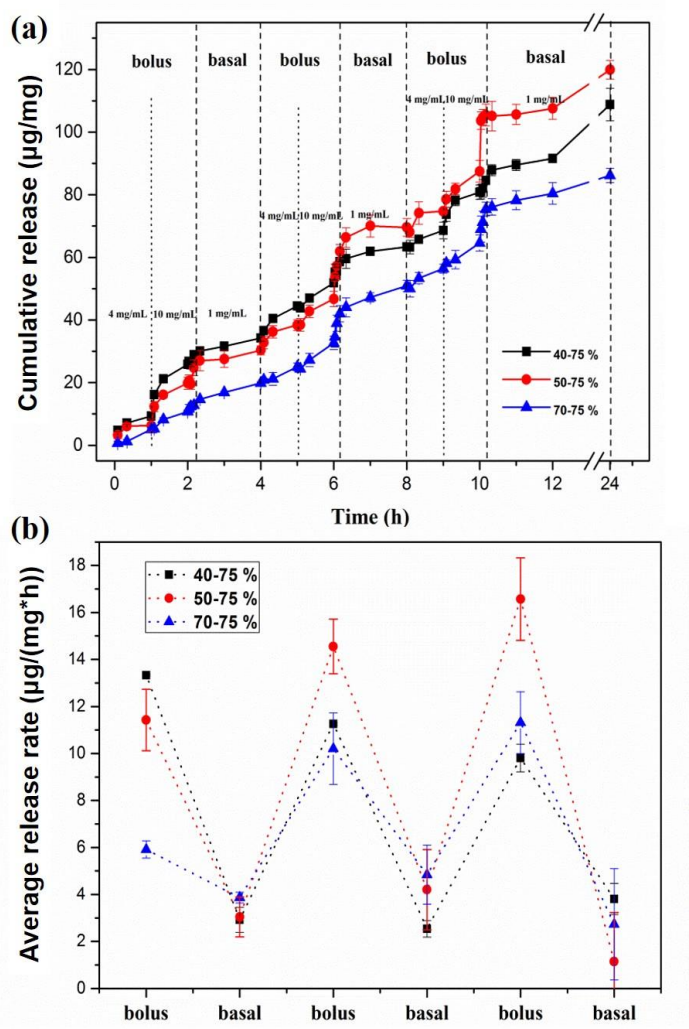

Fig. 4.3. (a) Cumulative release amount of insulin from microgels (per milligram) for a 24 h release cycle with three boluses for simulating three meals a day; (b) Average release rate of insulin as a function of bolus and basal glucose concentration in a 24 h release cycle. Data is presented as mean ± SD (n = 3).

The glucose-responsive insulin release behavior of Con A-DexG microgels can be found in Fig. 4.3. As shown in Fig. 4.3 a, higher release amount were achieved for all three groups at a hyperglycemic environment (4 an 10 mg/mL [33]) compared with normal glucose level (1 mg/mL). When subjecting to periodically changed glucose concentration from hyperglycemic to normal level, insulin release from these three groups all exhibited corresponding bolus and basal amounts in response to glucose concentration changes. The average release rate of insulin as a function of bolus and basal glucose concentration change is calculated from the release data in Fig. 4.3 a and shown in Fig. 4.3 b, indicating the insulin release profiles of microgels

with different compositions can keep similar pulsatile pattern.

Meanwhile, the *in vitro* release data revealed the effects of designed Con A-DexG composition on insulin delivery. From Fig. 4.3 a and b, it can be found that the insulin release rate during the first bolus-basal cycle (the first 4 hours) meets the following sequence: 40-75% > 50-75% > 70-75%, owing to the increased crosslinking density and decreased remaining Con A binding sites in the microgel network. However, the release rate of 40-75% microgels decreased during the second and third bolus-basal cycles while the release rate of 50-75% and 70-75% microgels gradually increased, indicating different composition of Con A-DexG network may cause different ways in the change of release rate. In addition, comparing the three curves in Fig. 4.3 a, we can find the burst release of insulin in the initial 20 minutes is dramatically reduced from 7.17 % (40-75%) to 5.50 % (50-75%) and 1.01 % (70-75%) with increased crosslinking density of Con A-DexG network. Also, the overall release amount of 70-75% microgels after 24 h was only 68 % compared to the insulin loading amount, while the 40-75% and 50-75% microgels reached to near 100% release after 24 h. The above results substantiated that the adjustment of Con A sites occupation during the network formation process could efficiently affect the burst release, release rate and overall release amount of insulin, as well as change the variation tendency of release rate during the whole release period.

4.3.6 Bioactivity of released insulin

The bioactivity of released insulin from microgels were evaluated by Fluorescence (FL) and circular dichroism (CD) spectra, which analyzed the tertiary and secondary conformational structure of insulin, respectively [34, 35]. The aim of this experiment is to find if there's the spectrophotometric evidence for deterioration of insulin structure with the assumption that denaturation would reflect a loss of bioactivity. Taking microgel 50-75% as a typical example, Figure 4.4 compares the FL and CD spectra of released insulin with that of standard insulin. From Fig. 4.4 a, it can be found that the released insulin and standard insulin exhibited similar peaks with an emission maximum at about 305 nm, indicating that the tertiary structure of

released insulin was not distorted. Additionally, the released insulin displayed similar characteristic peaks at about 208 nm and 223 nm on CD spectra (see Fig. 4.4 b) compared with standard insulin, indicating that the secondary conformational structure of released insulin can match that of native insulin. Both FL and CD results confirmed there was no significant conformational change observed for the released insulin from the microgels.

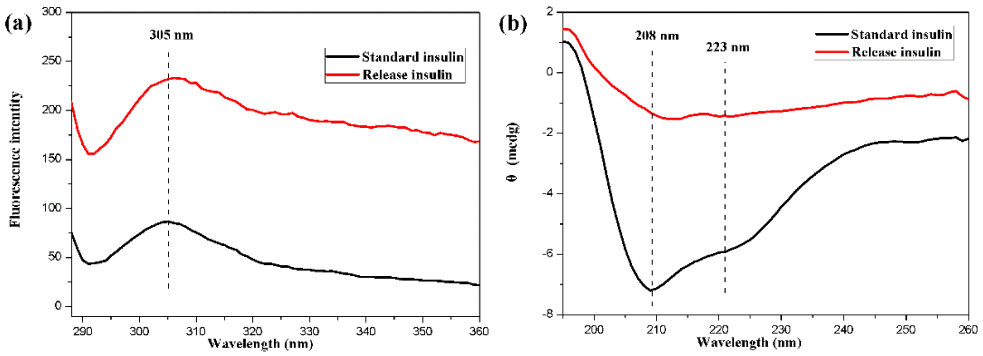

Fig. 4.4. Fluorescence (a) and circular dichroism (b) spectra of standard insulin and released insulin, showing similar tertiary and secondary structure.

4.3.7 In vitro cytotoxicity analysis

The *in vitro* cytotoxicity of the microgels with different compositions was assessed by CCK-8 assay. Human dermal fibroblast cells (HDF) were used as model cells considering the potential subcutaneous injection administration of the microgels into human patients. In the cell culture experiments, we used the concentration 10 μg/mL and 100 μg/mL to test the cytotoxicity of microgels [23]. The viability of HDF culture for 1, 4 and 7 days is illustrated in Fig. 4.5. It could be seen that most of the experiments showed higher cell viability (> 80%) for HDF cells, and no statistically significant differences were observed in the cell viability of HDF culture for 1, 4 and 7 days in the presence of microgels with 10 μg/mL and 100 μg/mL compared with the negative control group ($p < 0.05$ was considered as significant difference in the T-test), respectively. The obtained results suggested that the microgels were nontoxic to HDF cells.

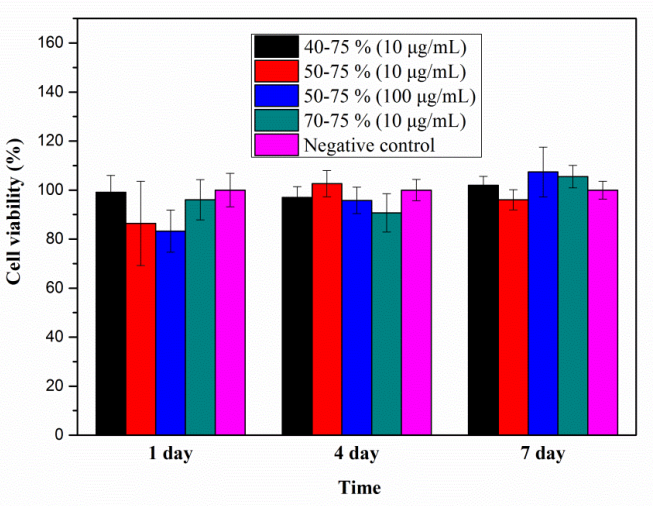

Fig. 4.5. *In vitro* cytotoxicity evaluation of microgels with concentrations of 10 μg/mL and 100 μg/mL by CCK-8 assay using HDF cells. Data is presented as mean ± SD (n = 6).

4.4 Conclusions

In this chapter, we performed the GPC-LLS and NMR tests to obtain the absolute molecular weight of polysaccharide ligands (dextran and DexG) and then measured the binding affinity with Con A by ITC. Interestingly, we found that the affinities of glucose and the terminal groups on dextran/DexG with Con A are on the same order of magnitude. By combining the result of the affinity analysis and the ligand binding equilibrium theory, we were able to account for the principle/mechanism of glucose-responsiveness in the Con A-sugar affinity-based system and successfully resolve the controversy relevant to the Con A principle in literature. In addition, Con A-DexG hydrogel-networks with varying response rates were developed by the design of the network composition and the corresponding microgels were fabricated by the high-speed shear emulsification method. The results of the *in vitro* insulin release revealed that the microgels with 40-75%, 50-75%, 70-75% composition could maintain bolus and basal insulin release in response to different glucose concentrations, and the network composition could affect the burst release, release rate and overall release amount of insulin. Further, the FL and CD data supported the idea that insulin remained active as the secondary and tertiary conformational structures of the released insulin were not disturbed. The HDF cell viability

assessment suggested that the microgels possessed no *in vitro* cytotoxicity. These results indicated the promise of using such microgels for individual diabetes care in the future.

REFERENCES

[1] Gordijo CR, Koulajian K, Shuhendler AJ, Bonifacio LD, Huang HY, Chiang S, et al. Nanotechnology - enabled closed loop insulin delivery device: In vitro and in vivo evaluation of glucose - regulated insulin release for diabetes control. Advanced Functional Materials. 2011;21:73-82.

[2] Gu Z, Dang TT, Ma M, Tang BC, Cheng H, Jiang S, et al. Glucose-responsive microgels integrated with enzyme nanocapsules for closed-loop insulin delivery. ACS Nano. 2013;7:6758-66.

[3] Massaro M, Cavallaro G, Colletti CG, D'Azzo G, Guernelli S, Lazzara G, et al. Halloysite nanotubes for efficient loading, stabilization and controlled release of insulin. Journal of Colloid and Interface Science. 2018;524:156-64.

[4] Elleri D, Biagioni M, Allen JM, Kumareswaran K, Leelarathna L, Caldwell K, et al. Safety, efficacy and glucose turnover of reduced prandial boluses during closed - loop therapy in adolescents with type 1 diabetes: a randomized clinical trial. Diabetes, Obesity and Metabolism. 2015;17:1173-9.

[5] Wang Y, Dassau E, Doyle III FJ. Closed-Loop Control of Artificial Pancreatic $\beta $-Cell in Type 1 Diabetes Mellitus Using Model Predictive Iterative Learning Control. IEEE Transactions on Biomedical Engineering. 2010;57:211-9.

[6] Yin R, Wang K, Du S, Chen L, Nie J, Zhang W. Design of genipin-crosslinked microgels from concanavalin A and glucosyloxyethyl acrylated chitosan for glucose-responsive insulin delivery. Carbohydrate Polymers. 2014;103:369-76.

[7] Di J, Yu J, Ye Y, Ranson D, Jindal A, Gu Z. Engineering synthetic insulin-secreting cells using hyaluronic acid microgels integrated with glucose-responsive nanoparticles. Cellular and Molecular Bioengineering. 2015;8:445-54.

[8] Lutolf MP. Biomaterials: Spotlight on hydrogels. Nature Materials. 2009;8:451-3.

[9] Zhu J, Marchant RE. Design properties of hydrogel tissue-engineering scaffolds. Expert Review of Medical Devices. 2011;8:607-26.

[10] Yin R, Bai M, Zhang B, Wang K, Zhang H, Yang S, et al. Understanding drug delivery from a system perspective: Concept and demonstration. Nano/Micro Engineered and Molecular Systems (NEMS), 2017 IEEE 12th International Conference on: IEEE; 2017. p. 698-701.

[11] Qi W, Yan X, Duan L, Cui Y, Yang Y, Li J. Glucose-sensitive microcapsules from glutaraldehyde cross-linked hemoglobin and glucose oxidase. Biomacromolecules. 2009;10:1212-6.

[12] Kim JJ, Park K. Modulated insulin delivery from glucose-sensitive hydrogel dosage forms. Journal of Controlled Release. 2001;77:39-47.

[13] Jin X, Zhang X, Wu Z, Teng D, Zhang X, Wang Y, et al. Amphiphilic random glycopolymer based on phenylboronic acid: synthesis, characterization, and potential as glucose-sensitive matrix. Biomacromolecules. 2009;10:1337-45.

[14] Taylor M, Gregory R, Tomlins P, Jacob D, Hubble J, Sahota T. Closed-loop glycaemic control using an implantable artificial pancreas in diabetic domestic pig (Sus scrofa domesticus). International journal of Pharmaceutics. 2016;500:371-8.

[15] Sinha VR, Trehan A. Biodegradable microspheres for protein delivery. Journal of Controlled Release. 2003;90:261-80.

[16] Byrne JD, Betancourt T, Brannonpeppas L. Active targeting schemes for nanoparticle systems in cancer therapeutics. Advanced Drug Delivery Reviews. 2008;60:1615-26.

[17] Yin R, Tong Z, Yang D, Nie J. Glucose-responsive insulin delivery microhydrogels from methacrylated dextran/concanavalin A: preparation and in vitro release study. Carbohydrate Polymers. 2012;89:117-23.

[18] Li J, Qu X, Payne GF, Zhang C, Zhang Y, Li J, et al. Biospecific Self‐Assembly of a Nanoparticle Coating for Targeted and Stimuli‐Responsive Drug Delivery. Advanced Functional Materials. 2015;25:1404-17.

[19] Sato K, Imoto Y, Sugama J, Seki S, Inoue H, Odagiri T, et al. Sugar-induced disintegration of layer-by-layer assemblies composed of concanavalin A and glycogen. Langmuir.

2005;21:797-9.

[20] Greenbaum CJ. Insulin resistance in type 1 diabetes. Diabetes/metabolism Research and Reviews. 2002;18:192-200.

[21] Raz I, Riddle MC, Rosenstock J, Buse JB, Inzucchi SE, Home PD, et al. Personalized management of hyperglycemia in type 2 diabetes. Am Diabetes Assoc; 2013. p. 1779-88.

[22] Kahn SE, Hull RL, Utzschneider KM. Mechanisms linking obesity to insulin resistance and type 2 diabetes. Nature. 2006;444:840-6.

[23] Bai M, He J, Kang L, Nie J, Yin R. Regulated basal and bolus insulin release from glucose-responsive core-shell microspheres based on concanavalin A-sugar affinity. International Journal of Biological Macromolecules. 2018;113:889-99.

[24] Yin R, Wang K, Han J, Nie J. Photo-crosslinked glucose-sensitive hydrogels based on methacrylate modified dextran–concanavalin A and PEG dimethacrylate. Carbohydrate Polymers. 2010;82:412-8.

[25] Benzeval I. Development of responsive polymers for drug delivery applications: University of Bath; 2009.

[26] Karewicz A, Zasada K, Szczubiałka K, Zapotoczny S, Lach R, Nowakowska M. “Smart” alginate–hydroxypropylcellulose microbeads for controlled release of heparin. International Journal of Pharmaceutics. 2010;385:163-9.

[27] Mandal DK, Kishore N, Brewer CF. Thermodynamics of lectin-carbohydrate interactions. Titration microcalorimetry measurements of the binding of N-linked carbohydrates and ovalbumin to concanavalin A. Biochemistry. 1994;33:1149-56.

[28] Benzeval I, Bowyer A, Hubble J. The influence of degree-of-branching and molecular mass on the interaction between dextran and Concanavalin A in hydrogel preparations intended for insulin release. European Journal of Pharmaceutics and Biopharmaceutics. 2012;80:143-8.

[29] Bhagavan N.V. HC-E. Enzymes and Enzyme Regulation. Essentials of Medical Biochemistry. 2011.

[30] Sigurskjold BW. Exact analysis of competition ligand binding by displacement isothermal titration calorimetry. Analytical Biochemistry. 2000;277:260-6.

[31] Engelking LR. Enzyme Kinetics. Textbook of Veterinary Physiological Chemistry (Third Edition). 2015.

[32] Bai M.R. HJ, Yin R.X., Nie J. Regulated insulin release from core-shell microspheres with glucose-responsive core and photo-crosslinkable shell. International Journal of Biological Macromolecules. 2018; 113: 889-899.
[33] Tanna S, Sahota TS, Sawicka K, Taylor MJ. The effect of degree of acrylic derivatisation on dextran and concanavalin A glucose-responsive materials for closed-loop insulin delivery. Biomaterials. 2006;27:4498-507.
[34] Amidi M, Pellikaan HC, de Boer AH, Crommelin DJ, Hennink WE, Jiskoot W. Preparation and physicochemical characterization of supercritically dried insulin-loaded microparticles for pulmonary delivery. European Journal of Pharmaceutics and Biopharmaceutics. 2008;68:191-200.
[35] Kelly SM, Jess TJ, Price NC. How to study proteins by circular dichroism. Biochimica et Biophysica Acta (BBA)-Proteins and Proteomics. 2005;1751:119-39.

APPENDIX A

GPC-LLS and GPC tests

Gel permeation chromatography (GPC) combined with static laser light scattering (GPC-LLS) is convenient for the measurement of absolute molecular weight and its distribution without the aid of standard samples [1]. The GPC-LLS tests of dextran samples (methacrylate modified and unmodified dextran) were performed on the DAWN DSP multi-angle laser photometer with 690 nm laser wavelength (Dawn Eos, Wyatt, USA). Hydrolyzed dextran column was used. The column temperature was maintained at 25 °C. The flow rate was 1 mL/min and mobile phase was 0.025 M phosphate buffer (pH 7.4) with added 0.05 M NaCl. The refractive index increment (dn/dc) of dextran samples at 633 nm and 25 °C was 0.15 g^{-1} cm^3 in aqueous solution. GPC measurement of samples without LLS (Waters, USA) was also performed using the same dextran column and mobile phase.

NMR test

Proton nuclear magnetic resonance (^{1}H NMR) spectroscopy (600 MHz, Bruker AV600 Bruker Corp., Germany) was used to confirm the structure of modified dextran samples and calculate the degree of substitution (DS) of dextran, using DMSO-*d6* as solvent at room temperature (298 K).

Table A.1. The number-average molecular weight, weight-average molecular weight and molecular weight dispersity of different DexG samples.

Samples	DexG T40-20%	DexG T70-20%	DexG T200-20%
Mn (Da)	982	6853	61226
Mw (Da)	7351	8297	97735
Dispersity	7.48	1.21	1.59

Table A.2. The number-average molecular weight, weight-average molecular weight and molecular weight dispersity of different unmodified dextran samples.

Samples	Dextran T40	Dextran T70	Dextran T100	Dextran T200
Mn (Da)	33690	62581	32306	159732
Mw (Da)	42006	63929	78115	394743
Dispersity	1.25	1.02	5.09	2.47

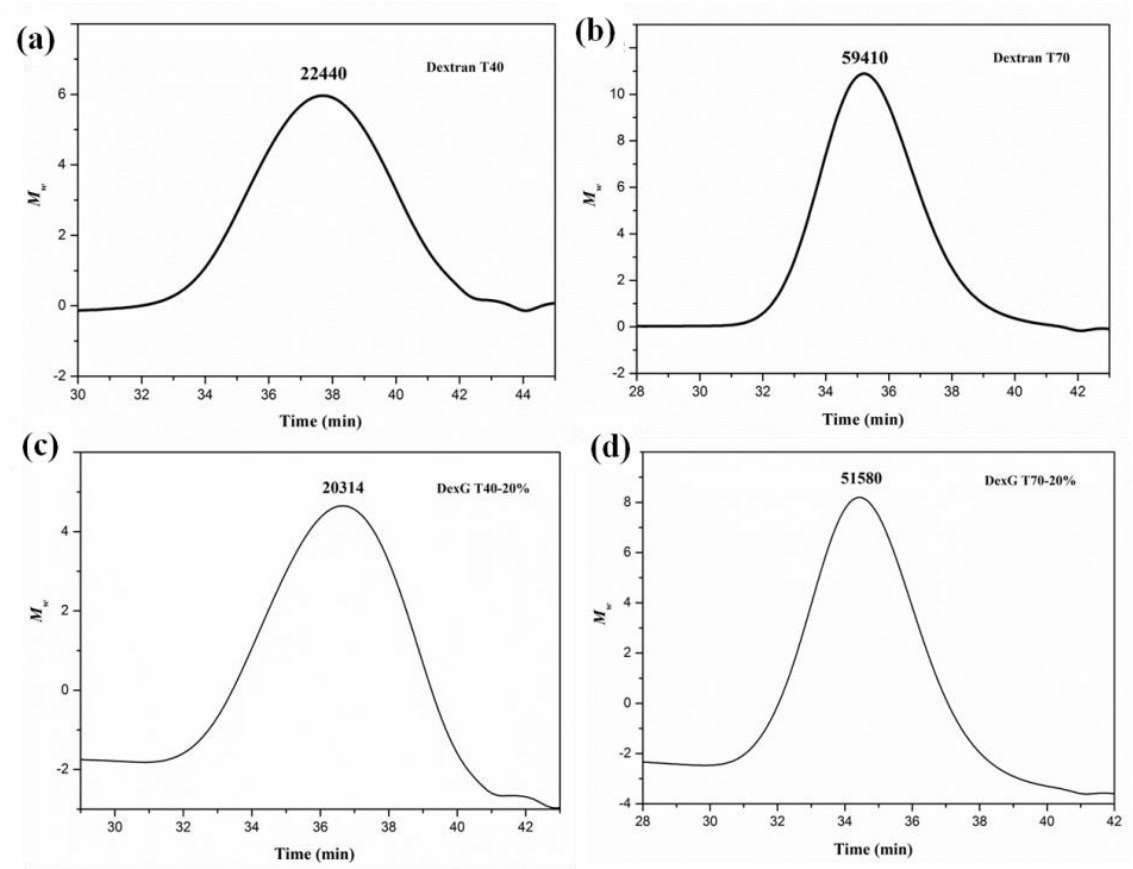

Fig. A.1. GPC traces of unmodified dextran T40 (a), T70 (b), and methacrylate modified DexG T40-20% (c) and T70-20% (d).

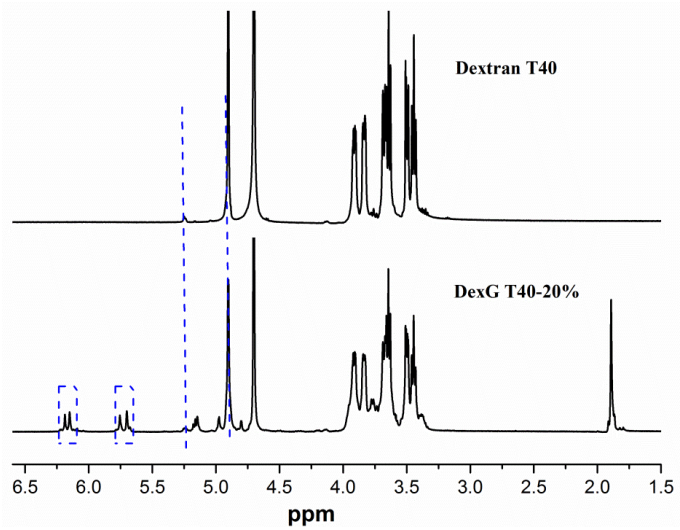

Fig. A.2. The ^{1}H NMR spectra of Dextran T40 and DexG T40-20%.

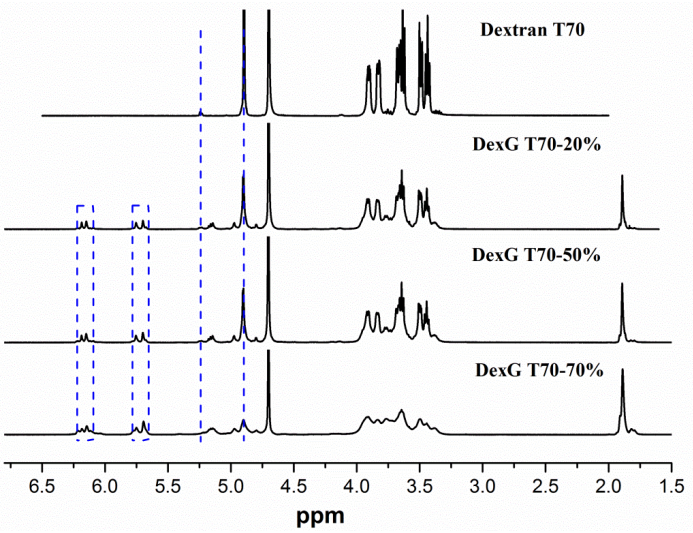

Fig. A.3. The ^{1}H NMR spectra of Dextran T70 and its derivatives DexG with different degree of substitution.

The ^{1}H NMR spectra of Dextran T40, DexG T40-20%, Dextran T70, DexG T70-20%, DexG T70-50% and DexG T70-70% are shown in Fig. A.2 and Fig. A.3, respectively. The DS is defined as the percentage of substituted pyranose rings per 100 rings, and calculated according to our previous study[2]. Briefly, the branching degree of dextran is calculated by the ratio of the integrals at 5.3 and 4.9 ppm, which represents the ratio of the proton at the anomeric carbon of the α-1,3 linkages to the proton at the anomeric carbon of the α-1,6 linkages. The DS of DexG is calculated as *100X/Y*, in which *X* was the average peak area of the protons at the double

bond (i.e., the average of integrals at 5.75 and 6.2 ppm), and *Y* was the integral of the anomeric proton at 4.9 ppm multiplied by (1-branching degree) with the addition of the integral of the anomeric proton at 5.3 ppm multiplied by the branching degree.

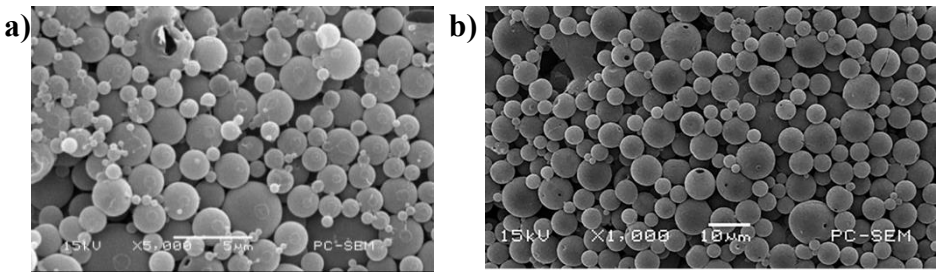

Fig. A.4. SEM images of DexG microgels without Con A (a) and Con A-DexG/Dex-CCH core-shell microgels with hydrophobic surface (b).

REFERENCES

[1] Zhang L, Zhang M, Zhou Q, CHEN J, ZENG F. Solution properties of antitumor sulfated derivative of α-(1→ 3)-D-glucan from Ganoderma lucidum. Bioscience, Biotechnology, and Biochemistry. 2000;64:2172-8.

[2] Yin R, Wang K, Han J, Nie J. Photo-crosslinked glucose-sensitive hydrogels based on methacrylate modified dextran–concanavalin A and PEG dimethacrylate. Carbohydrate Polymers. 2010;82:412-8.

CHAPTER 5 INTEGRATED CLOSED-LOOP INSULIN DELIVERY SYSTEM WITH PROLONGED INSULIN RELEASE BEHAVIOR

*This chapter is derived from an article published in **Materials Science & Engineering C**, 2019, 96, 374-382. Available online: https://doi.org/10.1016/j.msec.2018.11.032.*

5.1 Introduction

Diabetes mellitus is a disorder characterized by the body's inability (Type 1) or deficiency (Type 2) to produce enough insulin in the glucose metabolic process, resulting in high blood glucose levels over a prolonged period [1, 2]. Diabetes currently affects over 382 million people globally [3]. Alternatively to the conventional multi-dose insulin injection, which is painful and inaccurate [4], the artificial pancreas, known also as closed-loop control of blood glucose in diabetes, is a highly desirable therapy for type 1 and advanced type 2 diabetes [5]. The artificial pancreas delivers insulin in response to changes of the glucose level in real-time [6]. Until now, there are two basic strategies to achieve the closed-loop insulin delivery: (i) insulin infusion pumps directed by a control algorithm with a continuous glucose monitor (or sensor), also known as the traditional artificial pancreas in a narrow definition [6] and (ii) chemically controlled systems based on glucose-responsive hydrogels [7], also known as synthetic artificial pancreas [1, 2]. In the last decade, chemically controlled insulin delivery systems have been viewed as a better alternative than pump-based systems in terms of the effectiveness of the closed-loop delivery function, as realization of the process, namely from the continuous glucose-sensing to the glucose-triggered insulin release in a small and implantable system, is much easier compared with that of the process involving insulin pumps [1, 8, 9]. Most of the chemically controlled closed-loop insulin delivery systems developed so far is based on glucose oxidase [10-12], concanavalin A (Con A)-sugar affinity [13] and phenylboronic acid [14]. The Con A-sugar affinity-based system has promise for clinical use. The first *in vivo* test in a live diabetic domestic pig has been done by Taylor's group by using an implantable artificial pancreas made from crosslinkable-dextran/Con A complex [15], and human trials for the

artificial pancreas may begin soon. Our group has also developed a glucose-responsive small and implantable system based on Con A-polysaccharides interaction [16-18]. Both the closed-loop delivery of insulin in response to a change of the blood glucose level [19] and with a long-term supply of insulin [20] are important for diabetes patients. However, a combination of these two goals in a chemically controlled small and implantable system is still challenging yet highly desirable [1].

An integrated or hybrid or composite drug scaffold by introduction of drug-loaded nano- or micro-carriers into 3D micro- or macro-scaffold is a promising way to address the above challenge and have attracted a lot of attentions these years. Zhang's group has incorporated VEGF-containing PLGA/PEG microspheres into an engineered collagen-chitosan scaffold to achieve a prolonged and controlled delivery of growth factors and to enhance the vascularization of soft tissue [21]. They performed an experiment on a rat model. By eight weeks, the integrated scaffold had significantly increased the amount of microvasculature, and the persistent adipose and ECM deposits. Nanda and co-workers developed collagen porous scaffolds hybridized with insulin-releasing PLGA microbeads to control the release of bioactive insulin for a sufficient duration in a cell culture environment, in which the release of insulin can be additionally modulated in porous biodegradable scaffolds for specific cellular requirements [22]. The hybrid scaffolds exhibited an insulin release of nearly 70% after four weeks. By contrast, 85%–95% of the insulin were released from the free microbeads during the same period. Also, the initial burst from the hybrid scaffolds was reduced to less than one-fourth of the initial release from the free microbeads. Besides the application in tissue engineering, integrated systems have also been applied to drug delivery for further protection and control of drugs. In Li's group, a composite hydrogel system containing insulin-loaded glucose-responsive nano-carriers to enhance the oral delivery efficiency of insulin was developed [23]. The outer hyaluronic acid (HA) hydrogel can provide additional protection for insulin and delay the decomposition of nano-carriers in Gastrointestinal (GI) tract. Di and co-workers incorporated insulin-loaded glucose-responsive nano-carriers into HA microgels to avoid the burst release and reduce loss of glucose oxidase in nano-carriers [2]. The blood glucose levels in mice treated with the integrated microgels maintained in the normoglycemic state for up to

8 days without peaks of hyperglycemia, while the blood glucose level in mice treated with the non-integrated microgels (i.e., microgels encapsulating insulins) maintained a normoglycemic state for 1 day.

In the study reported in the present chapter, we developed a novel engineered synthetic artificial pancreas, which was capable of releasing insulin in a glucose-responsive fashion and achieved a prolonged period of release. This novel artificial pancreas was made by means of the integration of Con A-based glucose-responsive microspheres into a biodegradable scaffold (a chitosan hydrogel). The unique properties of chitosan [24-26], including antimicrobial activity, biocompatibility and biodegradability [27, 28], make it a good candidate in the applications of tissue engineering, drug delivery [29-32], immunoadjuvants, food and cosmetics [21]. In the study reported in this paper, glucose-responsive insulin-loaded microspheres were first fabricated via a high-speed shear-emulsion based crosslinking method and then integrated into chitosan hydrogels to make a scaffold-based synthetic artificial pancreas. Chitosan acts as a mechanical support and protection for insulin-loaded microspheres, and the degradation of chitosan hydrogels enables the erosion-dependent leakage of insulin microspheres, thus providing a prolonged closed-loop insulin delivery. The morphology, insulin loading capacity, degradation, *in vitro* insulin release behavior and cytotoxicity of the artificial pancreas (i.e., integrated scaffold) were investigated and discussed in detail.

5.2 Materials and methods

5.2.1 Materials

Concanavalin A (extracted from Jack Bean, M_w= 102 kDa, containing Ca^{2+} and Mn^{2+}) was purchased from Medicago Inc. (Canada). Insulin (bovine pancreas), tris (AR, 99.9 %), and dialysis membranes were obtained from Shanghai Yuanye Bio-Technology Co., Ltd (Shanghai, China). D-glucose anhydrous (AR), cyclohexane, ammonium persulfate and sodium bisulfite were purchased from ENOX (Jiangsu, China). Polyethylene glycol (600) diamethacrylate

(PEGDMA) was obtained from TCI Inc. (USA). Chitosan (viscosity 20-300 cP for 1 wt. % in 1% acidic acid at 25 ℃, degree of deacetylation (D.D) = 75%-85%) was purchased from Sigma Aldrich (St. Louis, MO, USA). Acetic acid, acetone and hydrochloric acid were obtained from Shanghai Lingfeng Chemical Reagent Co. (Shanghai, China). Sodium tripolyphosphate (STPP) was purchased from Macklin Biochemical Co. Ltd. (Shanghai, China). Fluorescamine (FSM), sodium tertraborate decahydrate, boric acid and glucose were obtained from Aladdin Corp.(Shanghai, China). Human dermal fibroblasts cell line (HDF) was supplied by Biovector Science lab, Inc. (Beijing, China) and Cell Counting Kit-8 assay (CCK-8) was purchased from Dojindo Molecular Technologies, Inc. (Kumamoto, Japan). Phosphate buffer saline (PBS, pH7.4) was supplied by Sigma (USA). Deionized water from ultrapure water machine (Sichuan optimal PuChao pure science and technology co., LTD, China) was used for preparation of all the solutions and reagents. Glycidyl methacrylated dextran (Dex-GMA) was synthesized via ring-opening reaction of glycidyl methacrylate with dextran using the same method in our previous study [15]. The degree of substitution (DS) of Dex-GMA used in this study is 26.92 (the ratio of substituted glucopyranosyl rings to unmodified glucopyranosyl rings).

5.2.2 Fabrication of glucose-responsive insulin-loaded microspheres

Glucose-responsive insulin-loaded microspheres were prepared according to our previous work [18] by high-speed water-in-oil (W/O) emulsification based crosslinking method (see Scheme 5.1 a). Briefly, 39.9 g of organic phase containing 39 g of cyclohexane and 0.9 g of Span 80 as stabilizer was emulsified with aqueous phase (2 mL) containing 30.82 mg of Dex-GMA, 3.1 mg of PEGDMA, 1 mL of Con A solution (23.29 mg of pre-activated Con A was dissolved in 1 mL of 0.05 mol/L HCl-Tris buffer solution with pH 7.2) and 1 mL of insulin solution (10 mg of insulin was dissolved in 1 mL of 0.1 mol/L HCl solution) by stirring at 5,000 rpm for 2 min, followed by the addition of 0.925 g of initiator solution (a mixture of 3 mmol/L ammonium persulfate and 3 mmol/L sodium bisulfite). After continuous high-speed dispersion for 20 minutes, the emulsion was mechanically stirred for 24 h to achieve the purpose of further hardening and standing for core-layer microspheres. Then, 150 mL of isopropanol was added,

and the microspheres were separated by centrifugation at 10, 000 rpm. After that, these obtained microspheres were washed with isopropanol and deionized water 3 times, respectively. Finally, the core-layer microspheres were dried by freeze-drying and stored at 4℃ for further use.

5.2.3 Preparation of integrated scaffold

Chitosan (5 mg/mL) was dissolved in 2% acetic acid and then blended with insulin-loaded microspheres (10 mg/mL) in an ultrasonic water bath (Ningbo Scientz Biotechnology Co., LTD., China) for 3h at 25 ℃ to achieve homogeneous mixture [33]. The mixture was then molded in a polytetrafluoroethylene (PTFF) square frame template with 25 square grids (2 mm in height, 10 mm in width, and 2 mm gap between grids) (see Scheme 5.1 b). Next, the template was transferred to a chamber with the temperature of -20℃ for freezing. After 4h, the frozen mold was immersed into 10% (w/v) sodium tripolyphosphate (STPP) solution for 3h at room temperature to crosslink the chitosan hydrogels. The obtained scaffolds were washed with PBS (pH 7.4) and deionized water 3 times, respectively, to remove excessive cross-linkers and acidic reagent. The washed scaffolds were subjected to a second freezing for 4h and freeze-drying for 48h to obtain the final scaffolds. Pure chitosan scaffolds without the integration of insulin-loaded microspheres were prepared under the same condition as a control group for degradation test.

5.2.4 Morphological characterization of microspheres and scaffolds

The morphology of microspheres and scaffolds was determined by a JSM-6360LA scanning electron microscope (SEM) at an accelerating voltage of 15 kV, respectively. Prior to the observation, the specimen was fixed on stubs with sputter coated with gold. At least 50 microspheres from each SEM picture were evaluated with the software Image J and an average size as well as a standard deviation was calculated. For scaffold morphology, both surface and cross-section were observed. The specimens were cryofractured in liquid nitrogen to obtain the cross-section.

5.2.5 Insulin loading capacity

The confirmation of insulin loading as well as insulin quantification in the prepared insulin-loaded microspheres and scaffolds was carried out using fluorescamine (FSM) method for covalent labelling [34]. Aliquots (20 – 150 µL) from insulin stock solution with the concentration of 0.001 mg/mL, 0.01 mg/mL, 0.1 mg/mL and 1 mg/mL prepared in HCl (0.01M) were placed into 2 mL tubes and mixed with 400 µL phosphate buffer (pH 7.4) and 300 µL borate buffer (pH 9.0, 100 mM), respectively. 75 µL of FSM solution in acetone (0.125 mg/mL) was added into each tube. After shaking vigorously for 30 s, the derivatization could proceed for three more minutes after adjusting the volume to 1mL with distilled water. Finally, fluorescence intensities of the insulin solutions were measured by using a microplate reader (Bio Tech, USA) with an excitation monochromatic wavelength and emission monochromatic wavelength of 390 and 475 nm, respectively. The insulin concentration in the obtained standard curves was in the range of 0.025-5.0 µg/mL. For insulin quantification, at certain time intervals, 100 µL of the releasing medium was taken out by a micropipette and mixed with borate buffer and FSM solution using the above method. The released amount of insulin was then determined using a microplate reader after derivatization of insulin with FSM according to the calibration curve (see Fig. B.1 in APPENDIX B). The insulin entrapment capacity (EC) during the insulin loading process, i.e., microspheres fabrication, the loading capacity (LC) of microspheres and scaffolds were calculated by the following equations [35]:

$$\mathrm{EC}\% = \frac{\text{Loaded insulin}}{\text{Total insulin}} \times 100\% \quad (5\text{-}1)$$

$$\mathrm{LC(microsphere)}\% = \frac{\text{Loaded insulin}}{\text{Microsphere weight}} \times 100\% \quad (5\text{-}2)$$

$$\mathrm{LC\ (scaffold)}\% = \frac{\text{Loaded insulin}}{\text{Scaffold weight}} \times 100\% \quad (5\text{-}3)$$

where total insulin is the initial amount of insulin added in the loading process, and the loaded insulin for microspheres and scaffolds was measured following a prolonged release experiment after all the loaded insulin was released.

5.2.6 Scaffold degradation test

In vitro degradation of chitosan scaffolds with or without microspheres was evaluated for 28 days with the addition of lysozyme (Sigma, powder, white, ~70000U/mg) from chicken egg white. Briefly, scaffolds were immersed in 5 mL of PBS (pH 7.4) containing 6 μg/mL lysozyme [4], and incubated at 37 ℃ to mimic the *in vivo* conditions. The degradation medium was replaced with fresh solution every 72 hours. At predetermined times, samples with the same volume were washed with deionized water and freeze-dried for mass loss measurement. The percentage mass loss was determined by the following equation [5]:

$$\text{Mass loss}\% = \frac{[W_i - W_t]}{W_i} \times 100\% \qquad (5\text{-}4)$$

where W_i is the initial dry weight of the scaffold and W_t is the final weight after 0, 1, 2, 4, 7, 14 and 28 days of incubation. The degradation ratio was determined for each scaffold. The experiment was performed in triplicates.

5.2.7 In vitro insulin release test

5.2.7.1 Glucose-responsive release test

The integrated scaffolds immersed in 1.5 mL of PBS (pH 7.4) were placed in a dialysis bag (MD34(8000-14000) D, Solarbio, USA) and then the whole entity was put into a 50 mL tube with 15 mL release medium (PBS, pH 7.4, with different glucose concentrations). Insulin release was analyzed by incubating these scaffolds at 37℃ ± 0.5℃ while shaking (100 r/min) as a function of time. Responsive release of insulin was achieved in response to stepwise changes of glucose concentration (4-10-1 mg/mL). At appropriate time intervals, 100 μL of the released insulin in the tube was taken out, fluorescent labeled by fluorescamine and quantitatively measured by using a microplate reader at an excitation wavelength of 390 nm and emission wavelength of 475 nm. The release study was continued after replacement with an equal volume of fresh solution to maintain a constant volume. The release data were

expressed as mean ± standard deviation (S.D.) based on three independent measurements. The glucose-responsive release behavior of free microspheres was performed by using the same procedure for comparison.

5.2.7.2 Prolonged release experiments

The following prolonged release experiments were designed to prove that scaffolds can release insulin for a longer time compared with microspheres. For the release from free microspheres, 8 mg of insulin-loaded microspheres were placed into a dialysis bag with 1.5 mL PBS (pH 7.4), and the dialysis bag was then put into a release tube containing glucose solution (10 mg/mL, PBS 7.4). For the release from integrated scaffolds, four scaffolds were placed into a release tube containing glucose solution (10 mg/mL, PBS 7.4) with 6 μg/mL lysozyme. The release medium was replaced with fresh solution every 24 hours, and the released insulin was measured using the above FSM method. After prolonged release tests, the free microspheres and scaffolds were collected, washed, and freeze-dried for 48 hours. Subsequently, glucose-stimulus release experiments (see 2.7.1) were performed on the microspheres and scaffolds again to see the difference of their glucose-responsiveness after prolonged experiments. The release data were expressed as mean ± standard deviation (S.D.) based on three independent measurements. Student's t-test (Origin 2019) was utilized to determine statistical significance between two groups. The $p < 0.05$ was considered as statistically significant.

5.2.8 Insulin activity measurement

The activity of released insulin was determined by analysis of the structural stability by using both fluorescence (FL) spectrophotometer and circular dichroism (CD). For FL measurement, samples were tested at an excitation wavelength of 276 nm and emission wavelength of 305 nm, and the standard insulin solution was set to 0.02 mg/mL [36]. For the CD study, released insulin and standard insulin were measured at 25 ◦C with a cell path length of 0.1 cm, a bandwidth of 1 nm, and a response time of 1 s. The standard insulin solution was prepared in

PBS (pH 7.4) to a final concentration of 0.1 mg/mL. The samples were scanned from 190 to 260 nm at a resolution of 1.0 nm and a scanning speed of 100 nm/min, and the data were compared at the characteristic peaks of about 208 nm and 223 nm. All circular dichroism data were expressed as mean residue ellipticity [3, 6]. For both the FL and CD tests, each sample was repeated three times, and the final data is the average of three measurements.

5.2.9 In vitro cell proliferation evaluation

Human dermal fibroblasts cell line (HDF Biovector Science lab, Inc.) was cultured for 24h in a 5% CO_2 atmosphere at 37 °C in high glucose Dulbecco's modified Eagle's medium (DMEM, GE Healthcare Life Sciences), supplemented with 10 % (v/v) Fetal Bovine Serum (FBS, Gibco, USA) and 1 % (v/v) streptomycin penicillin (Sigma, USA), all provided by Life technologies. Then the HDF cells were activated by the addition of 0.25% Trypsin-EDTA (1X) (gibco, Canada) for 3 min. A certain concentration of cell suspension (2000 cells/100 μL) was formed by dilution. Next, sterilized scaffolds (by soaking in 75% alcohol and then immersing in PBS buffer for 2 days) were added in 100 μL of DMEM and 100 μL of HDF cells suspension. Cells were seeded to the medium without scaffolds for reference (negative control). The medium was changed every three days. After culturing for 1, 4 and 7 days, the DMEM medium was removed and 200 μL of Counting Kit-8 (CCK-8, Dojindo Molecular Technologies, Kumamoto, Japan) solution was added to each well, after which the cells were incubated for another 2h at 37 °C. The optical density (O.D.) was then evaluated by measuring the absorbance of the CCK-8 solution using a microplate reader (Bio-Tech, USA) at a wavelength of 450 nm.

5.3 Results and Discussion

5.3.1 Fabrication and characterization of insulin-loaded microspheres

Concanavalin A-sugar affinity-based glucose-responsive microspheres made by Dex-GMA/Con A (the structure of Dex-GMA and Con A can be seen in Scheme 5.1c) were used to

encapsulate insulin and supply a chemically controlled closed-loop insulin delivery function [16-18]. A high-speed shear-emulsion based crosslinking method was implemented for the preparation of insulin loaded glucose-responsive microspheres (see Scheme 5.1 a).

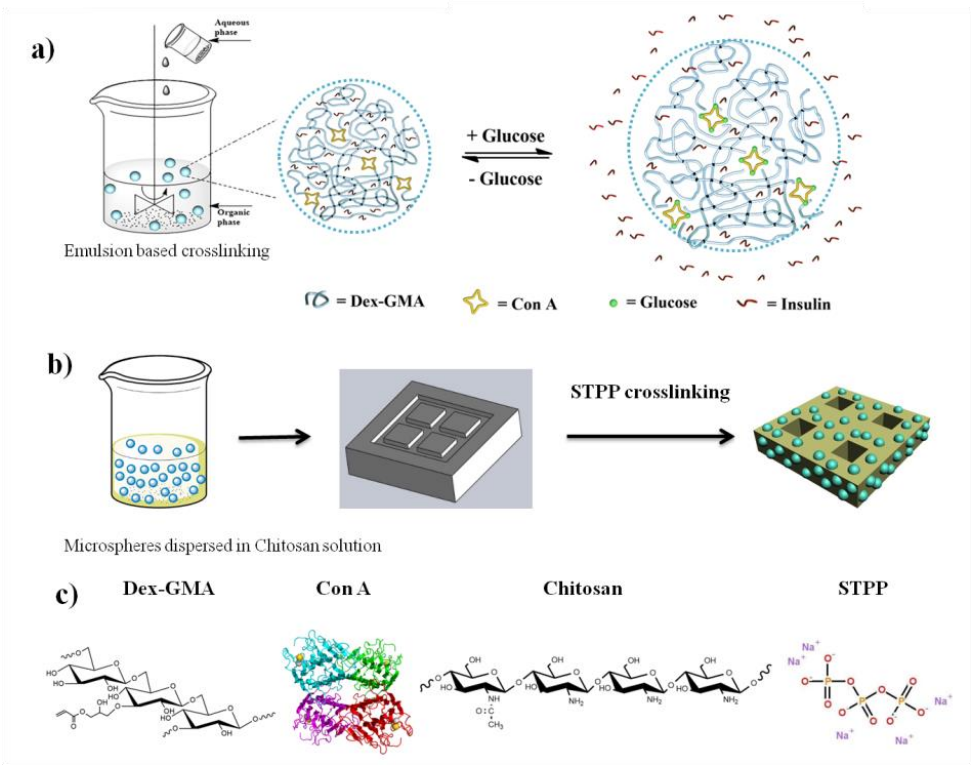

Scheme 5.1. Fabrication process and glucose-responsive structural change of microspheres (a); preparation process of integrated scaffold (b); and the chemical structure of Dex-GMA, Con A, Chitosan and STPP (c).

The morphology and size distribution based on SEM observation are shown in Fig. 5.1. The microspheres had a spherical shape with smooth surface (Fig. 5.1a and Fig. 5.1b). The size distribution profile of microspheres (Fig. 5.1c) indicated a high monodispersity with the average diameter of 2.3 ± 0.6 µm. Most of the microspheres (over 90%) were between 1 and 3 µm in diameter. With the increase of high-speed (5000 rpm) shearing time from 20 min (Fig. 5.1a and 5.1b) to 40 min (Fig. B.2 a in the supplementary data) and 70 min (Fig. B.2b), the size scale of obtained microspheres decreased from micro-level (1-3µm in Fig.5.1a) to nano-level (200-500 nm in Fig. B.2a and < 100 nm in Fig. B.2b). During the insulin loading process, the insulin loading capacity and encapsulation capacity of the obtained microspheres are about 10.0 % ± 0.1 % and 78.0 % ± 0.7 %, respectively. These insulin-loaded microspheres were used for

further preparation of the integrated scaffold and insulin release test.

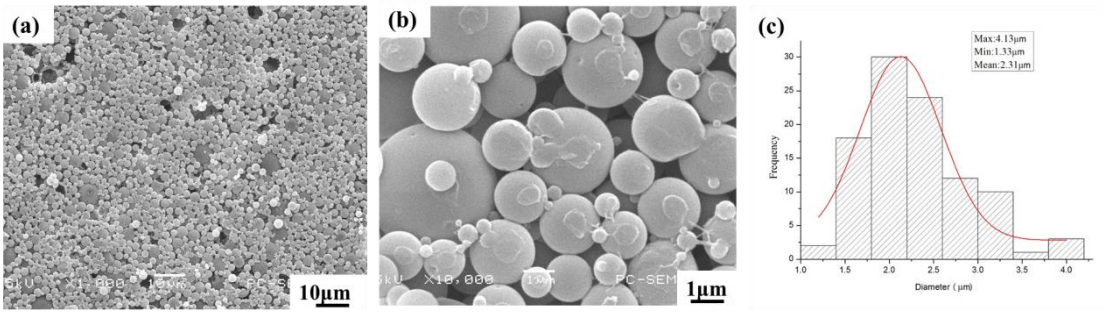

Fig. 5.1. SEM images of insulin-loaded microspheres with low (a) and high (b) magnification and (c) size distribution of microspheres.

5.3.2 Preparation and characterization of integrated scaffold

Insulin-loaded microspheres with glucose-responsiveness were embedded in chitosan hydrogels to form an integrated scaffold as a synthetic artificial pancreas. The integrated scaffold was prepared by freeze-drying the mixture of microspheres and chitosan aqueous solution casted in a template, followed by crosslinking by STPP (see Scheme 5.1). The overall appearance of the integrated scaffold is shown in Fig. 5.2a, the surface morphology is shown in Fig. 5.2b, and the cross-section morphology is shown in Fig. 5.2c. From Fig. 5.2, it can be found that an interconnected porous microstructure was obtained on both the surface (Fig. 5.2b) and cross-section (Fig. 5.2c) with more regular pores on the cross-section than on the surface. The average pore size and porosity was calculated by gray analysis method using the software Image J [37]. The average diameter of the pores is calculated as 2.19±0.78 μm, and the porosity of the integrated scaffold is 42.40±5.64%. In addition, micro-protrusions which are related to microspheres can be observed in both Fig. 5.2b and 5.2c (yellow circle), indicating that insulin-loaded microspheres were distributed throughout the scaffold. The insulin loading capacity of the integrated scaffold was about 4.6%±0.2%.

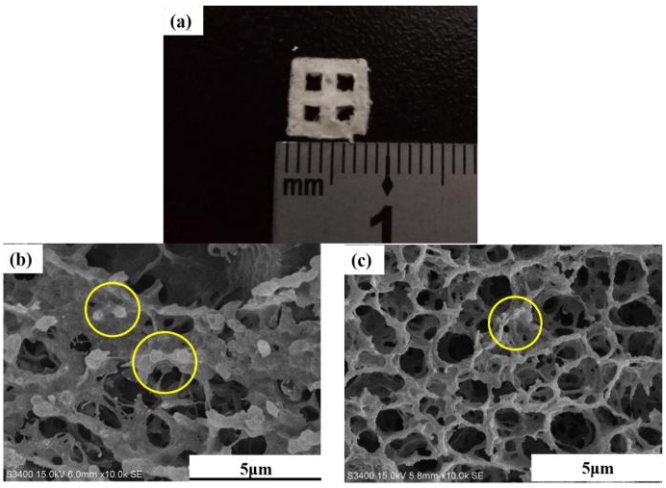

Fig. 5.2. The integrated scaffold containing insulin-loaded microspheres. (a) the overall appearance, (b) surface morphology, (c) cross-section morphology.

5.3.3 Scaffold degradation behavior

In the literature, lysozyme degrades chitosan by cleaving 1,4-β-glycosidic bond in the chitosan backbone, and chitosan was shown to be resistant to lysozyme after deacetylation to the extent of 85 % or more [14, 38]. Therefore, in this study, we chose the chitosan with 75-85% degree of deacetylation and a 6 µg/mL concentration of lysozyme similar to *in vivo* environment for *in vitro* degradation test [39]. The degradation of the chitosan scaffold without microspheres (chitosan-only scaffold) and the integrated scaffold with the insulin-loaded microspheres were analyzed by monitoring weight loss during the incubation period of 4 weeks in PBS (pH 7.4) with the presence of lysozyme (Fig. 5.3). The weight loss profile demonstrated a faster weight loss of integrated scaffold in the first week compared to chitosan-only scaffold, indicating that the leak out of insulin-loaded microspheres happened mainly in the first week. After two weeks of degradation, the integrated scaffold reached similar mass loss as the chitosan-only scaffold, which revealed the insulin-loaded microspheres dispersed inside the integrated scaffold may be completely leaked to the environment. The overlapped degradation curves of these two scaffolds during the last two weeks confirmed that there were no microspheres left in the integrated scaffold after two weeks' degradation. At the end of degradation test (four weeks), the integrated scaffold and chitosan-only scaffold had similar mass remaining of about 83%.

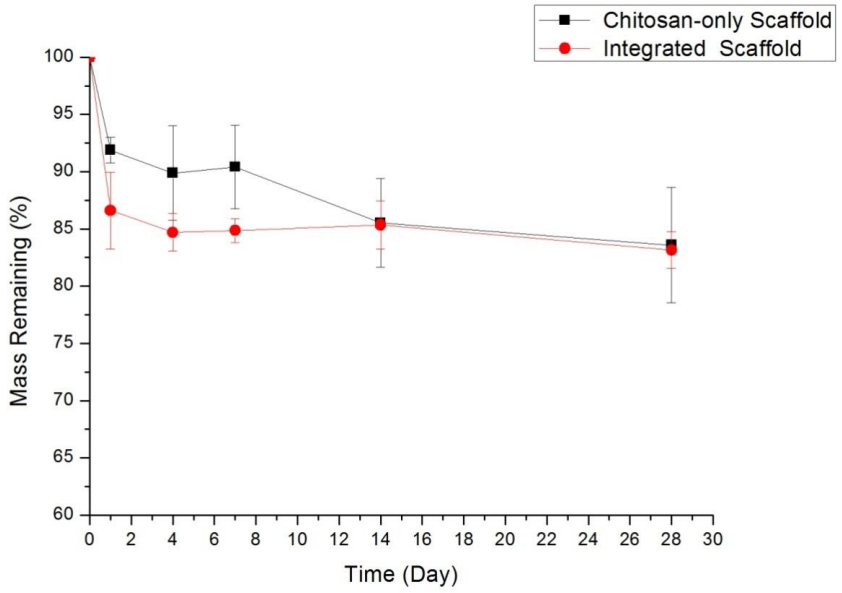

Fig. 5.3. Degradation behavior of the scaffolds with or without integration of insulin-loaded microspheres (represented by the integrated scaffold and chitosan-only scaffold) for four weeks in PBS (pH 7.4) with an *in vivo*-like concentration of lysozyme (6 μg/mL). Data is presented as mean ± SD (n = 3).

5.3.4 In vitro insulin release analysis

Generally, insulin dosing can be separated into two regimens: basal and bolus insulin, where basal insulin is responsible for fasting conditions with normal glucose level, while bolus insulin is required for hyperglycemia conditions after meals [6]. Insulin delivery rates should increase rapidly after each meal and return to basal rates within 2-3 h [40]. Therefore, in this study, *in vitro* insulin release under glucose-stimulus changing from hyperglycemia condition (4 and 10 mg/mL) to normal glucose level (1 mg/mL), which mimics the physiological conditions, was tested on the closed-loop insulin delivery behavior of the synthetic artificial pancreas (i.e., the integrated scaffold)

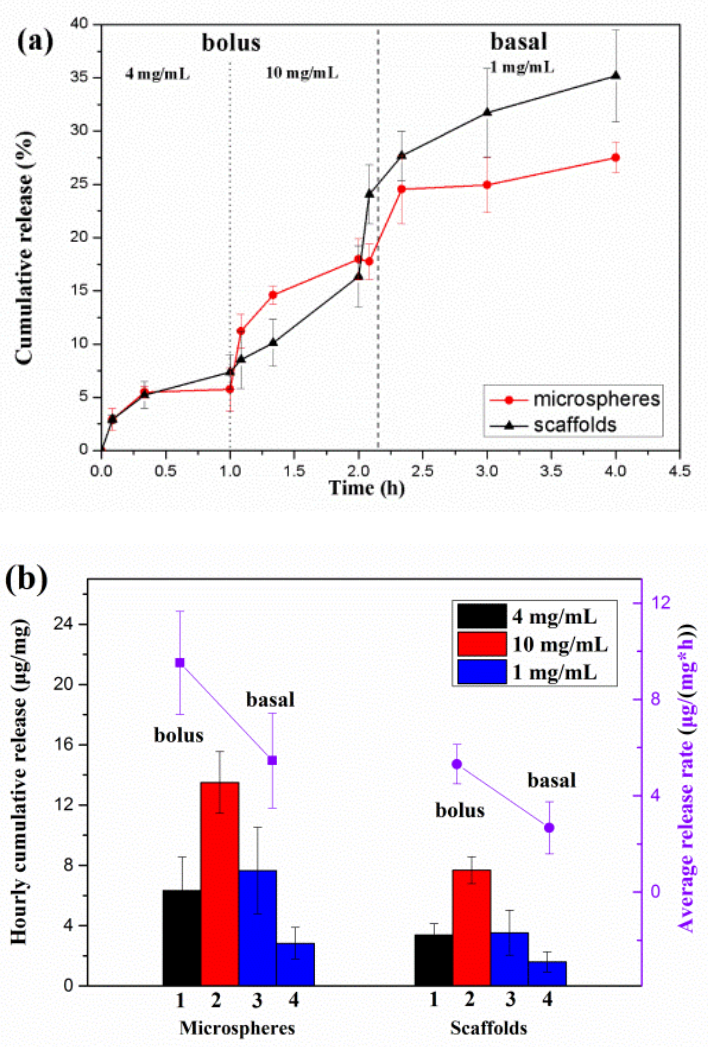

Fig. 5.4. (a) The *in vitro* bolus and basal insulin release kinetics under stepwise changed glucose-stimulus at 37 ℃ and (b) hourly cumulative release amount and average release rate of insulin from free microspheres and scaffolds as a function of bolus and basal glucose stimuli. Data is presented as mean ± SD (n = 3).

Bolus and basal insulin release kinetics as a function of bolus (4 and 10 mg/mL) and basal (1 mg/mL) glucose stimuli are shown in Fig. 5.4. Hourly cumulative release amount and average release rate of insulin from both free microspheres and scaffolds were obtained under stepwise changing glucose-stimulus. It can be seen from Fig. 5.4a that the insulin release kinetics from free microspheres and scaffolds has the similar pattern - the trend of gradual increase in high glucose concentration (4 and 10 mg/mL) and being steady in low glucose concentration (1 mg/mL). When subject to the periodic change of glucose concentration from the hyperglycemic

to normal level, insulin release from both the free microspheres and the integrated scaffolds exhibited bolus and basal release rate and release amount (Fig. 5.4b) in response to the change of glucose concentration. The aforementioned results suggest that the integrated scaffold can keep the glucose-responsive insulin release property inherited from the corresponding microspheres, which is accounted for by the reversible crosslinking/dissociation structural change of the Con A/Dex-GMA network in response to the increase/decrease of glucose level [19] (see Scheme 5.1a).

To verify whether the integrated scaffolds can provide a longer-time insulin supply than the free microspheres, we designed the prolonged *in vitro* insulin release test under the hyperglycemia condition for the comparison of the integrated scaffold and free microspheres. In order to perform the insulin release from the integrated scaffold under degradation condition, it is noted that 6 μg/mL of lysozyme was added in the release medium of the integrated scaffold to achieve the scaffold degradation and erosion-dependent leakage of embedded microspheres. From Fig. 5, it can be seen that the insulin release from the integrated scaffolds shows significant difference versus that from the free microspheres. Fig. 5.5a and Fig. 5.5b show the cumulative insulin release profiles and daily insulin release amount from the integrated scaffolds as well as their corresponding free microspheres. After a 1-day release period, an initial burst of about 17% was observed in the release profile of free microspheres, which was nearly 2-fold of the initial release from the integrated scaffolds.

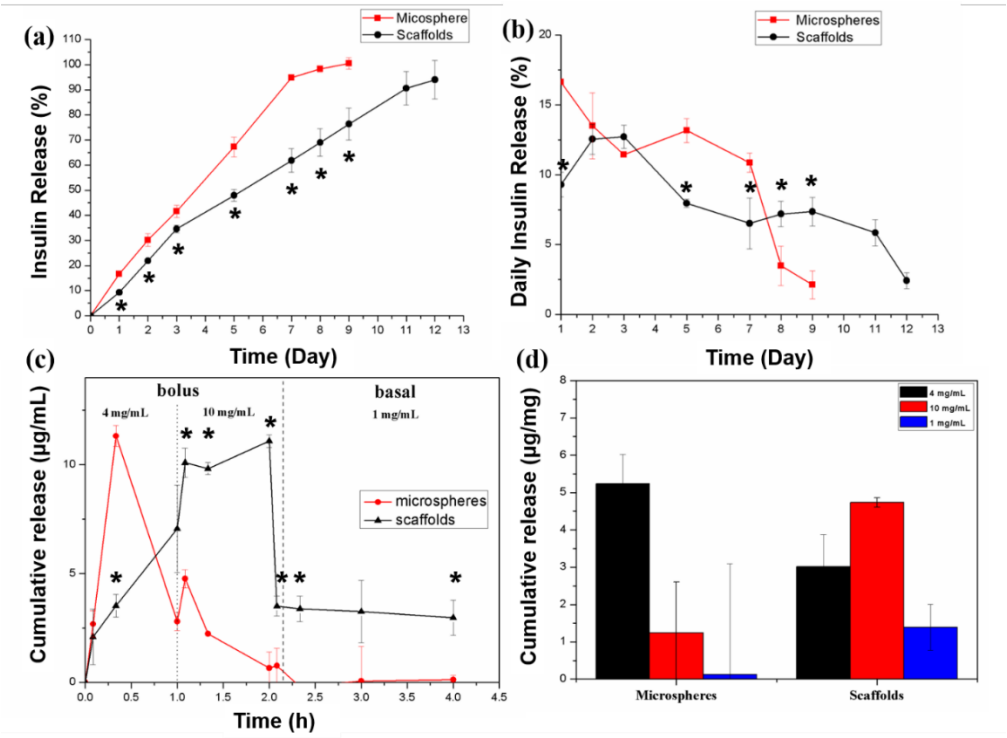

Fig. 5.5. (a) Cumulative insulin release; (b) daily release amount for 12 days from integrated scaffold and for 9 days from free microspheres under hyperglycemia environment; (c) insulin release concentration under stepwise changed glucose-stimulus; (d) accumulated insulin release amount after 1 h-releasing in each glucose level (4, 10 and 1 mg/mL) from integrated scaffold and free microspheres after 12 days and 9 days prolonged exposure to hyperglycemia environment, respectively. Data is presented as mean ± SD (n = 3). Significant differences are marked with asterisks (*p < 0.05 versus microspheres group).

In addition, the integrated scaffolds exhibited an insulin release of nearly 92 % after 12 days; however, during 9 day-release, nearly 98 % of the insulin was released from the free microspheres. These results indicated a prolonged insulin release behavior as well as lower burst release from the integrated scaffolds compared with the corresponding free microspheres. Moreover, as shown in Fig. 5.5b, the insulin release amount on day 2 and day 3 from the integrated scaffolds demonstrated a gradual increase, but the insulin release from the free microspheres obviously decreased during the same period. It is worth mentioning that in the first few days, the integrated scaffold had faster weight loss than the chitosan-only scaffold (Fig. 5.3), suggesting that the embedded microspheres underwent a gradual leaching process owing

to the degradation of chitosan.

Furthermore, to substantiate that the scaffold can supply a prolonged insulin release and, in the meantime, maintain the closed-loop insulin delivery in response to the change of glucose level, we performed glucose-stimulus insulin release experiments after prolonged release. Fig. 5.5c and Fig. 5.5d exhibit that the integrated scaffold can maintain the glucose-responsive insulin release behavior after 12 day-release, while the free microspheres could not release insulin in response to the change of glucose level after 9 day-release, revealing that the integrated scaffold has the ability of combining closed-loop insulin delivery and long-term insulin supply.

5.3.5 Bioactivity of released insulin

Fluorescence (FL) spectrophotometer and circular dichroism (CD) spectroscopy were used to evaluate the tertiary and secondary conformational structure of insulin, respectively [41]. Figure 5.6 compares the FL and CD spectra of released insulin from the integrated scaffolds and the free microspheres with that of standard insulin. From Fig. 5.6a and Fig. 5.6b it can be found that the standard insulin and released insulin from the integrated scaffolds and the free microspheres after 1 day-release and exhibited a similar emission peak at about 305 nm on FL spectra and similar characteristic peaks at 208 nm and 223 nm on CD spectra, indicating that the tertiary and secondary conformational structure of released insulin can match that of native insulin (the native insulin here served as standard insulin). Besides, after accumulated insulin release for a relatively long period (12 days for the integrated scaffolds and 9 days for the free microspheres, as shown in Section 3.4), the tertiary and secondary structure of released insulin were tested again by FL and CD spectra (see Fig. 5.6c and 5.6d). There was no significant conformational change observed for the released insulin from the integrated scaffolds according to the FL and CD spectra. However, the released insulin from free microspheres demonstrated shifted fluorescence emission peak compared with standard insulin, indicating the tertiary structure of released insulin from free microspheres after 9 day-release may be significantly changed. As a result, these results revealed that compared with the free microspheres, the

scaffolds may be able to protect the bioactivity of insulin for a longer time.

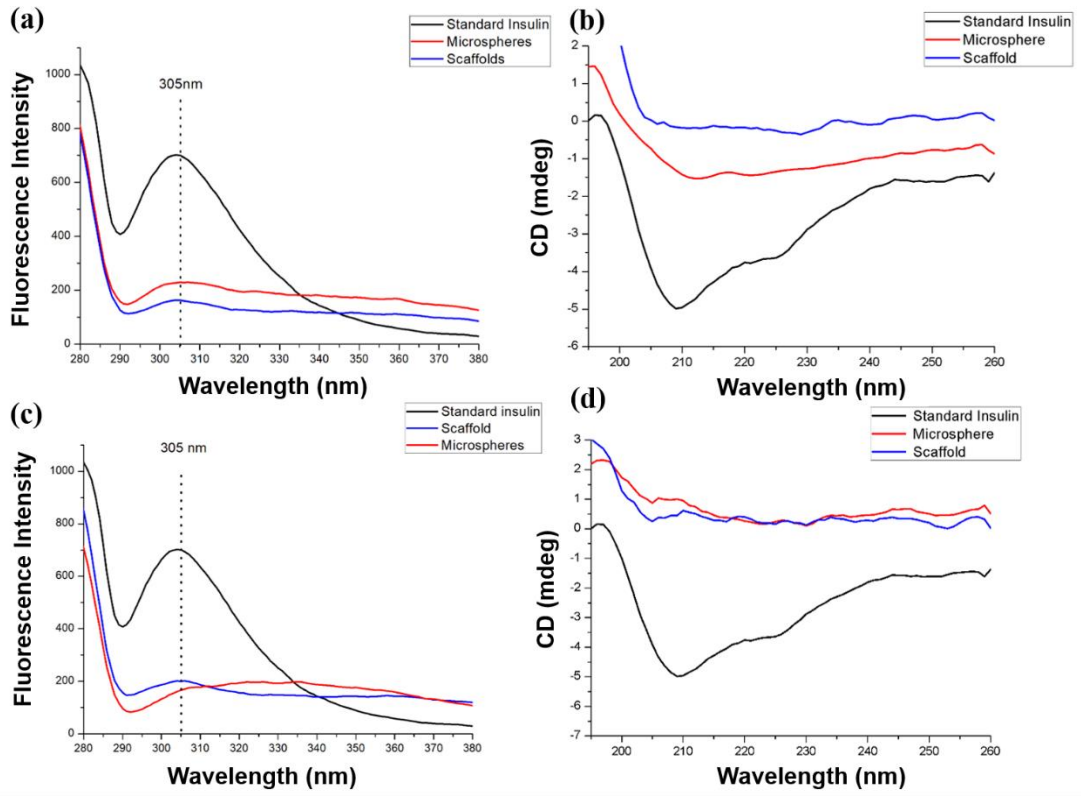

Fig. 5.6. Fluorescence (a, c) and circular dichroism (b, d) spectra of released insulin and standard insulin. The released insulin from integrated scaffold and free microspheres after the first day (a, b) and the last day (c, d) of prolonged insulin release was tested for comparison.

5.3.6 Cell proliferation

The proliferation of HDF cells on the integrated scaffold was assessed by CCK-8 assay [42, 43] at days 1, 4 and 7 (see Fig. 5.7) in order to understand any potential cytotoxicity of the integrated scaffold. The experiment showed that proliferation of HDF cells on the integrated scaffold increased gradually throughout the incubation period for up to 7 days. No statistically significant differences were observed in cell growth for 1 and 4 days with the integrated scaffold compared with the control group ($p < 0.05$ was considered as significant difference in the T-test). Although there was significant difference after 7 days in cell growth between the

integrated scaffold and control group, the cell viability on the integrated scaffold at day 7 was 30 % higher than that at day 4. These results demonstrated the HDF cells can proliferate well on the integrated scaffold, suggesting the integrated scaffold is of safe for biomedical applications [44].

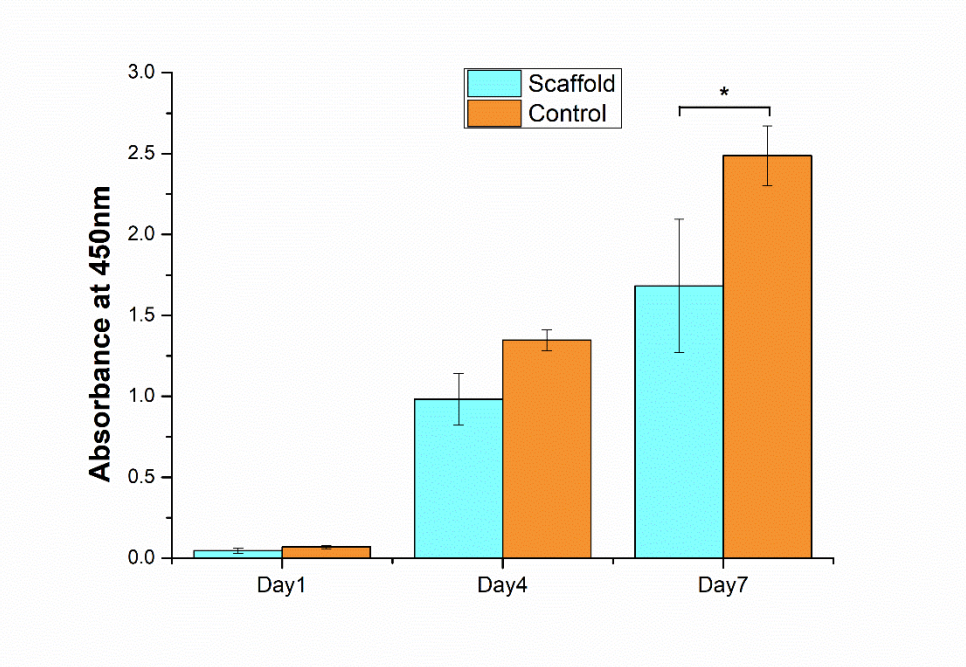

Fig. 5.7. Cell proliferation of HDF cells cultured on integrated scaffold and in the medium without scaffold (control group) after 1, 4 and 7 days. Data is presented as mean ± SD (n = 6).

5.4 Conclusions

In this study, glucose-responsive insulin-loaded microspheres were firstly fabricated via a high-speed shear-emulsion based crosslinking method and then integrated into chitosan hydrogels to make a scaffold-based synthetic artificial pancreas. *In vitro* experiments showed the scaffold exhibited a longer insulin supply as well as a lower burst release compared with free microspheres and could keep the glucose-responsive insulin release property inherited from the corresponding microspheres even after 12 day-release. The released insulin was suggested to remain active, and the culture of HDF cells on the scaffold showed good cell proliferation during 7 days incubation. These results suggested the scaffold-based synthetic artificial

pancreas have a great promise in the application of insulin delivery for diabetes care.

REFERENCES

[1] Gordijo CR, Koulajian K, Shuhendler AJ, Bonifacio LD, Huang HY, Chiang S, et al. Nanotechnology-Enabled Closed Loop Insulin Delivery Device: In Vitro and In Vivo Evaluation of Glucose-Regulated Insulin Release for Diabetes Control. Advanced Functional Materials. 2011;21:73-82.

[2] Di J, Yu J, Ye Y, Ranson D, Jindal A, Gu Z. Engineering synthetic insulin-secreting cells using hyaluronic acid microgels integrated with glucose-responsive nanoparticles. Cellular and Molecular Bioengineering. 2015;8:445-54.

[3] Mo R, Jiang T, Di J, Tai W, Gu Z. Emerging micro- and nanotechnology based synthetic approaches for insulin delivery. Chemical Society reviews. 2014;43:3595-629.

[4] Jeandidier N, Boivin S. Current status and future prospects of parenteral insulin regimens, strategies and delivery systems for diabetes treatment. Advanced Drug Delivery Reviews. 1999;35:179-98.

[5] Cobelli C, Renard E, Kovatchev B. Artificial pancreas: past, present, future. Diabetes. 2011;60:2672-82.

[6] Wang Y, Dassau E, Francis J. Doyle I. Closed-Loop Control of Artificial Pancreatic β -Cell in Type 1 Diabetes Mellitus Using Model Predictive Iterative Learning Control. IEEE Transactions on Biomedical Engineering. 2010;57:211-9.

[7] Ravaine V, Ancla C, Catargi B. Chemically controlled closed-loop insulin delivery. Journal of Controlled Release. 2008;132:2-11.

[8] Uchiyama T, Watanabe J, Ishihara K. Implantable polymeric artificial pancreas. Journal of Biomaterials Science, Polymer Edition. 2004;15:1237-62.

[9] Yu J, Zhang Y, Ye Y, Disanto R, Sun W, Ranson D, et al. Microneedle-array patches loaded with hypoxia-sensitive vesicles provide fast glucose-responsive insulin delivery. Proceedings of the National Academy of Sciences of the United States of America. 2015;112:8260-5.

[10] Qi W, Yan X, Duan L, Cui Y, Yang Y, Li J. Glucose-sensitive microcapsules from glutaraldehyde cross-linked hemoglobin and glucose oxidase. Biomacromolecules.

2009;10:1212-6.

[11] Chen Z, Wang J, Sun W, Archibong E, Kahkoska AR, Zhang X, et al. Synthetic beta cells for fusion-mediated dynamic insulin secretion. Nature Chemical Biology. 2017;14:86.

[12] Naveed A. Bakh ABC, Michael A. Weiss, Robert S. Langer, Daniel G. Anderson, Zhen Gu, Sanjoy Dutta, Michael S. Strano. Glucose-responsive insulin by molecular and physical design. Nature Chemistry. 2017;9:937-43.

[13] Kim JJ, Park K. Modulated insulin delivery from glucose-sensitive hydrogel dosage forms. Journal of Controlled Release. 2001;77:39-47.

[14] Jin X, Zhang X, Wu Z, Teng D, Zhang X, Wang Y, et al. Amphiphilic random glycopolymer based on phenylboronic acid: synthesis, characterization, and potential as glucose-sensitive matrix. Biomacromolecules. 2009;10:1337-45.

[15] Taylor MJ, Gregory R, Tomlins P, Jacob D, Hubble J, Sahota TS. Closed-loop glycaemic control using an implantable artificial pancreas in diabetic domestic pig (Sus scrofa domesticus). International Journal of Pharmaceutics. 2016;500:371-8.

[16] Yin R, Wang K, Du S, Chen L, Nie J, Zhang W. Design of genipin-crosslinked microgels from concanavalin A and glucosyloxyethyl acrylated chitosan for glucose-responsive insulin delivery. Carbohydrate Polymers. 2014;103:369-76.

[17] Yin R, Han J, Zhang J, Nie J. Glucose-responsive composite microparticles based on chitosan, concanavalin A and dextran for insulin delivery. Colloids and surfaces B, Biointerfaces. 2010;76:483-8.

[18] Yin R, Tong Z, Yang D, Nie J. Glucose-responsive insulin delivery microhydrogels from methacrylated dextran/concanavalin A: preparation and in vitro release study. Carbohydrate Polymers. 2012;89:117-23.

[19] Hovorka R. Closed-loop insulin delivery: from bench to clinical practice. Nature Reviews Endocrinology. 2011;7:385-95.

[20] Tomar L, Tyagi C, Kumar M, Kumar P, Singh H, Choonara YE, et al. In vivo evaluation of a conjugated poly(lactide-ethylene glycol) nanoparticle depot formulation for prolonged insulin delivery in the diabetic rabbit model. International Journal of Nanomedicine. 2013;8:505-20.

[21] Zhang Q, Hubenak J, Iyyanki T, Alred E, Turza KC, Davis G, et al. Engineering

vascularized soft tissue flaps in an animal model using human adipose–derived stem cells and VEGF+ PLGA/PEG microspheres on a collagen-chitosan scaffold with a flow-through vascular pedicle. Biomaterials. 2015;73:198-213.

[22] Nanda HS, Kawazoe N, Zhang Q, Chen S, Chen G. Preparation of collagen porous scaffolds with controlled and sustained release of bioactive insulin. Journal of Bioactive and Compatible Polymers. 2014;29:95-109.

[23] Li L, Jiang G, Yu W, Liu D, Chen H, Liu Y, et al. A composite hydrogel system containing glucose-responsive nanocarriers for oral delivery of insulin. Materials Science & Engineering C, Materials for Biological Applications. 2016;69:37-45.

[24] Xiaohui W. Structures and Properties of Chitosan-Starch-Sodium Benzoate Blend Films. Wuhan University Journal. 2003.

[25] Hu X, Tang Y, Wang Q, Li Y, Yang J, Du Y, et al. Rheological behaviour of chitin in NaOH/urea aqueous solution. Carbohydrate Polymers. 2011;83:1128-33.

[26] Hu X, Du Y, Tang Y, Wang Q, Feng T, Yang J, et al. Solubility and property of chitin in NaOH/urea aqueous solution. Carbohydrate Polymers. 2007;70:451-8.

[27] Adekogbe I, Ghanem A. Fabrication and characterization of DTBP-crosslinked chitosan scaffolds for skin tissue engineering. Biomaterials. 2005;26:7241-50.

[28] Mi F-L, Shyu S-S, Wu Y-B, Lee S-T, Shyong J-Y, Huang R-N. Fabrication and characterization of a sponge-like asymmetric chitosan membrane as a wound dressing. Biomaterials. 2001;22:165-73.

[29] Zhang X, Zhang H, Yin L, Hu R, Qiu T, Yin Y, et al. A pH-Sensitive Nanosystem Based on Carboxymethyl Chitosan for Tumor-Targeted Delivery of Daunorubicin. Journal of Biomedical Nanotechnology. 2016;12:1688-98.

[30] Yang Y, Wang S, Wang Y, Wang X, Wang Q, Chen M. Advances in self-assembled chitosan nanomaterials for drug delivery. Biotechnology Advances. 2014;32:1301-16.

[31] Wang Q, Zhang N, Hu X, Yang J, Du Y. Chitosan/polyethylene glycol blend fibers and their properties for drug controlled release. Journal of Biomedical Materials Research Part A. 2008;85A:881-7.

[32] Hu R, Zheng H, Cao J, Davoudi Z, Wang Q. Synthesis and In Vitro Characterization of Carboxymethyl Chitosan-CBA-Doxorubicin Conjugate Nanoparticles as pH-Sensitive Drug

Delivery Systems. Journal of Biomedical Nanotechnology. 2017;13:1097-105.

[33] Zhang Q, Hubenak J, Iyyanki T, Alred E, Turza KC, Davis G, et al. Engineering vascularized soft tissue flaps in an animal model using human adipose-derived stem cells and VEGF+PLGA/PEG microspheres on a collagen-chitosan scaffold with a flow-through vascular pedicle. Biomaterials. 2015;73:198-213.

[34] Basan H, Gümüşderelioğlu M, Tevfik Orbey M. Release characteristics of salmon calcitonin from dextran hydrogels for colon-specific delivery. European Journal of Pharmaceutics and Biopharmaceutics. 2007;65:39-46.

[35] Li X, Fu M, Wu J, Zhang C, Deng X, Dhinakar A, et al. pH-sensitive peptide hydrogel for glucose-responsive insulin delivery. Acta Biomaterialia. 2017;51:294-303.

[36] Elleri D, Biagioni M, Allen JM, Kumareswaran K, Leelarathna L, Caldwell K, et al. Safety, efficacy and glucose turnover of reduced prandial boluses during closed - loop therapy in adolescents with type 1 diabetes: a randomized clinical trial. Diabetes, Obesity and Metabolism. 2015;17:1173-9.

[37] Yin R, Zhang N, Wang K, Long H, Xing T, Nie J, et al. Material design and photo-regulated hydrolytic degradation behavior of tissue engineering scaffolds fabricated via 3D fiber deposition. Journal of Materials Chemistry B. 2017;5:329-40.

[38] Tomihata K, Ikada Y. In vitro and in vivo degradation of films of chitin and its deacetylated derivatives. Biomaterials. 1997;18:567-75.

[39] Tomar L, Tyagi C, Kumar M, Kumar P, Singh H, Choonara YE, et al. In vivo evaluation of a conjugated poly (lactide-ethylene glycol) nanoparticle depot formulation for prolonged insulin delivery in the diabetic rabbit model. International Journal of Nanomedicine. 2013;8:505.

[40] Weinzimer SA, Steil GM, Swan KL, Dziura J, Kurtz N, Tamborlane WV. Fully automated closed-loop insulin delivery versus semiautomated hybrid control in pediatric patients with type 1 diabetes using an artificial pancreas. Diabetes Care. 2008;31:934-9.

[41] Kelly SM, Jess TJ, Price NC. How to study proteins by circular dichroism. Biochimica et Biophysica acta. 2005;1751:119-39.

[42] Kim SE, Song SH, Yun YP, Choi BJ, Kwon IK, Bae MS, et al. The effect of immobilization

of heparin and bone morphogenic protein-2 (BMP-2) to titanium surfaces on inflammation and osteoblast function. Biomaterials. 2011;32:366-73.
[43] Liu H, Peng H, Wu Y, Zhang C, Cai Y, Xu G, et al. The promotion of bone regeneration by nanofibrous hydroxyapatite/chitosan scaffolds by effects on integrin-BMP/Smad signaling pathway in BMSCs. Biomaterials. 2013;34:4404-17.
[44] Ye T, Yan S, Hu Y, Ding L, Wu W. Synthesis and volume phase transition of concanavalin A-based glucose-responsive nanogels. Polymer Chemistry. 2014;5:186-94.

APPENDIX B

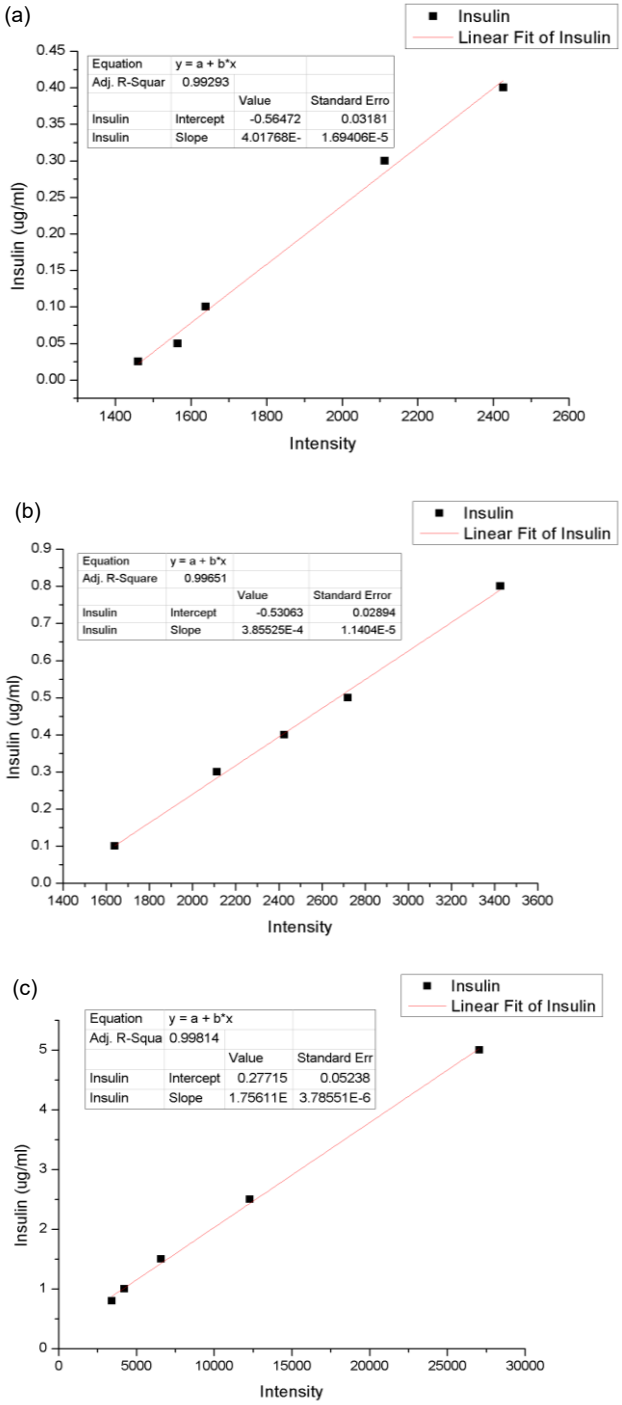

Fig. B.1 Insulin calibration curves generated at excitation and emission wavelength of 390 nm and 475 nm from a series of insulin concentrations using fluorescamine as indicator. Three curves were obtained according to fluorescence intensity:

Intensity $\leqslant$ 2050 (a); 2050 < Intensity $\leqslant$ 3825 (b); Intensity > 3825 (c).

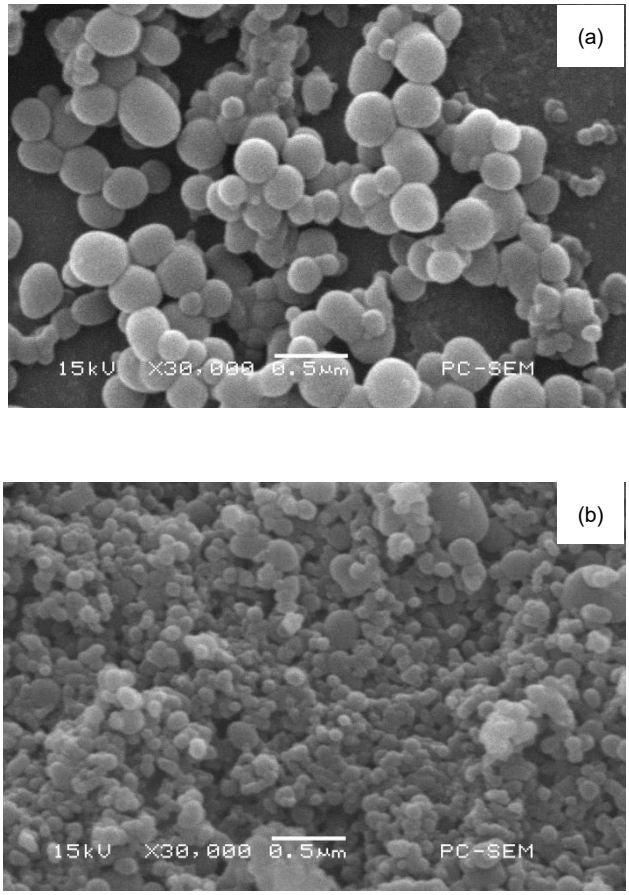

Fig. B.2 SEM images of insulin-loaded microspheres obtained with different shearing time at high speed (5000 rpm): 40 min (a) and 70 min (b)

CHAPTER 6 MATHEMATICAL MODELLING

This chapter is submitted as ***Ruixue Yin*** *et al. "MATHEMATICAL MODELLING OF GLUCOSE-RESPONSIVE BEHAVIOR OF CONCANAVALIN A-SUGAR AFFNITY BASED HYDROGELS" to* ***Theoretical and Experimental Chemistry*** *in 2021 (under review).*

6.1 Introduction

An artificial closed-loop system, known as the artificial pancreas, can quickly respond to changes of blood sugar levels and release insulin instantly. It aims to be a better therapeutic method than the insulin multi-injection method and has attracted widespread attention in the fields of materials, mechanics, and biology. A chemically controlled closed-loop system relies on responsive materials that can quickly respond to slight but critical changes in the environment. The changes in the environment can include temperature, pH, electrolyte concentration, biomolecules (such as glucose, enzymes, antigens, etc.) and fields (electric and magnetic fields). Glucose responsive materials that can sense blood glucose concentration and release insulin in response to changes of glucose level have a great potential to develop the chemically controlled closed-loop insulin delivery system for improved diabetes care [1-4].

At present, three glucose-responsive materials have been investigated to develop the chemically controlled closed-loop insulin delivery system. There is glucose oxidase, concanavalin A (Con A), and phenylboronic acid. Among them, the Con A-sugar affinity-based system is the most promising one for clinical use due to its strongest specificity to glucose [4]. The first *in vivo* test in a live diabetic domestic pig was performed by Taylor's group by using an implantable artificial pancreas made from crosslinked dextran-Con A hydrogel.

This chapter presents a mathematical model for the glucose-responsive process of Con A-sugar affinity based chemically controlled system based on the swelling and variable diffusion coefficient theory [5]. The model was preliminarily validated based on the swelling ratio Q.

After that, the influence of glucose concentration as well as other parameters on the swelling ratio was studied.

6.2 The swelling model of the Con A-DexG hydrogel

The hydrogel in this study has two major parts: Con A and DexG. DexG has carbon-carbon double bonds, and the double bonds can crosslink to form the chemical crosslinking of the hydrogel. DexG also has terminal glucose groups, and the terminal glucose groups can bind with Con A to form physical affinity crosslinking of the hydrogel. The crosslinked network absorbs water to an equilibrium swelling state, thus allowing the transport of macromolecular drugs, nutrients, and cellular wastes.

The Con A and DexG mixture acts as a concentrated solution at full hydration with osmotic forces causing the hydrogel swell. The combination of covalent and affinitive cross-linking bonds makes the hydrogel act like a spring against this force. When competitive glucoses are introduced into the hydrogel network, the amount of affinitive crosslink bonds decreases, leading to less resistance to osmotic forces and enhanced swelling.

Flory-Rehner [6] proposed a theory to explain the relationship between crosslink density and the swelling of rubber compounds. Peppas and Merrill [7] modified the original equation to establish a polymer network swelling equation:

$$\frac{1}{\bar{M}_c} = \frac{2}{\bar{M}_n} - \frac{\frac{\bar{v}}{V_1}\cdot[\ln(1-v_{2,s})+v_{2,s}+\chi_1 {v_{2,s}}^2]}{v_{2,r}\cdot\left[\left(\frac{v_{2,s}}{v_{2,r}}\right)^{\frac{1}{3}}-0.5\frac{v_{2,s}}{v_{2,r}}\right]} \tag{6-1}$$

where $\overline{M_c}$ is the number average molecular mass of the polymer chain between cross-links, $\overline{M_n}$ is the number average molecular mass of the polymer chain, $\bar{v}$ is the partial specific volume of the polymer, V_1 is the molar volume of water, χ_1 is the Flory-Huggins polymer-solvent interaction parameter, $v_{2,s}$ is the polymer fraction of the hydrogel at equilibrium swelling, $v_{2,r}$ is the polymer fraction of the hydrogel after gel formation.

The swelling ratio can be calculated by the ratio of the polymer fraction of the hydrogel after gel formation to the polymer fraction of the hydrogel at equilibrium swelling, shown in equation 6-2:

$$Q = \frac{v_{2,r}}{v_{2,s}} \tag{6-2}$$

The volume increase caused by swelling will be regarded as a decrease in the polymer composition, so the swelling ratio will be greater than 1.

The total number of cross-links was determined by finding the respective number of affinity and covalent bonds. The number of covalent bonds was assumed to equal the number of methacrylate groups measured for DexG molecules as it was assumed that each bind to a Con A molecule. Affinity cross-links were calculated by solving the binding equations (4-4) to (4-7) in Chapter 4. It was assumed that there was only one dextran binding to one Con A tetramer. Although this is not strict, the model is greatly simplified.

According to the binding equations (4-4) to (4-7) in Chapter 4, the equilibrium constants of DexG-Con A and Con A-glucose binding are given by

$$K_1 = \frac{c_{\mathrm{DexGConA}}}{(c_{\mathrm{DexG\ total}} - c_{\mathrm{DexGConA}})(c_{\mathrm{ConA\ total}} - c_{\mathrm{DexGConA}} - c_{\mathrm{GluConA}})} \tag{6-3}$$

$$K_2 = \frac{c_{\mathrm{GluConA}}}{(c_{\mathrm{Glu\ total}})(c_{\mathrm{ConA\ total}} - c_{\mathrm{DexGConA}} - c_{\mathrm{GluConA}})} \tag{6-4}$$

where $c_{\mathrm{ConA\ total}}$ is the initial concentration of Con A, $c_{\mathrm{DexG\ total}}$ is the initial concentration of DexG, $c_{\mathrm{Glu\ total}}$ is the initial concentration of glucose that is set to 0.022mol/L based on the concentration of blood sugar after meal in diabetic patients (it is noted that the glucose concentration could be any value within the range of hyperglycemia, and here just shows a typical concentration), c_{DexGConA} is the concentration of resultant DexG-Con A complex, c_{GluConA} is the concentration of resultant Glu-Con A complex, and K_1 and K_2 are the equilibrium constants of DexG-Con A and Con A-glucose binding reactions, respectively. It should be note that in the calculation of K_2, the assumption of $c_{\mathrm{Glu\ total}} \approx c_{\mathrm{Glu\ total}} - c_{\mathrm{Glu\ ConA}}$ is applied owing to the value of $c_{\mathrm{Glu\ total}}$ is much higher than that of $c_{\mathrm{Glu\ ConA}}$.

In order to calculate $c_{DexGConA}$, Equation (6-4) needs to be rearranged and substituted into Equation (6-3). This leads to a quadratic equation, i.e.:

$$K_1 c_{DexGConA}{}^2 = (K_1 c_{DexG\ total} + K_1 c_{ConA\ total} + K_2 c_{Glu\ total} + 1) c_{DexGConA} + K_1 c_{ConA\ total} c_{DexG\ total} \quad (6\text{-}5)$$

By calculating the concentration of covalent bonds and affinity cross-links, the average molecular weight between crosslinks can be calculated:

$$\bar{M}_c = \frac{c_p \bar{M}_n}{c_{DexGConA} + c_{covalent}} \quad (6\text{-}6)$$

where c_p is the concentration of polymer DexG in the hydrogel, and $c_{covalent}$ can be calculated by the following equation:

$$c_{covalent} = c_{substituent\ group} = c_{DexG\ total} \times \text{The number of substituents in a chain}$$
$$= c_{DexG\ total} \times \left(\frac{62580}{162} \times branching\ degree + 2\right) \times DS \quad (6\text{-}7)$$

where the branching degree is characterized as 4.8% and the DS is characterized as 20.6% by NMR spectrum.

The concentrations of the components are governed by the degree of swelling; therefore, calculation of the swelling must be done iteratively. The swollen polymer fraction can be used to calculate the mesh size of the hydrogel [8]:

$$\xi = v_{2,s}{}^{-\frac{1}{3}} \cdot \left(C_n \cdot \frac{2\overline{M_c}}{M_r}\right)^{\frac{1}{2}} \cdot l \quad (6\text{-}8)$$

where C_n is the Flory characteristic ratio, M_r is the molecular mass of repeat unit, l is the unit length along the polymer backbone.

Then, the mesh size can be used to calculate the variable diffusion coefficient D based on the deviation from the liquid phase diffusivity[9, 10]:

$$D = D_0 \left(1 - \frac{a}{\xi}\right)^{e^{\frac{-1}{Q-1}}} \quad (6\text{-}9)$$

where D_0 is the liquid phase diffusivity of the solute, a is the hydrodynamic radius of the solute.

6.3 Results and discussion

6.3.1 Parameters calculation and validation

By using MATLAB software, the parameters can be calculated according to equations (6-1) to (6-9). The initial values and parameters calculated are shown in Table 6.1.

For model validation, the calculated swelling ratio Q was compared with the obtained Q by experiments in [11]. At the glucose level of 0.022 mol/L, the measured equilibrium swelling ratio Q of glucose-responsive Con A-DexG hydrogel samples by weighting method was about 4.75 ± 0.06 (n=3), while the calculated Q was 6.625 by the above mathematical model. The values are on the same order of magnitude, but the calculated result is not within the error bar of experimental result. There might be a structural reason for this disagreement. It is noted that the weighting method to get the swelling data has significant operating error; and the assumptions that were made in mathematical modelling may cause significant modelling errors. Nevertheless, the mathematical modelling may help to predict the swelling and diffusion tendency besides experiments.

Table 6.1 Initial values and parameters calculated based on equations 6-1 to 6-9.

Parameters	Value	References
$c_{\text{ConA total}}$	2.28×10^{-4} mol/L	--
$c_{\text{DexG total}}$	4.18×10^{-4} mol/L	--
$c_{\text{Glu total}}$	0.022mol/L	--
K_1	5354L/mol	[13]
K_2	323L/*mol*	[13]
c_{p}	4.18×10^{-4} mol/L	--
$v_{2,\text{r}}$	0.106g/g	--
$\overline{M_n}$	62580g/mol	[43]
χ_1	0.48	[44]
$\bar{v}$	0.62	[44]
V_1	18cm^3/mol	[44]
C_n	5	[44]
M_r	162g/mol	[44]
l	4.6×10^{-10}m	[44]
a	7.5nm	[44]
D_0	5.5×10^{-11} m^2/s	[44]
c_{covalent}	1.77×10^{-3}mol/L	Calculated
c_{DexGConA}	1.432×10^{-4}mol/L	Calculated
$\overline{M_c}$	27345.779g/mol	Calculated
$v_{2,s}$	0.016	Calculated
ξ	7.5×10^{-8}m	Calculated
Q	6.625	Calculated
D	$5.036 \times 10^{-11}\text{m}^2/\text{s}$	Calculated

6.3.2 Influence of glucose concentration on swelling and diffusion behavior

The parameter values at different glucose levels were calculated by MATLAB programming to

discuss the influence of glucose concentration on the calculation results of the model. The range of glucose concentration was 0-0.06 mol/L.

(1) the concentration of DexG-Con A complex $c_{DexGConA}$

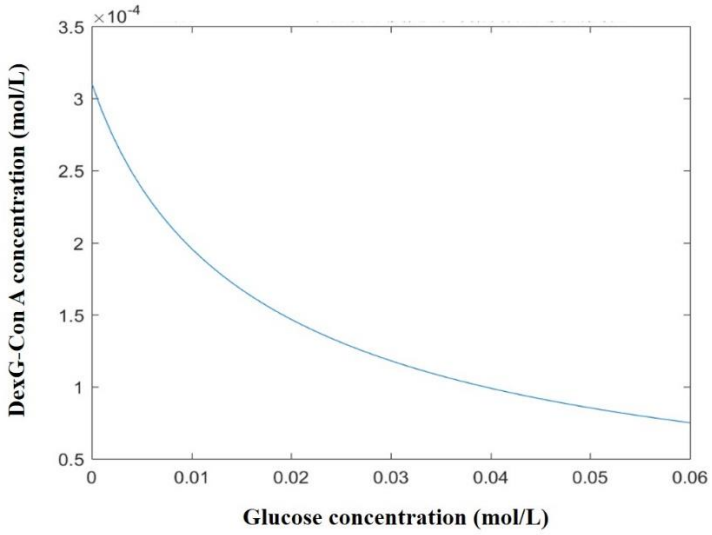

Fig. 6.1 The concentration change of the generated DexG-Con A complex with varied glucose concentration.

As it can be seen from Fig. 6.1, the concentration of generated DexG-Con A complex decreases with increase of glucose level. According to the ligand competition equilibrium equations (4-4) and (4-5) in Chapter 4, with an increase of the glucose concentration, the chemical equilibrium of equation (4-5) shifts to the right side of the equation, generating more Con A-Glu complex. Meanwhile, the amount of Con A binding sites decreases, which also promotes the left shift of equation (4-4), leading to the decrease of DexG-Con A complex.

(2) the number average molecular mass of the polymer chain between cross-links $\overline{M_c}$

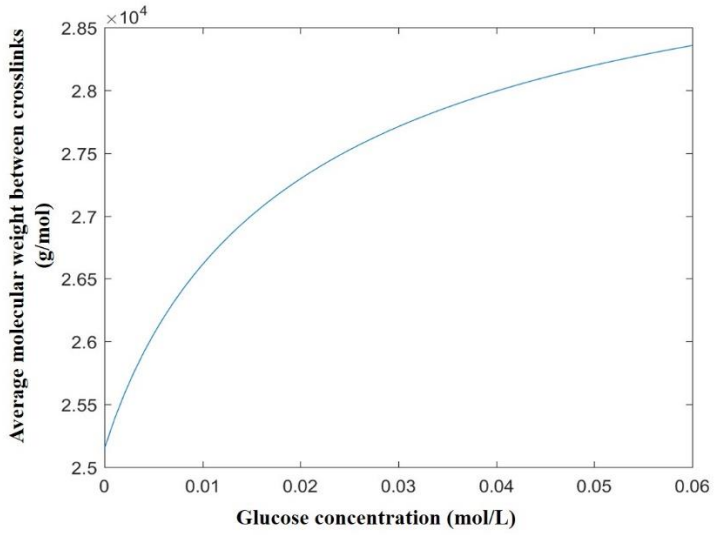

Fig. 6.2. The change of number average molecular mass of the polymer chain between cross-links with varied glucose concentration.

According to the aforementioned discussion, the concentration of DexG-Con A complex decreases with increased glucose concentration, resulting in a looser molecular network. The number average molecular mass of the polymer chain between cross-links increases correspondingly.

(3) the swelling ratio Q

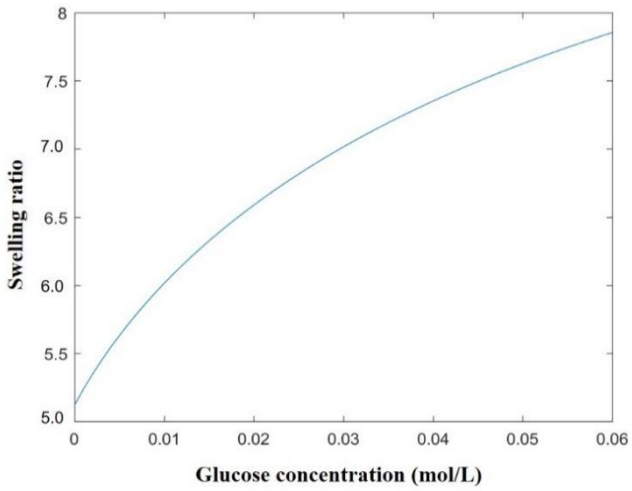

Fig. 6.3 The swelling ratio change with varied glucose concentration

The calculated Q>1 indicates that the hydrogel swells in the glucose solution. With the increase of glucose concentration, the swelling degree of hydrogel increases, and Q value increases,

which is in good agreement with the conclusion obtained by experiments in our previous study [11].

(4) the polymer fraction of the hydrogel at equilibrium swelling $v_{2,s}$

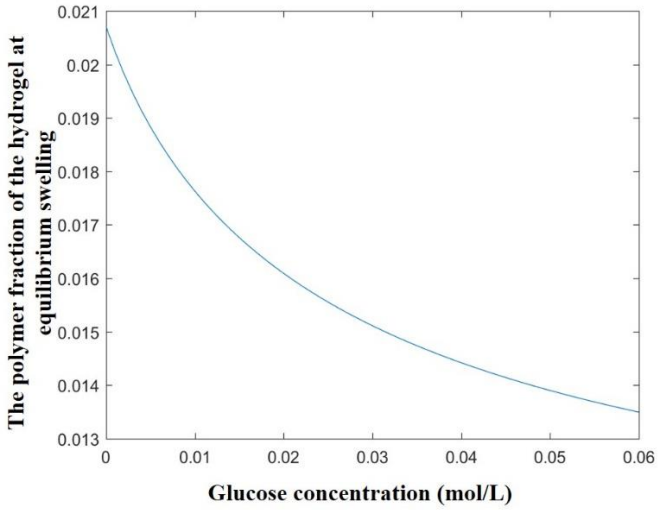

Fig. 6.4 The polymer fraction of the hydrogel at equilibrium swelling change with varied glucose concentration.

As discussed above, with the increase of glucose concentration, the swelling degree of the hydrogel increases. Accordingly, more water enters the hydrogel system, leading to the decrease of the volume fraction of the polymer at equilibrium swelling.

(5) the mesh size ξ

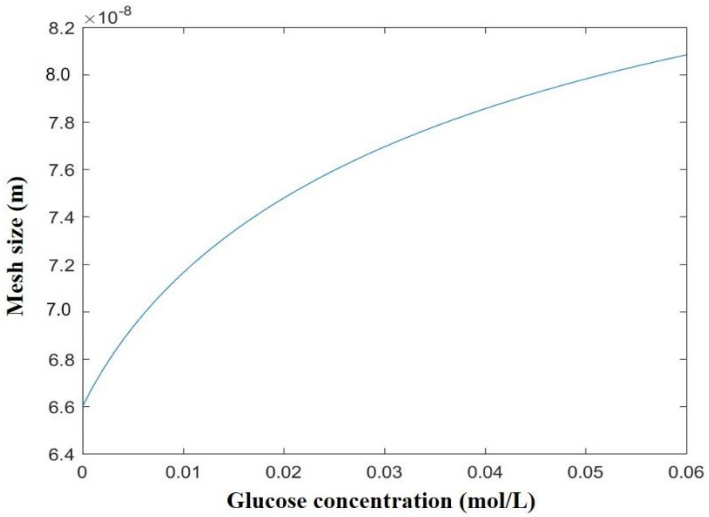

Fig. 6.5 The mesh size change with varied glucose concentration

As glucose concentration increases, the swelling ratio increases and the molecular network of the hydrogel becomes looser and looser, leading to an increase of the mesh size.

(6) the diffusion coefficient D

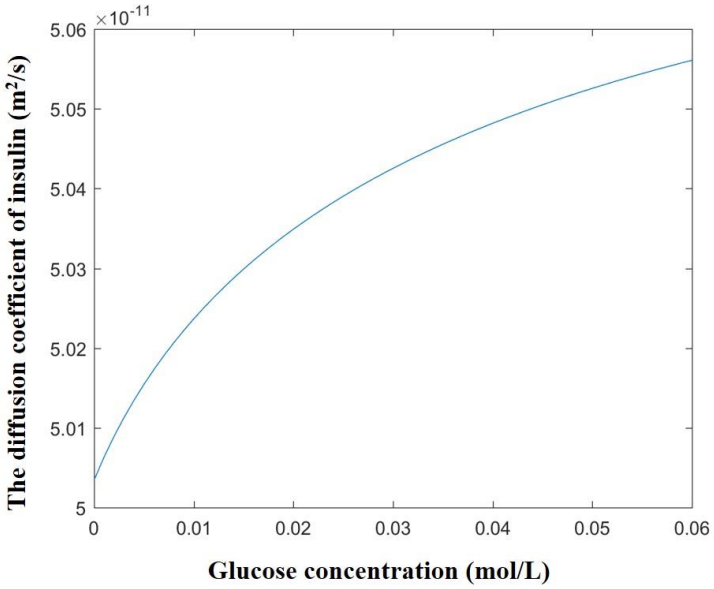

Fig. 6.6 The relationship between the variable diffusion coefficient of insulin and glucose concentration.

The diffusion coefficient governs the insulin release rate during drug release process. As can be seen in Fig. 6.6, the diffusion coefficient of insulin in the hydrogel gradually increases with an increase of glucose concentration. It is reasonable that as the mesh size of the hydrogel increases, it is easier for insulin to release through the hydrogel network.

6.4 Conclusions

In this study, a glucose-responsive swelling model controlled by seven main equations was established and solved to investigate the glucose-responsive behavior of Con A-DexG hydrogel. The model was validated by the comparison of calculated swelling ratio Q and the measured Q obtained by weighting method. The model may be a supplementary to experimental methods to predict the glucose-responsive behavior. The effect of glucose concentration change on the swelling model was also explored. This study was a preliminary work for mathematical

modeling and simulation of the glucose-responsive process of Con A-sugar affinity based chemically controlled systems. By the control of variables Q and D, the molecular structure and composition of Con A-DexG hydrogel may be possible to be tailored designed to meet the specific need of patients.

REFERENCES

[1] Jin X, Zhang X, Wu Z, Teng D, Zhang X, Wang Y, et al. Amphiphilic random glycopolymer based on phenylboronic acid: synthesis, characterization, and potential as glucose-sensitive matrix. Biomacromolecules. 2009;10:1337-45.

[2] Kim JJ, Park K. Modulated insulin delivery from glucose-sensitive hydrogel dosage forms. Journal of Controlled Release. 2001;77:39-47.

[3] Qi W, Yan X, Duan L, Cui Y, Yang Y, Li J. Glucose-sensitive microcapsules from glutaraldehyde cross-linked hemoglobin and glucose oxidase. Biomacromolecules. 2009;10:1212-6.

[4] Taylor M, Gregory R, Tomlins P, Jacob D, Hubble J, Sahota T. Closed-loop glycaemic control using an implantable artificial pancreas in diabetic domestic pig (Sus scrofa domesticus). International Journal of Pharmaceutics. 2016;500:371-8.

[5] Lamberti G. How mathematical modeling tools are helping the pharmaceutical sciences. International Journal of Pharmaceutics. 2015;496:157-8.

[6] Flory PJ, Rehner Jr J. Statistical mechanics of cross-linked polymer networks I. Rubberlike elasticity. The Journal of Chemical Physics. 1943;11:512-20.

[7] Flory PJ. Principles of polymer chemistry: Cornell University Press; 1953.

[8] Mason MN, Metters AT, Bowman CN, Anseth KS. Predicting controlled-release behavior of degradable PLA-b-PEG-b-PLA hydrogels. Macromolecules. 2001;34:4630-5.

[9] Lustig SR, Peppas NA. Solute diffusion in swollen membranes. IX. Scaling laws for solute diffusion in gels. Journal of Applied Polymer Science. 1988;36:735-47.

[10] Peppas NA, Reinhart CT. Solute diffusion in swollen membranes. Part I. A new theory. Journal of Membrane Science. 1983;15:275-87.

[11] Yin R, Wang K, Han J, Nie J. Photo-crosslinked glucose-sensitive hydrogels based on methacrylate modified dextran–concanavalin A and PEG dimethacrylate. Carbohydrate Polymers. 2010;82:412-8.

CHAPTER 7 CONCLUSIONS AND FUTURE WORK

7.1 Conclusions

In this thesis, the principle or mechanism of the Con A-based chemically controlled closed-loop insulin delivery system has been characterized and explained. Based on the principle, systems with modulated insulin release rate and prolonged insulin supply period have been designed. Also, a mathematical model for the glucose-responsive process of Con A-sugar system based on swelling and variable diffusion coefficient theory has been developed. The work presented in this thesis has demonstrated that all the research objectives proposed in Chapter 1 have been achieved and the conclusions can be summarised as follows:

(1) With respect to Objective 1, the competitive displacement of glucose from Con A-DexG complex is possible for two reasons. The first reason is that the affinity of Con A-glucose is similar to the affinity of the terminal groups (on DexG) with Con A. The second reason is that the glucose molecules may have a chance to bind with the remaining Con A sites. The principle of the Con A-based system, especially glucose triggering the dissociation of glycogen composites from Con A, is valid.

(2) With respect to Objective 2, the chemically controlled closed-loop insulin delivery system with different Con A-DexG compositions can maintain bolus and basal insulin release in response to different glucose concentrations, and the network composition can affect the burst release, release rate and overall release amount of insulin.

(1) With respect to Objective 3, the integrated system can achieve a longer insulin delivery as well as a lower burst release compared with the free microsphere and can keep the glucose-responsive insulin release property inherited from the free microsphere after 12 days of release.

(2) With respect to Objective 4, the simplified mathematical model for the Con A-based system is valid. The swelling ratio Q and diffusion coefficient D are two variables in the model, and they can help design the molecular structure of the hydrogel (i.e., a mixture of Con A and DexG) with a potential to design a personalized insulin delivery system.

7.2 Contributions

This thesis has several contributions in the field of drug delivery and the sub-field of insulin delivery. In the field of drug delivery, this thesis has provided a robotic model for drug delivery systems, and this model is a general reference framework for any intelligent drug delivery system. Indeed, with this model, the Con A-based insulin delivery system is a molecular robot, which may lead to a new field called molecular robots as opposed to the existing field of molecular machines. It is worth mentioning that in mechanical engineering, a machine is usually with no intelligence, but a robot has an intelligence. Thus, robots can perform more intelligent tasks that machines for human beings. Another contribution in the field of drug delivery is that the principle of Con A-based system has a generalized implication to drug delivery systems, namely via a network deformation process along with the binding and dis-binding of molecules in the network may come up with a real-time and event driven automatic responsive drug delivery system.

In the field of insulin delivery for diabetes care, this thesis has consolidated our understanding of the principle of Con A-based systems, especially having successfully addressed the controversy surrounding the principle. This thesis has also pioneered a personalised responsive insulin delivery, which can delivery insulin more precisely to individual patients. This improved precision in insulin delivery is important, as both low and high glucose levels are harmful.

7.3 Future work

Along with the work presented in this thesis, some further studies that may be needed are as follows.

First, improvement of the mathematical model for the Con A-based system is warranted. The equations in this study are empirical-based, and the variables such as swelling ratio Q and

diffusion coefficient D are event-variant parameters rather than time-variant. The proposed model in Chapter 6 cannot be applied to predict the time-varied insulin release dynamics. In future work, the time-dynamic drug release process and the hydrogel swelling process need to be coupled through the extension of Fick's law.

Second, considering the heterogeneity of individual diabetes patients regarding the manifestations of disease, symptoms, co-morbidities, genetic predisposition, and variance in molecular sensitivity to drugs, personalized medicine, which refers to the tailoring of medical treatments based on individual characteristics of each patient has gained more attention in diabetes care. Sufficient insulin should be delivered for each patient according to different degrees of insulin resistance. For the development of the future chemically controlled closed-loop insulin delivery system, there is a high demand of developing a system, composition of which can be varied to achieve the desired response rate based on individual requirements for each patient. To achieve this goal, a study is warranted on finding characteristics of patients that are responsible for individual requirements, with which to derive individual demands of insulins by combining both glucose level and these characteristics.

Third, the design of the Con A-DexG affinity based closed-loop insulin delivery system needs to be optimized to improve the stability, reliability, robustness and/or resilience of the system.

Finally, combining different insulin sources in the chemically controlled closed-loop system is another worthy research direction in the future. It is noted that there are different types of exogenous insulin in clinics, including ultra-short acting, short acting, lente, semi-lente, and ultra-lente insulin with different onsets and duration of action. Different insulin types may lead to different hypoglycemic dynamics if applied with Con A-system. Beside the clinical insulin types, nano-insulin dosage form with special functionality may bring other possibility for insulin delivery. For example, our group has developed a kind of nanomagnetic-insulin that has a better glycemic control with longer effective drug duration while not causing hypoglycemia and a magnetic-modulated hypoglycemic dynamics. The nanomagnetic-insulin opens the possibility of the recycle and reuse of insulin *in vivo* with the aid of magnetic remote-control

technique.

APPENDIX C LIST OF PUBLICATIONS

1. **Ruixue Yin*,** Xu Qian, Liangfa Kang, Kemin Wang*, Hongbo Zhang, Shih-Mo Yang, Wenjun Zhang. A step towards glucose control with a novel nanomagnetic-insulin for diabetes care. ***International Journal of Pharmaceutics***, 2021, 601: 120587.
2. **Ruixue Yin*,** Jing He, Meirong Bai, Cong Huang, Kemin Wang*, Hongbo Zhang, Shih-mo Yang, Wenjun Zhang. Engineering Synthetic Artificial Pancreas Using Chitosan Hydrogels Integrated with Glucose-Responsive Microspheres for Insulin Delivery, ***Materials Science and Engineering: C***, 2019, 96, 374-382.
3. **Ruixue Yin***, Meirong Bai, Jing He, Jun Nie, Wenjun Zhang*. Concanavalin A-sugar affinity based system: Binding interactions, principle of glucose-responsiveness, and modulated insulin release for diabetes care. ***International Journal of Biological Macromolecules***, 2019, 124, 724-732.
4. Meirong Bai, Jing He, Liangfa Kang, Jun Nie, **Ruixue Yin***. Regulated basal and bolus insulin release from glucose-responsive core-shell microspheres based on Concanavalin A-sugar affinity, ***International Journal of Biological Macromolecules***, 2018, 113, 889-899.
5. **R.X. Yin** *, M.R. Bai, B. Zhang, K.M. Wang, H.B. Zhang, S.M. Yang, W.J. Zhang*, J.W. Wang. Understanding Drug Delivery from a System Perspective: Concept and Demonstration. The 12th Annual IEEE International Conference on Nano/Micro Engineered and Molecular Systems (IEEE-NEMS), April 9-12, 2017, Los Angeles, USA.
6. Ang Chen, **Ruixue Yin**, Lin Cao, Chenwang Yuan and Wenjun Zhang*, Soft Robots: Concept and Research Directions, 24th International Conference on Mechatronics and Machine Vision in Practice (M2VIP), Auckland, New Zealand, November 21-23, 2017 .
7. Chenwang Yuan, Ge Chen, **Ruixue Yin**, Wenjun Zhang*, A New Under-Actuated Resilient Robot, IEEE International Conference on Systems, Man and Cybernetics (SMC), Banff, Canada, October 5-8, 2017.

APPENDIX D COPYRIGHT PERMISSIONS

The copyright permissions of the following papers presented in the thesis are listed here:

R.X. Yin *, M.R. Bai, B. Zhang, K.M. Wang, H.B. Zhang, S.M. Yang, W.J. Zhang*, J.W. Wang. Understanding Drug Delivery from a System Perspective: Concept and Demonstration. The 12th Annual IEEE International Conference on Nano/Micro Engineered and Molecular Systems (IEEE-NEMS), April 9-12, 2017, Los Angeles, USA.

Ruixue Yin*, Meirong Bai, Jing He, Jun Nie, Wenjun Zhang*. Concanavalin A-sugar affinity based system: Binding interactions, principle of glucose-responsiveness, and modulated insulin release for diabetes care. ***International Journal of Biological Macromolecules***, 2019, 124, 724-732.

Ruixue Yin*, Jing He, Meirong Bai, Cong Huang, Kemin Wang*, Hongbo Zhang, Shih-mo Yang, Wenjun Zhang. Engineering Synthetic Artificial Pancreas Using Chitosan Hydrogels Integrated with Glucose-Responsive Microspheres for Insulin Delivery, ***Materials Science and Engineering: C***, 2019, 96, 374-382.

Understanding drug delivery from a system perspective: Concept and demonstration

Conference Proceedings: 2017 IEEE 12th International Conference on Nano/Micro Engineered and Molecular Systems (NEMS)
Author: R.X. Yin
Publisher: IEEE
Date: April 2017

Thesis / Dissertation Reuse

The IEEE does not require individuals working on a thesis to obtain a formal reuse license, however, you may print out this statement to be used as a permission grant:

Requirements to be followed when using any portion (e.g., figure, graph, table, or textual material) of an IEEE copyrighted paper in a thesis:

1) In the case of textual material (e.g., using short quotes or referring to the work within these papers) users must give full credit to the original source (author, paper, publication) followed by the IEEE copyright line © 2011 IEEE.
2) In the case of illustrations or tabular material, we require that the copyright line © [Year of original publication] IEEE appear prominently with each reprinted figure and/or table.
3) If a substantial portion of the original paper is to be used, and if you are not the senior author, also obtain the senior author's approval.

Requirements to be followed when using an entire IEEE copyrighted paper in a thesis:

1) The following IEEE copyright/ credit notice should be placed prominently in the references: © [year of original publication] IEEE. Reprinted, with permission, from [author names, paper title, IEEE publication title, and month/year of publication]
2) Only the accepted version of an IEEE copyrighted paper can be used when posting the paper or your thesis on-line.
3) In placing the thesis on the author's university website, please display the following message in a prominent place on the website: In reference to IEEE copyrighted material which is used with permission in this thesis, the IEEE does not endorse any of [university/educational entity's name goes here]'s products or services. Internal or personal use of this material is permitted. If interested in reprinting/republishing IEEE copyrighted material for advertising or promotional purposes or for creating new collective works for resale or redistribution, please go to http://www.ieee.org/publications_standards/publications/rights/rights_link.html to learn how to obtain a License from RightsLink.

If applicable, University Microfilms and/or ProQuest Library, or the Archives of Canada may supply single copies of the dissertation.

BACK CLOSE WINDOW

Copyright Clearance Center RightsLink

Home | Help | Email Support | Sign in | Create Account

Concanavalin A-sugar affinity based system: Binding interactions, principle of glucose-responsiveness, and modulated insulin release for diabetes care

Author: Ruixue Yin,Meirong Bai,Jing He,Jun Nie,Wenjun Zhang
Publication: International Journal of Biological Macromolecules
Publisher: Elsevier
Date: 1 March 2019

Journal Author Rights

Please note that, as the author of this Elsevier article, you retain the right to include it in a thesis or dissertation, provided it is not published commercially. Permission is not required, but please ensure that you reference the journal as the original source. For more information on this and on your other retained rights, please visit: https://www.elsevier.com/about/our-business/policies/copyright#Author-rights

BACK CLOSE WINDOW

Copyright Clearance Center RightsLink

Home | Help | Email Support | Sign in | Create Account

Engineering synthetic artificial pancreas using chitosan hydrogels integrated with glucose-responsive microspheres for insulin delivery

Author: Ruixue Yin,Jing He,Meirong Bai,Cong Huang,Kemin Wang,Hongbo Zhang,Shih-Mo Yang,Wenjun Zhang
Publication: Materials Science and Engineering: C
Publisher: Elsevier
Date: March 2019

Journal Author Rights

Please note that, as the author of this Elsevier article, you retain the right to include it in a thesis or dissertation, provided it is not published commercially. Permission is not required, but please ensure that you reference the journal as the original source. For more information on this and on your other retained rights, please visit: https://www.elsevier.com/about/our-business/policies/copyright#Author-rights

BACK CLOSE WINDOW

The copyright permissions of figures in Chapter 1 are listed here:

Permission of Fig. 1.1

AMERICAN DIABETES ASSOCIATION LICENSE
TERMS AND CONDITIONS

Jun 06, 2021

This Agreement between University of Saskatchewan -- Ruixue Yin ("You") and American Diabetes Association ("American Diabetes Association") consists of your license details and the terms and conditions provided by American Diabetes Association and Copyright Clearance Center.

License Number	5082990130056
License date	Jun 06, 2021
Licensed Content Publisher	American Diabetes Association
Licensed Content Publication	Diabetes
Licensed Content Title	Artificial Pancreas: Past, Present, Future
Licensed Content Author	Claudio Cobelli,Eric Renard,Boris Kovatchev
Licensed Content Date	Nov 1, 2011
Licensed Content Volume	60
Licensed Content Issue	11
Type of Use	Thesis/Dissertation
Requestor type	Student

Portion	chart/graph/table/figure
Number of charts/graphs/tables/figures	1
Rights for	Main product
Duration of use	Life of current edition
Creation of copies for the disabled	no
With minor editing privileges	no
For distribution to	Worldwide
In the following language(s)	Original language of publication
With incidental promotional use	no
The lifetime unit quantity of new product	0 to 499
Title	PRINCIPLE AND PERFORMANCE OF CONCANAVALIN A-SUGAR AFFINITY BASED CLOSED-LOOP INSULIN DELIVERY SYSTEM
Institution name	University of Saskatchewan
Expected presentation date	Aug 2021
Order reference number	13 of Chapter 1

Portions	Fig. 3
Requestor Location	University of Saskatchewan 57 CAMPUS Drive, saskatoon Saskatoon, SK S7N 5A9 Canada Attn: University of Saskatchewan
Total	0.00 CAD

Permission of Fig. 1.2